Daniel Maria Hirschl

Master Thesis 2017:E12 supervised by
Univ.-Prof. Dipl.-Ing. Dr.mont. Gerhard Thonhauser

Experimental Design to Investigate the Casing Smearing Effect

dpe DEPARTMENT PETROLEUM ENGINEERING

MONTAN UNIVERSITÄT

This thesis is dedicated to my parents,
Monika and Michael

Affidavit

I declare in lieu of oath that I wrote this thesis and performed the associated research myself using only literature cited in this volume.

Eidesstattliche Erklärung

Ich erkläre an Eides statt, dass ich diese Arbeit selbständig verfasst, andere als die angegebenen Quellen und Hilfsmittel nicht benutzt und mich auch sonst keiner unerlaubten Hilfsmittel bedient habe.

_____

Daniel Maria Hirschl, 07 March 2017

Abstract

One of the main reasons why Casing while Drilling (CwD) was growing more and more interest in the oil and gas industry is the so called "smearing effect". Due to the eccentric motion of the casing string crushing of the cuttings takes place along the string. It is assumed that the casing string smears the mixture of fine-sized cuttings and mud onto the wellbore wall. The result in most of the cases is a low permeability layer, which is assumed to stabilize the wellbore wall and consequently increases the overall drilling margin.

This is in contrast to the ordinary methods of fluid loss prevention. Normally a filter cake develops due to the difference in formation and mud pressure. No mechanical action is involved in the creation of the cake. In this case, it is not desirable if the drillstring makes contact with the wellbore wall. Furthermore, the cuttings remain at its original size because no crushing action takes place. Therefore, the influence of the cuttings on the filter cake quality is negligible.

The main goal for both methods is the same but the underlying mechanism is different.

The thesis analyses the underlying mechanisms in theory and defines the most influential parameters for both methods. Furthermore, the geomechanical impact on the area surrounding the wellbore regarding CwD is analysed. Finally, an experimental design is proposed which, if implemented, enables the user to directly compare filter cakes created by one of the two methods.

Zusammenfassung

Einer der Hauptgründe für die Verwendung von Casing while Drilling ist der sogenannte "smearing-effect". Aufgrund der exzentrischen Bewegung des Bohrstranges, der in diesem Fall aus Verrohrung besteht, wird das Bohrklein an der Bohrlochwand zerbrochen. Anschließend schmiert der Bohrstrang die Mischung aus Bohrschlamm und zerkleinertem Bohrklein an die Wand und erzeugt so einen Filterkuchen mit niedriger Permeabilität.

Dies ist im Gegensatz zu den normalerweise eingesetzten Methoden zur Vermeidung von Bohrschlammverlust in die Formation. Normalerweise entsteht alleine durch den Druckunterschied zwischen Bohrschlamm und Formation ein Filterkuchen an der Bohrlochwand. Der Bohrstrang hat darauf keinen Einfluss. Das Bohrklein behält seine Originalgröße und hat auf die Qualität des Filterkuchens keinen Einfluss.

Das Ziel beider Methoden ist das Gleiche. Man möchte verhindern dass es zu einem Verlust von Bohrschlamm in die Formation kommt. Der zugrunde liegende Mechanismus ist jedoch unterschiedlich.

Diese Arbeit analysiert den zugrunde liegenden Mechanismus beider Methoden und jene Parameter die auf das Ergebnis den größten Einfluss haben. Des Weiteren wird der geomechanische Einfluss von Casing while Drilling auf die umliegende Formation untersucht. Abschließend wird ein Design für ein Experiment vorgeschlagen das einen direkten Vergleich der Filterkuchen beider Methoden ermöglichen soll.

Acknowledgements

I would like to thank my parents, Monika and Michael for their continuous support since the start of my studies.

I would also like to thank my siblings for reminding me that there is also a life besides studying and for being so patient with a “workaholic”.

Contents

Chapter 1 Introduction

The positive impact of Casing while Drilling (CwD) on wellbore stability is based on the theory of the "smearing effect". However, the "smearing effect" itself is not fully understood yet because several different theories exist [1]. Some of them focus on the coating of the wellbore wall with the crushed cuttings, which prevent the propagation of fractures. Others claim that early propping of already existing fractures with the crushed cuttings is the main reason for the wellbore strengthening effect. The biggest problem with all these theories is that none of them have been brought to the test directly by trying to simulate smearing in an experiment.

Additionally, it would be interesting to have a direct comparison between a regular filter cake and one that was created by smearing. This would especially be interesting for different properties such as permeability, thickness and the filter cake surface (from a microscopic point of view).

The thesis itself can be subdivided in the introduction and six chapters. The first chapter focuses on a literature review and assessment of the most influential parameters for the build-up of regular filter cake and one created by CwD. In the next chapter the geomechanical aspects of CwD are discussed and the most important findings are highlighted. Afterwards, already existing technologies to investigate the filter-cake build up are analysed regarding their applicability. In the chapter about experimental setup a proposal for an apparatus is made which could investigate static and dynamic filter cake build-up as well as filter cake created by CwD. Finally, the experimental procedures of the apparatus are outlined.

Chapter 2 Literature Review

While drilling a well, one of the main objectives of the drilling mud is to stabilize the wellbore and ensure safe operations. The drilling mud creates a pressure inside the wellbore, which hinders fluid to enter the wellbore in an uncontrolled way. Nevertheless, it is equally important to prevent fluid loss into the formation. When drilling overbalanced the mud pressure is higher than the formation pressure and therefore fluid is going to enter the formation anyway. To prevent that it is necessary that a sufficient filter cake of good consistency is build-up on the wellbore wall.

Furthermore, the filter cake is the only barrier for the fluid between wellbore and formation. Therefore, it is of vital importance to have a fundamental understanding about the build-up process and the mud cake properties. The standard process of mud cake build up has been studied extensively but since CwD has become more popular a new phenomenon has been observed which is called the "smearing effect".

The following literature review examines the most important parameters that influence the build-up and the final properties of a regular filter cake and one created by smearing. The overall conclusion will then define the parameters which have the most influence and should be investigated during the experimental research.

2.1 Fundamentals of Filter Cake Build-up

The fundamental theory of filter cake build-up is already described in the introduction of this literature review. Nevertheless it is important to pay attention to the details. During drilling two different situations are observed in terms of filter cake build-up. If circulation is stopped only the hydrostatic pressure of the mud forces the build-up of a filter cake. This can be called a "static" system. During circulation, continuous fluid flow has a major influence on the filter cake build-up. In this case we are talking about a "dynamic" system.

2.1.1 Static Filter Cake Description

According to Dewan and Chenevert [2, p. 237] a minimum of three parameters are required to characterize a filter cake. They state that these parameters are porosity, permeability and a compressibility exponent. The compressibility exponent describes the dependence of porosity and permeability on pressure across the mud cake.

Porosity and permeability are well known parameters but in the case of filter cake build-up we are not talking about constant values anymore, as they vary with time due to compression of the filter cake in the build-up process. The following formulas are proposed by Dewan and Chenevert [2, p. 239] to describe this behaviour where v is the compressibility exponent, which ranges typically between 0.4 and 0.9. Additionally, reference permeability with a differential pressure of 1 psi is defined, which is called k_{mc0}. The equation for mud cake porosity looks similar, but it includes a multiplier δ,

which is in the range of 0.1 to 0.2 and is based on porosity-permeability crossplots for shaly sands.

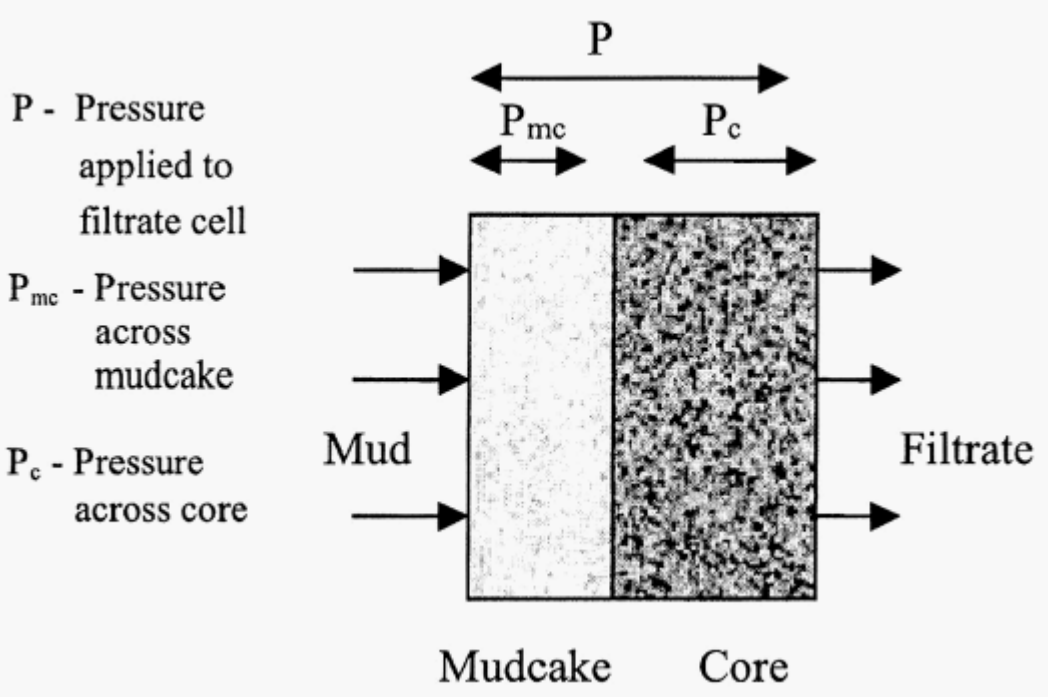

Figure 1: Model of filtration through a core [2, p. 239]

$$k_{mc}(t) = \frac{k_{mc0}}{P_{mc}^{v}}$$

Equation 1: Mudcake permeability determination [2, p. 239]

Where P_{mc} is the pressure across the mudcake, k_{mc0} is the reference permeability and v is the compressibility exponent.

$$\Phi_{mc}(t) = \frac{\Phi_{mc0}}{P_{mc}^{v*\delta}}$$

Equation 2: Mudcake porosity determination [2, p. 240]

Where Φ_{mc} is the mudcake porosity, Φ_{mc0} is the reference porosity and δ is the multiplier based on porosity-permeability crossplots for shaly sands.

The model above can be combined with investigations from a different study [3], which indicates that a filter cake consists of two different layers as depicted in the picture on the next page.

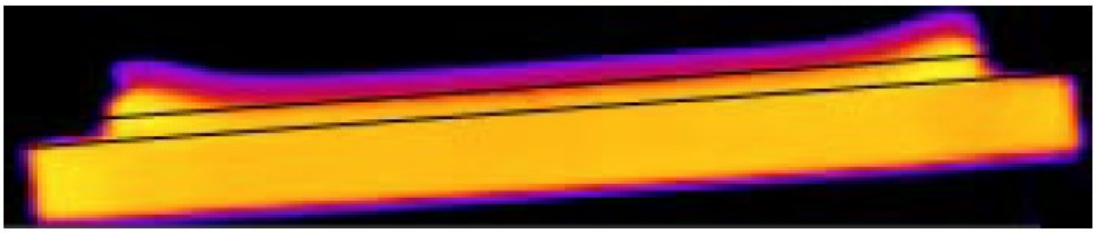

Figure 2: CT-Scan of Filter Cake with two-layer structure [3, p. 10]

Furthermore, investigations via SEM showed a clear difference in the composition of both layers.

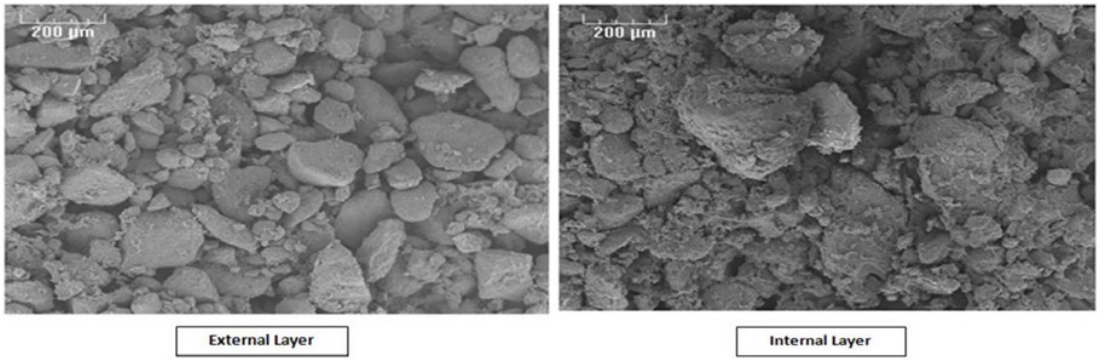

Figure 3: SEM-Scan of the internal and the external layer [4, p. 11]

Furthermore, during the process of build-up, the properties of the filter cake are not constant. Different periods of build-up and compression occur, which result in changing values for thickness, porosity and permeability of the filter cake.

2.1.1.1 Filter Cake Porosity

Porosity is calculated based on the CT-Number by the following equation.

$$\Phi = \frac{CT_{wet} - CT_{dry}}{CT_{water} - CT_{air}}$$

Equation 3: Porosity calculated from the CT-Number [5, p. 2]

Where CT_{wet} is the CT-Number of the scanned slice saturated with water, CT_{dry} is the CT-Number of the scanned slice when dry, CT_{water} is the CT-Number of water and CT_{air} is the CT-Number of air.

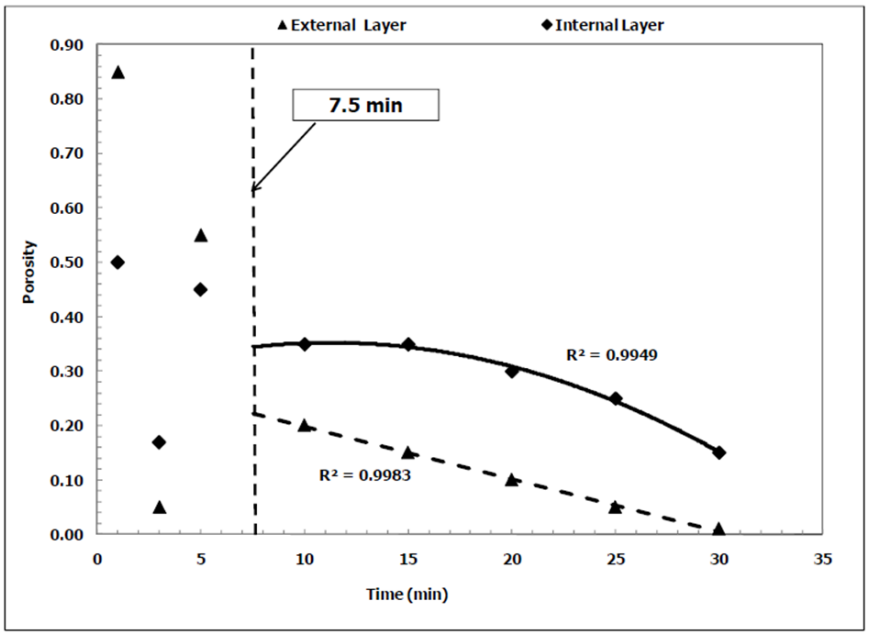

Figure 4: Filter cake porosity as a function of time [5, p. 11]

Before 7.5 minutes, it can be seen that different periods of compression and build-up are present as the porosity changes very fast from high to low values and vice versa. After 7.5 minutes, a more or less normal behaviour can be seen as porosity decreases with time. Additionally, the outer layer of the filter cake can be influenced by the particle size. As can be seen in Figure 3 the external layer experiences a very poor sorting resulting in a porosity that drops down to zero in this experiment [5, p. 11].

2.1.1.2 Filter Cake Thickness

The next parameter, to have a closer look at, is the filter cake thickness, during the same experiment.

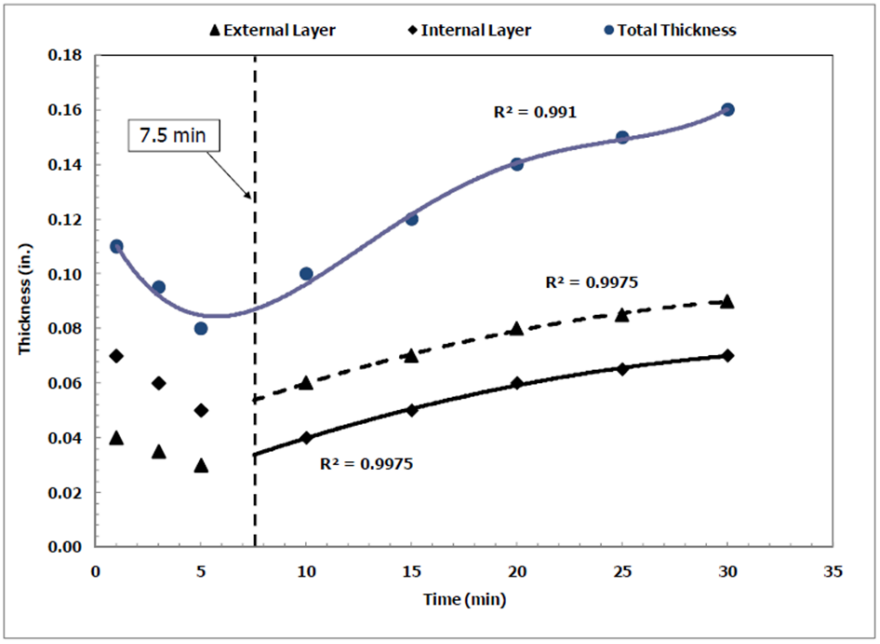

Figure 5: Filter cake thickness as a function of time [5, p. 12]

In the compression region, which is before 7.5 minutes, the filter cake thickness decreases for both layers. Afterwards, as the build-up rate is high enough, a normal trend can be observed, which shows an increase in filter cake thickness as time goes by. An interesting observation is the fact that the thickness of the internal filter cake is higher in the beginning than the external one. This is caused by the precipitation of large particles in the beginning. Afterwards, as porosity in the external filter cake decreases, less particles could move through the filter cake and the thickness of the external filter cake is therefore higher [5, p. 12].

2.1.1.3 Filter Cake Permeability

The last important parameter, which describes the filter cake is the permeability. The permeability needs to be calculated from empirical correlations. The following equation is used as an example because it was used for the following figure.

$$k_c = 112.7 * e^{-8.8*(1-\Phi_c)}$$

Equation 4: Empirical correlation for filter cake permeability from porosity [4, p. 5]

Where k_c is the permeability of the filter cake and Φ_c is the porosity of the filter cake.

This calculation results in the figure below, which is in line with the behaviour one would expect from a filter cake with decreasing porosity. As the porosity of the external layer decreases to zero and nearly no fluid can pass this layer anymore, the permeability reaches a very low value.

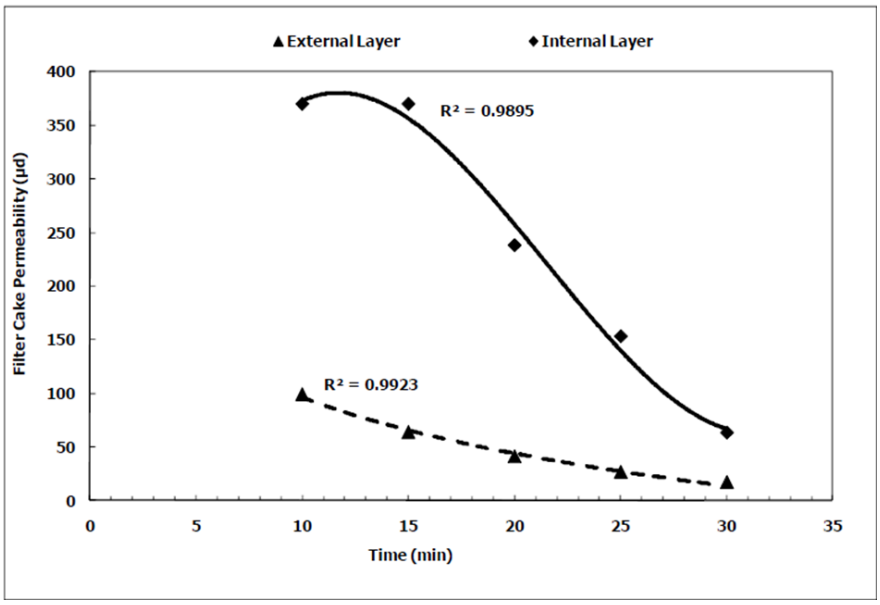

Figure 6: Filter cake permeability as a function of time [5, p. 13]

Nevertheless, all of the points mentioned above need to be treated with care due to the fact that all the values are indirectly derived. This means that porosity, permeability and thickness are derived based on the CT-number and empirical correlations.

2.1.2 Dynamic Filter Cake Description

To understand a dynamic system, we have to take this model another step further. During circulation of drilling mud the fluid flow in the annulus creates an additional force, which acts parallel to the filter cake surface. This force creates a shear stress onto the filter cake surface resulting in an erosion process. The rate of erosion is directly dependent on the amount of shear stress exerted on the filter cake surface [6, p. 2].

Furthermore, it needs to be mentioned that during dynamic filtration the filter cake build-up undergoes two different stages. [7, p. 3]. In the first stage deposition of particles takes place. The force that deposits the particles on the wellbore wall is higher than the force that removes particles from the surface. In the second stage equilibrium is reached. The forces of deposition and removal are equal. At this stage filter cake thickness does not change anymore.

Jiao and Sharma [8, p. 79] conducted experiments with water based mud on cores. They observed that the thickness of the mud cake is a sensitive function of the mud rheology, the mud shear rate and the permeability of the core. The deposition of clay particles during dynamic filtration is a function of two forces [8, p. 81]. A hydrodynamic drag force F_y. This force acts normal to the mud cake. The other force is a hydrodynamic shear force F_x which is imposed by the mud flow parallel to the mud cake.

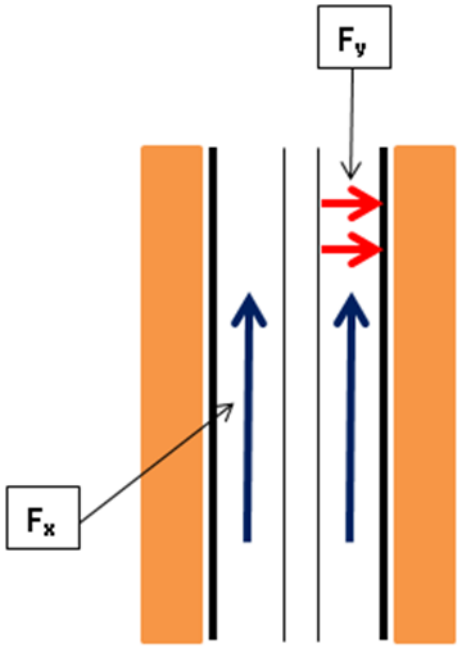

Figure 7: Dominant forces during mudcake deposition

As long as the following inequality is satisfied particles of a certain size are going to be deposited [8, p. 81].

$$F_x \leq f * F_y$$

Equation 5: Hydrodynamic force inequality [8, p. 81]

In the beginning, when the filtration rate is high, bigger particles are going to settle but when the filtration rate decreases, smaller particles are going to be deposited and finally, when the drag force is too small the equilibrium state is reached and no more particles are deposited on the filter cake surface [8, p. 3].

2.1.2.1 Filter Cake Porosity and Permeability

Dynamic conditions in the annulus can have a positive effect on the filter cake porosity. Due to the shear forces present, they could hinder fine particles to settle on top of the filter cake surface [4, p. 4]. This has not only a positive effect on the overall porosity but also on the permeability of the filter cake, which is especially critical if we later want to produce a reservoir fluid through the filter cake [9, p. 1]. Therefore, special attention has to be paid to the particle size distribution (PSD) in the drilling mud.

2.1.2.2 Particle Size Distribution

A wrong PSD can lead to an invasion of drilling fluid into the reservoir, which could actually lead to a positive skin [10, p. 1], which, in return, could result in bad production rates and costly stimulation operations. Therefore, it is necessary to have an optimized PSD in the drilling mud.

"It is commonly understood that a reservoir drilling fluid must be compatible with the reservoir rock, both chemically and physically" [10, p. 1]

The invasion of drilling fluid into the formation is closely related to the pore system and other fluid-flow channels in the reservoir rock [10, p. 1]. Therefore, it is necessary to have a fundamental understanding about the type, size and distribution of fluid-flow channels in the critical interval. Different techniques exist for characterizing these features. Thin sections, mercury injection, SEM and Micro CT are the most popular methods [10, pp. 2-4].

Based on the methods mentioned above the most important features to determine the particle size distribution, are:

- Dominant flow channels in the rock
- Dimension, Distribution and Connectivity of Pores
- Dimension, Distribution and Connectivity of Fractures

If we use sandstone as an example, the dominant fluid flow channels are interparticle pores. A full range of PSD of bridging material is proposed in this case [10, p. 5]. The following tables show the difference in a formation damage test with and without bridging particles.

Test Fluid	Initial Permeability [mD]	Volume of Filtration [ml] / [%] Pore Volume	Return Permeability [mD] / [%] Return	Flow Initiation Pressure [psi]
1	230.4	5.7 / 48.9	212.4 / 92.2	6.9
2	250.5	7.0 / 50.4	237.3 / 94.7	9.7
3	258.0	5.8 / 43.3	236.6 / 91.7	6.0

Table 1: Test results for a sandstone using bridging particles [10, p. 6]

Test Fluid	Initial Permeability [mD]	Volume of Filtration [ml] / [%] Pore Volume	Return Permeability [mD] / [%] Return	Flow Initiation Pressure [psi]
1	43.2	16.8 / 160.0	4.07 / 12.6	92.7
2	32.2	17.3 / 135.3	4.76 / 11.0	68.9
3	93.4	22.7 / 200.0	23.65 / 25.3	23.5

Table 2: Test results for a sandstone without bridging particles [10, p. 6]

It is obvious from the results above that the correct PSD makes a big difference as, the return permeability is much smaller and the volume of filtration is much higher.

Furthermore, it is important to know if a formation contains oversized pores such as limestone or dolomite. Tests have shown that if these pores are not bridged, fluid loss and formation damage can be high. Also, these tests have indicated, that having the D90 of the bridging particles equal to the common maximum pore size, combined with fine particles for the small pores, bridging of most of the pores can be achieved [10, p. 7].

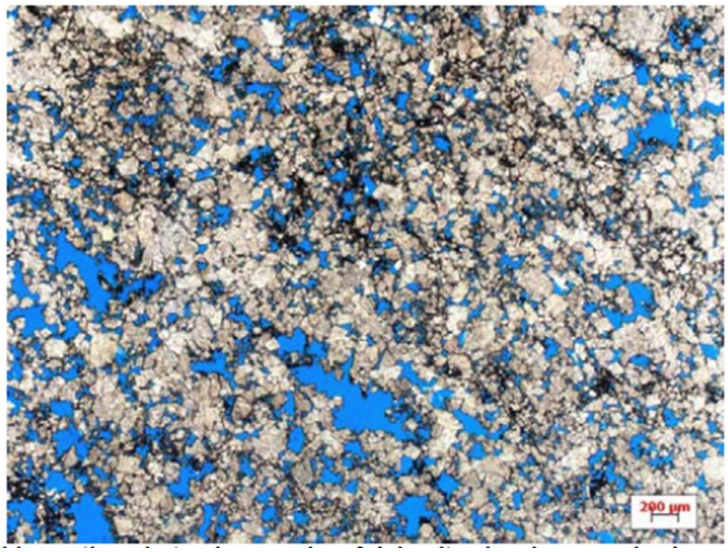

Figure 8: Thin section of a dolomite with oversized pores [10, p. 7]

Finally, there is one more situation in which PSD has a huge influence on the build-up of an appropriate filter cake. Carbonate rocks with well-developed fractures or other large-scale openings are critical as well. As long as these openings are not larger than 500 µm, the correct size of bridging particles could still bridge these features. Nevertheless, these features can even go into the centimetre scale. If this is the case new methods such as underbalanced drilling should be considered to minimize formation damage [10, p. 9].

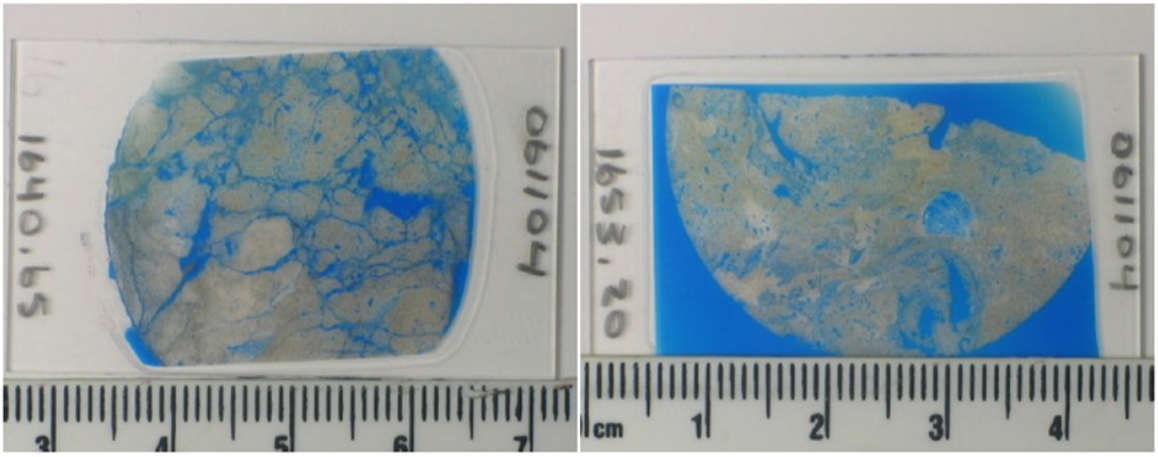

Figure 9: Thin sections of silty dolomite with vugs, channels, oversized pores [10, p. 9]

2.2 Fundamentals of the Smearing Effect

In general, "plastering" or "smearing" describes a special process of mud cake build-up during Casing while Drilling Operations. One of the most popular hypotheses describes this process as follows [11, p. 3]. The cuttings generated at the drill-bit are pulverized and smeared against the formation due to the combination of high annular velocity, pipe rotation and the proximity of casing wall to the borehole. This creates an impermeable mud cake on the wellbore wall.

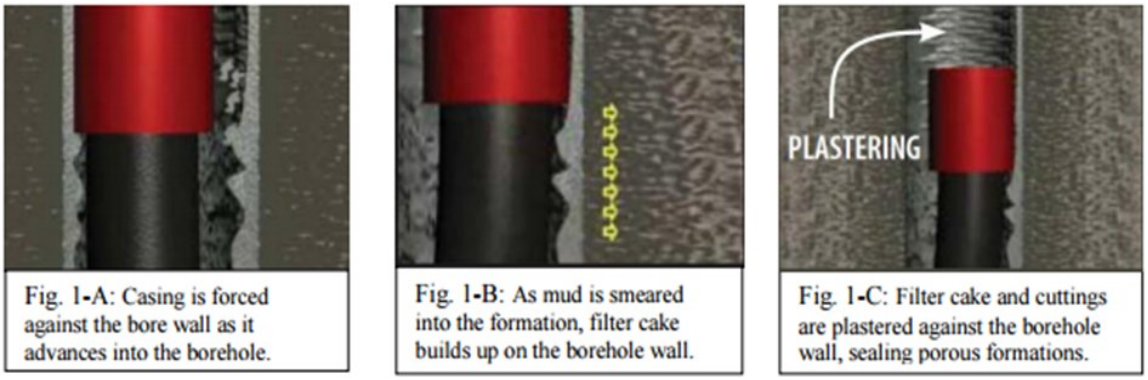

Figure 10: Proposed Plastering Mechanism [11, p. 3]

2.2.1 Objectives of Casing while Drilling

"Smearing" cuttings against the wellbore wall is a desired effect during CwD. Especially in lost circulation zones it can be very beneficial. Several successful case studies are mentioned in the literature [12, pp. 5-6]. By applying CwD it was possible to overcome lost circulation, wellbore instability and well control problems. Even the wellbore quality was improved. Furthermore, due to the "smearing" effect as a method for extending the overall drilling margin, CwD can be considered as a wellbore strengthening method. [1, p. 6]. Several theories exist about the underlying mechanism of strengthening the wellbore during CwD. The most reliable mechanism was proposed by van Oort and Razavi [1, pp. 6-7]. They claim that Fracture Propagation Resistance is responsible for the strengthening of the wellbore. They base their evidence on the results of open-hole leak-off tests, which were conducted while drilling with casing in the Alaskan Tarn Field [13, p. 8]. The test results are displayed in the figures below.

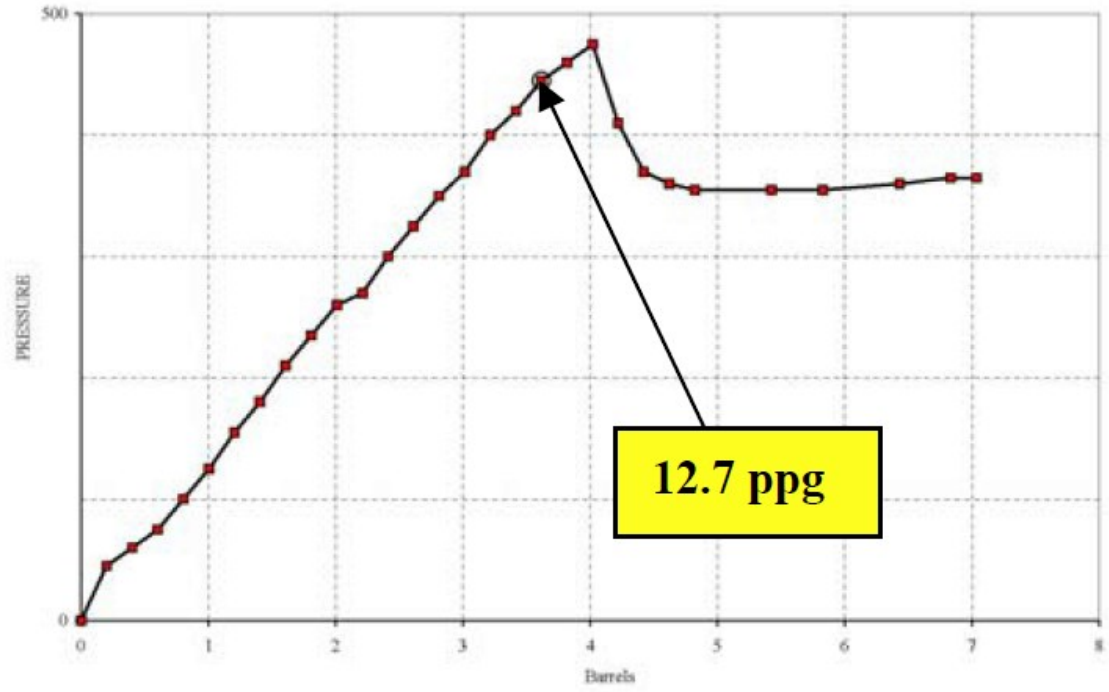

Figure 11: Leak-Off Test before CwD [13, p. 8]

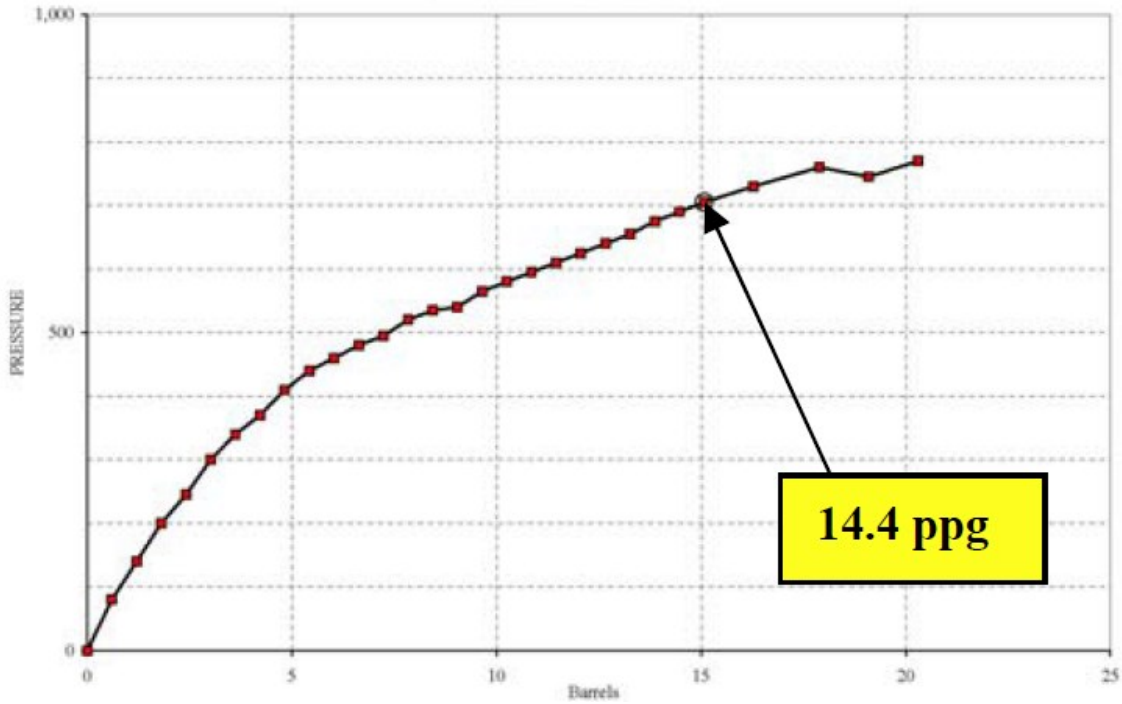

Figure 12: Leak-Off Test after CwD [13, p. 8]

It clearly indicates that the Fracture Initiation Pressure, before CwD was applied, is higher than the Fracture Reopening Pressure after CwD. Therefore, wellbore stress augmentation is not the reason for wellbore strengthening [1, p. 7]. If it would be the reason there need to be an increase from FIP to FRP. It is more likely that an increase in the Fracture Propagation Resistance is responsible for WBS. The figure above shows a

dramatic increase in the Fracture Propagation Pressure. This means that during CwD it is much harder for the fractures to propagate. A possible explanation for that is that tip-screen out occurs during CwD which seals the fracture tips and raises the FPP [1, p. 7].

2.2.2 Mechanical Parameters Influencing Filter-Cake Build-up in CwD

Due to the complexity of this process a variety of parameters have a significant influence on the smearing effect. The most important ones are discussed in detail in the sections below.

2.2.2.1 Eccentricity

Eccentricity can be described as how off-centre of the hole a pipe is within the open hole section [14, p. 10]. If a pipe is concentric it means that the eccentricity is zero. Nevertheless, it is very unlikely that a pipe is completely concentric, especially in CwD, it is desired that the pipe moves in an eccentric motion in the wellbore. As recently mentioned the wellbore strengthening effect of CwD is related to the occurring fractures. The direction of fracture propagation is related to the stress field.. Due to that the contact points of the casing with the wellbore should be similar with the direction of fracture occurrence because this makes a plastering of the induced fractures more likely. [15, p. 4] Nevertheless, eccentricity can't be controlled which makes this influence factor unpredictable.

2.2.2.2 Pipe Geometry

The large diameter of the casing is the primary drive for the "smearing" effect of casing while drilling [16]. Furthermore, the research of Karimi, Moellendick and Holt [16] identified the following parameters, with the corresponding explanations mentioned below, as critical for the success of "smearing" in a CwD operation. Considering the definition of eccentricity above, the influence of eccentricity is minor if the diameter of the used pipe gets bigger.

2.2.2.3 Contact Angle

As the tool joint has a bigger diameter than the pipe body and contact with the wellbore wall is more likely the contact angle is described with regards to the tool joint diameter. Depending on the diameter of the tool joint the contact angle of the tool joint is different. With decreasing tool joint diameter, the contact angle gets bigger. This leads to the problem that a small contact angle is necessary to guarantee a smooth contact of the tool joint with the wellbore wall. Otherwise there is a significant potential that contact of the tool joint with the wellbore leads to a damage of the filter cake. Furthermore, the curvature of the tool joint is another significant factor. If the curvature of the tool joint is similar to the curvature of the wellbore wall the contact forces are minimized and the contacting action is smoother.

2.2.2.4 Contact Area

A larger contact area is much more beneficial because plastering happens at the contact area of the pipe. Obviously, the contact area when using casing is much bigger. Therefore, plastering takes place faster and is much more effective.

2.2.2.5 Linear Speed of the Pipe before hitting the Wellbore Wall

The pipe contact should be as smooth as possible. Therefore, the linear speed should not be too high because this leads to a forceful momentum transfer onto the filter cake at the contact area. Due to the fact that the diameter of regular drill pipe is much smaller than for casing the distance the pipe needs to travel before hitting the wall is higher. This leads to a higher linear speed in case of the regular drill pipe.

2.2.2.6 Penetration Depth into the Filter Cake

With regards to the differences already mentioned it is obvious that the penetration depth into the filter cake for regular drill pipe needs to be higher. This is because the forces when the pipe hits the filter cake are distributed on a much smaller area. Nevertheless, another observation of Karimi, Moellendick, Holt [16] was that the risk for differential sticking is still higher for regular drill pipe. This investigation is highly interesting, because one would expect that the larger contact area of the casing is a much stronger contributor. They base this phenomenon on the fact that the differential pressure in case of a filter cake created by ”smearing” is much smaller because of the high quality of the filter cake.

2.2.2.7 Pipe to Wellbore Size Ratio

The pipe to wellbore size ratio is defined as the ratio of the pipe diameter and the wellbore diameter. The size ratio has a significant impact on the overall hydraulics [15, p. 9]. One of the benefits in terms of casing size is that the smaller annulus leads to higher velocities with lower flowrates compared to drill pipe and improves the hole cleaning efficiency. Nevertheless, it is necessary to keep an eye on the equivalent circulating density, which can be a serious issue if it exceeds the pore pressure. The bottomhole pressure is a function of the flowrate, but also the fluid model, which is used to calculate it can influence the result. The figure below shows that the change in bottomhole pressure depends highly on the size ratio. If the size ratio is higher than 0.7 the pressure increases significantly.

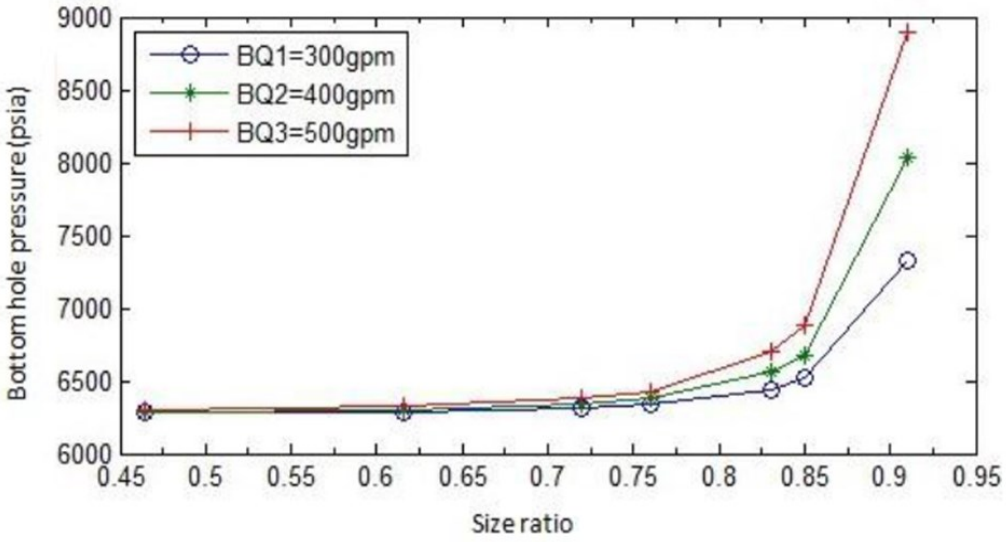

Figure 13: Bottomhole Pressure vs. Size Ratio [15, p. 11]

2.2.2.8 Particle Size Distribution

Since the cuttings are a significant contributor to the smearing effect [14, p. 1] it is necessary to have a clear understanding about the cuttings size. Obviously, the cuttings, which are created at the drill bit are not uniform in size. Therefore, a certain size distribution can be expected, which has a significant influence on the smearing effect. The following figure shows the PSD for a 13.5 ppg water based mud with and without lost circulation material (LCM). The LCM shifts the PSD to a higher number of finer particles compared to the normal mud.

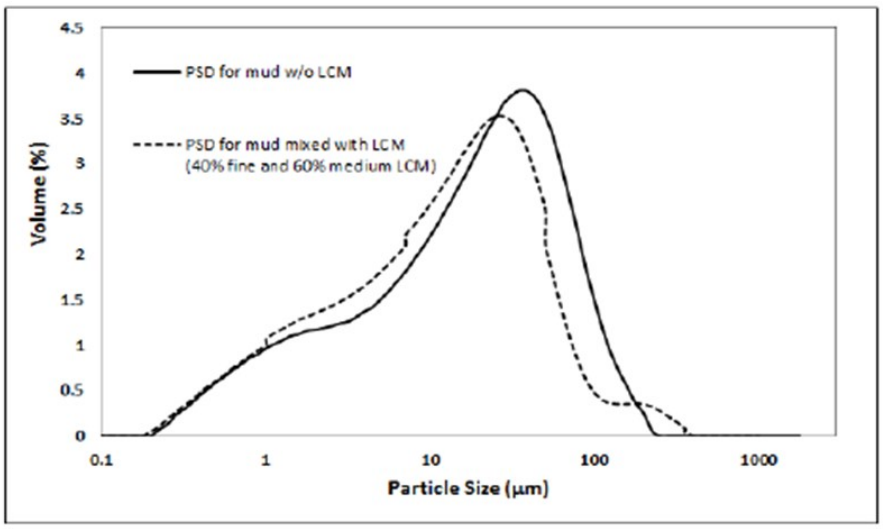

Figure 14: Particle size distribution [14, p. 6]

Furthermore, the real benefit of having finer particles can be seen when observing the results of the permeable plug testing in the figure below. The filtrate volume is significantly lower when using the mud with the LCM. Since CwD leads to smaller cuttings sizes due to the crushing action of the casing, it can be concluded that the created filter cake by "smearing" has enhanced properties in terms of fluid loss, compared to a filter cake which is created by normal drilling practices.

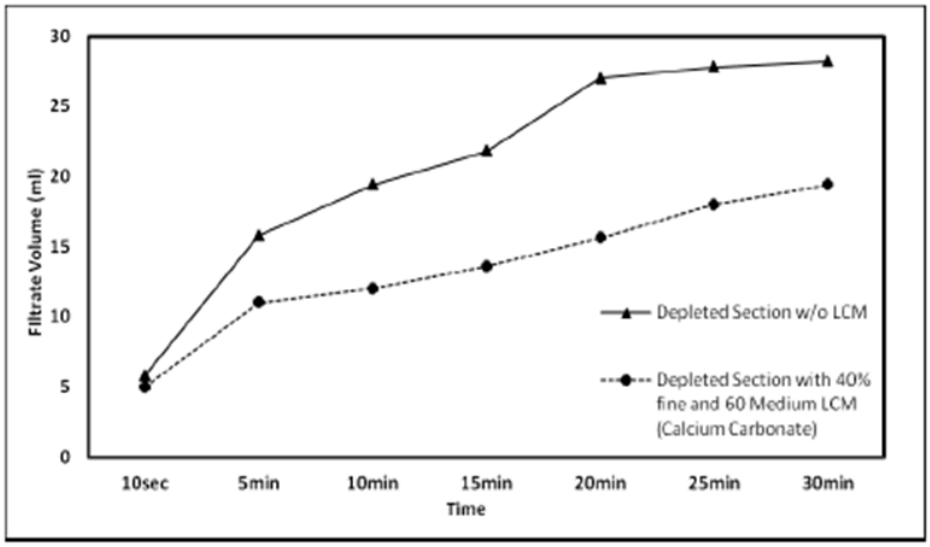

Figure 15: Permeable Plug Tester Filtrate Volume Result [14, p. 8]

2.3 Conclusion of the Literature Review

The comparison between a regular filter cake and one created by smearing has shown some interesting results. First of all, in both cases the particle size distribution is of vital importance. The structure of the filter cake and the volume of filtrate lost into the formation are highly influenced by the PSD. Additionally, porosity and permeability of a regular filter cake are a function of the PSD. So far this is not an intensive topic of research for filter cakes created by smearing, because only the influence on fluid loss performance was evaluated and not the influence on porosity and permeability itself Also, it is not possible to compare permeability and porosity in both of these cases directly because the purpose for a filter cake created by smearing is different. So far CwD is mostly applied in lost circulation situations and instable formations but not in reservoir intervals.

The biggest difference is that in normal drilling situations the pipe itself has nearly no influence on the build-up of the filter cake. In CwD the pipe itself is a major contributor to the filter cake build-up.

Finally, it is necessary to compare the status of research in these two categories. Several experiments exist to investigate the build-up and properties of regular filter cake in static and dynamic situations. So far only simulations and field investigations exist about the influence of different parameters on the filter cake properties during CwD. Therefore, the most important conclusion from this literature review is that a comparison between these two types of filter cakes should be treated with care. No experiment exists so far that investigates different influence parameters for a filter cake created during CwD. It is therefore highly recommended to push into the direction of developing an apparatus that can simulate all three conditions, static, dynamic and CwD filter cake build up.

Chapter 3 Geomechanical Aspects

The process of drilling a well into the earth leads to an alteration of the original stress state in the drilled rocks. The same alteration takes place during CwD operations. The following section is split into two parts. The first section describes the basic geomechanical concepts which are normally applied for investigating wellbore stability. The second part investigates the geomechanical conditions in the near wellbore region while applying CwD and highlights the differences to the normal conditions.

3.1 The in-situ Stress State

Formations beneath the ground are subject to compressive stresses. These stresses are anisotropic and non-homogenous [17] which means that they vary in magnitude based on their direction.

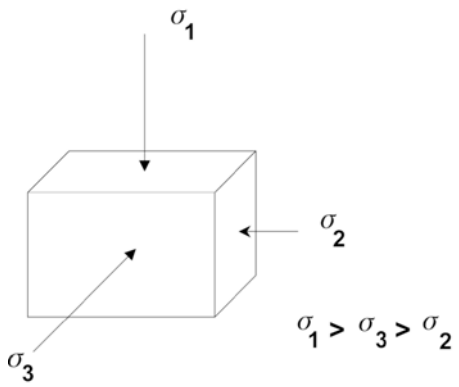

Figure 16: The three principal compressive stresses [18]

3.2 Stresses after Drilling a Well

The in-situ stress state is altered and the stresses are now acting directly onto the wellbore wall. This can cause a variety of types of wellbore failure, which may be referred as wellbore instabilities in general. In the case of CwD we are only going to consider the stress state of a vertical wellbore since CwD is so far not extensively used in combination with directional drilling.

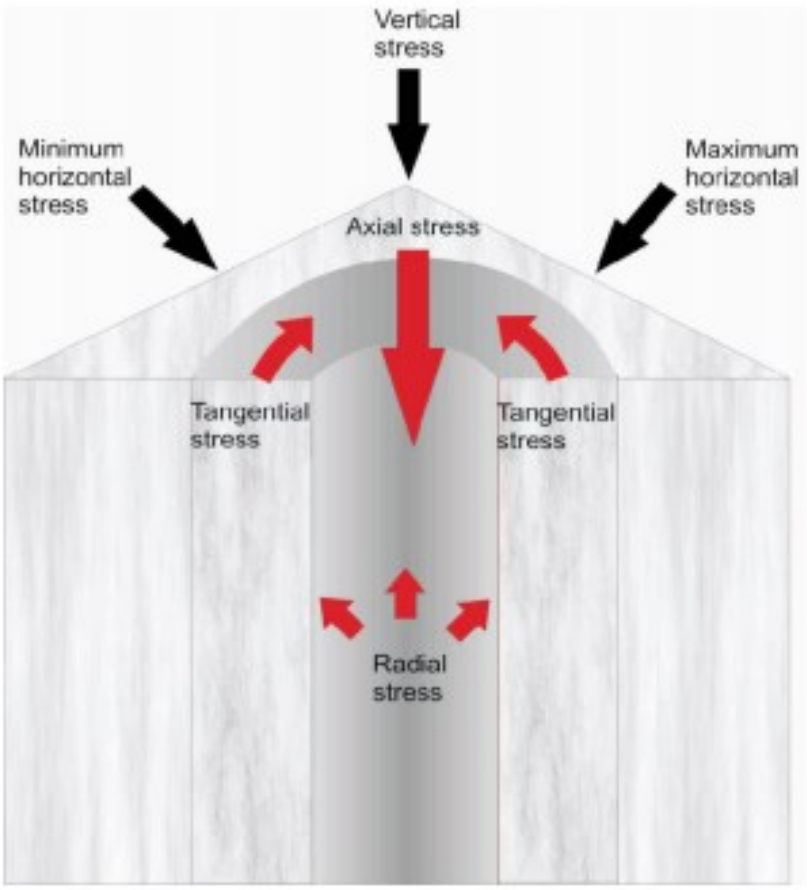

Figure 17: Direction of stresse in a vertical wellbore [19]

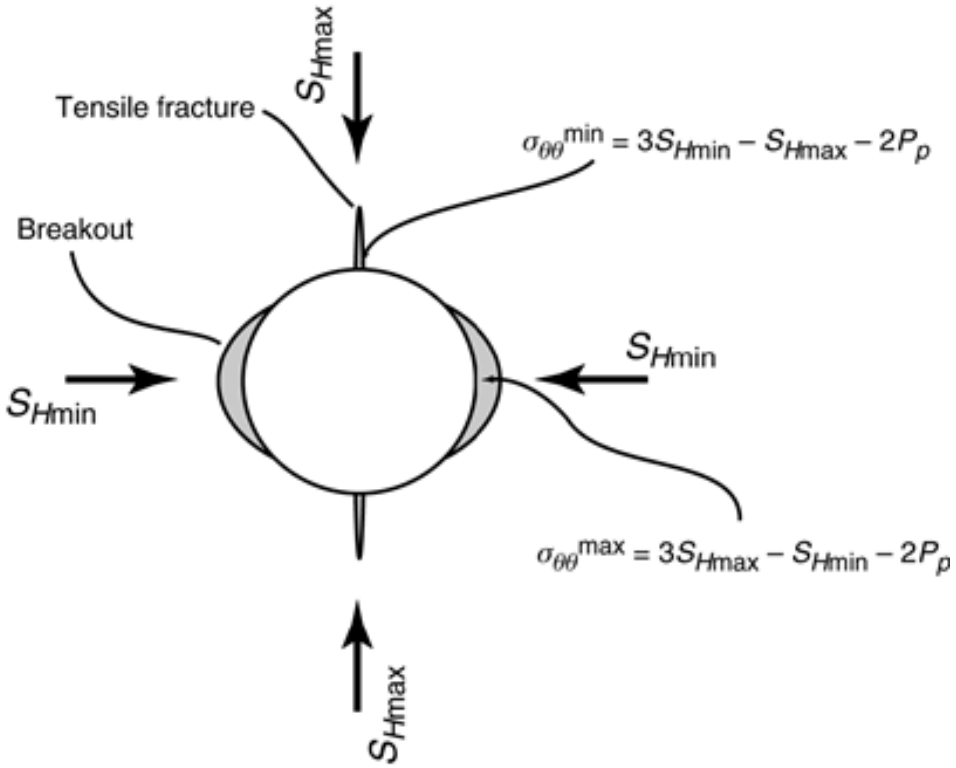

Figure 18: 2D representation of stresses around the wellbore [20]

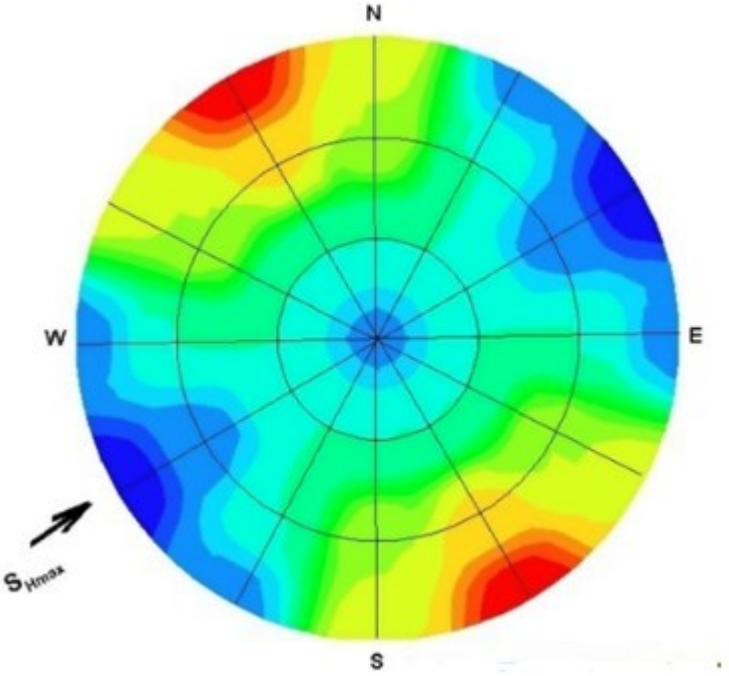

Figure 19: Distribution of stresses around the wellbore, compressive stresses are indicated in red and tensile stresses are indicated in blue [21]

Depending on the magnitude and the direction of the stresses the wellbore will face different failure modes. Failures can be categorized as tensile and compressive failure.

3.2.1 The Kirsch Equations

The Kirsch Equations [22] describe the stress state around the wellbore by three different stresses. The tangential or hoop stress σ_θ, the radial stress σ_r and the axial stress σ_z. Because in our case, the near wellbore region is subject of interest, only the simplified version of the equation is stated here. The complete form can be found in the Ápendix.

$$\sigma_\theta = (\sigma_H + \sigma_h) - 2 * (\sigma_H - \sigma_h) * \cos(2 * \theta) - \Delta P$$

$$\sigma_r = \Delta P$$

$$\sigma_z = \sigma_v - 2 * \nu * (\sigma_H - \sigma_h) * \cos(2 * \theta)$$

Equation 6: Simplified Kirsch Equations for the stress state at the wellbore wall [23]

Where σ_H is the maximum horizontal stress, σ_h is the minimum horizontal stress, θ is the angle around the wellbore and ΔP is the pressure difference between formation and mud.

Nevertheless, it needs to be stated that in this case the equations of Kirsch were developed assuming an isotropic homogeneous environment around the wellbore [24]. Furthermore, the equations have a lack in correctly displaying stresses because they treat the wellbore wall as a no flow boundary, which could lead to an underestimation of fracture pressure [25, p. 1].

A possible solution for this problem can be found by introducing a filter cake permeability coefficient δ [26, p. 913]. If the filter cake is totally sealing the coefficient becomes zero. For a totally permeable filter cake δ becomes unity. The following equations account for the additional stress, which acts on the formation due to fluid seepage through the filter cake.

$$\delta = \frac{(P_w - P_0)}{(P - P_0)}$$

Equation 7: Filter cake permeability coefficient [26, p. 913]

Where P_w is the pore pressure at the wellbore wall, P_0 is the pore pressure in the far field formation and P is the fluid column pressure in the borehole.

$$\sigma_{rp} = 0$$

$$\sigma_{\theta p} = \delta * \frac{\alpha * (1 - 2 * \nu)}{1 - \nu} * (P_w - P_0)$$

$$\sigma_{zp} = \delta * \frac{\alpha * (1 - 2 * \nu)}{1 - \nu} * (P_w - P_0)$$

Equation 8: Additional stresses due to fluid seepage [26, p. 913]

Where σ_{rp} is the additional radial stress, $\sigma_{\vartheta p}$ is the additional hoop stress, σ_{zp} is the additional axial stress, α is the Biot coefficient and ν is the Poisson's ratio.

By combining these two methods the influence of fluid seepage into the formation can be analysed more accurately.

3.2.2 Compressive Wellbore Failure

Compressive wellbore failure happens in the zones of maximum compressive stress around the wellbore. In these zones the compressive stress exceeds the compressive strength and failure occurs. If the rock has no residual strength so called breakouts will occur which fall into the wellbore and are washed away with the fluid flow.

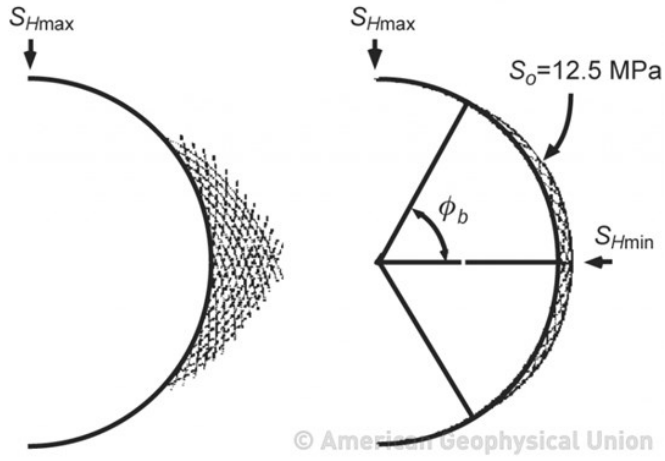

Figure 20: Compressive wellbore failure [27]

3.2.3 Tensile wellbore failure

The second type of failure category is the tensile failure resulting in fractures around the wellbore. In this case the tensile stresses exceed the tensile strength of the rock in the zone of maximum tensile stresses. The fracture direction is controlled by the magnitude and direction of the in-situ stress state. Fractures are going to open up perpendicular to the minimum horizontal stress in direction of the maximum horizontal stress.

3.3 Failure Criteria

Several different wellbore failure criteria exist. There is no universal solution, which can be applied. The two most common ones are introduced in the next section.

3.3.1 Linearized Mohr Coulomb Failure Criterion

This criterion is widely used in different engineering applications. Shear failure takes place across a plane. The normal stress and the shear stress are associated with a functional relation characteristic of the material [28, p. 15].

$$\tau = c + \mu * \sigma_n$$

Equation 9: Mohr-Coulomb failure criterion [28]

Where τ is the shear stress, c is the cohesion, μ is the tangens of the internal angle of friction and σ_n is the normal stress.

The linearized form of the Mohr-Coulomb criterion looks as follows [29]:

$$\sigma_1 = C_0 + q * \sigma_3$$

Equation 10: Linearized Mohr-Coulomb Equation

Where σ_1 is the maximum principal stress, σ_3 is the minimum principal stress, C_0 is the uniaxial compressive strength of the rock and q is calculated as follows:

$$q = \left[\left(\mu_i^2 + 1\right)^{\frac{1}{2}} + \mu_i\right]^2 = tan^2\left(\frac{\pi}{4} + \frac{\varphi}{2}\right)$$

Equation 11: Fitting parameter equation for linearized Mohr Coulomb criterion

$$\varphi = \tan^{-1}(\mu_i)$$

Equation 12: Coefficient of internal friction from angle of internal friction

Based on the equations above it is possible to come up with a failure criterion, which specifies a critical pressure, which would lead to either wellbore breakouts or fracturing. Nevertheless, only the two most common stress states for fracturing and breakout are used for deriving the equation that predicts failure. The two most common cases according to Gholami et. al [28] are:

$$\sigma_\theta > \sigma_z > \sigma_r$$

Equation 13: Most common stress state for wellbore breakout

$$\sigma_r > \sigma_z > \sigma_\theta$$

Equation 14: Most common stress state for inducing fractures

By analysing the Kirsch equations it is obvious that the tangential and axial stress equations reach a maximum value at θ is equal to ±π/2 and a minimum value when θ is equal to 0. As already mentioned breakouts are going to appear at the point of maximum compressive stress, when the tangential stress reaches a maximum. The Kirsch equations can then be simplified further to:

$$\sigma_\theta^{max} = 3 * \sigma_H - \sigma_h - \Delta P$$

$$\sigma_r = \Delta P$$

$$\sigma_z = \sigma_v + 2 * \nu * (\sigma_H - \sigma_h)$$

Equation 15: Simplified Kirsch equations for predicting wellbore breakouts

If we now consider the most common stress state for wellbore breakouts, as mentioned above, and substitute the simplified Kirsch equations into the linearized Mohr Coulomb failure criterion we end up with the following equation.

$$\Delta P = \frac{3 * \sigma_H - \sigma_h - \sigma_C}{1 + q}$$

Equation 16: Pressure difference wellbore and formation to avoid breakouts [28]

Where σ_C is the uniaxial compressive strength.

For predicting the fracture pressure, we follow exactly the same idea as above considering that fractures or tensile failure occurs at the point of minimum tangential stress, the Kirsch equations simplify as follows.

$$\sigma_\theta^{min} = 3 * \sigma_h - \sigma_H - \Delta P$$

$$\sigma_r = \Delta P$$

$$\sigma_z = \sigma_v - 2 * \nu * (\sigma_H - \sigma_h)$$

Equation 17: Simplified Kirsch equations for predicting fracture initiation in a wellbore

By substituting the equations into the linearized Mohr-Coulomb failure criterion the final equation for the allowed pressure difference between wellbore and formation is:

$$\Delta P = \frac{\sigma_C + q * (3 * \sigma_h - \sigma_H)}{1 + q}$$

Equation 18: Pressure difference wellbore and formation to avoid fractures [28]

3.3.2 Hoek-Brown Failure Criterion

The Hoek-Brown criterion uses the uniaxial compressive strength of the intact rock material as a scaling parameter, and it introduces two dimensionless strength parameters *m* and *s* [29]. The maximum principal stress at failure is given as:

$$\sigma_1 = \sigma_3 + \sigma_c * \sqrt{m * \frac{\sigma_3}{\sigma_c} + s}$$

Equation 19: Hoek-Brown failure criterion [29]

Hoek and Brown stated [30] that the parameter *m* depends on the rock type. The parameter *s* is dependent on the fact, whether the rock is intact or not. For a completely intact specimen *s* is equal to 1. In a completely granulated specimen or a rock aggregate *s* is equal to zero [29]. The Hoek-Brown criterion is generally more accepted than the Mohr-Coulomb failure criterion because it fits a non-linear model to the available data [28].

The same approach as before is applied to come up with two equations, which describe the allowable pressure difference between wellbore and formation to avoid fracturing or breakouts.

The following terms are simplified to shorten the final equation.

$$D = 3 * \sigma_H - \sigma_h$$

$$p = m * \sigma_c$$

$$\Delta P = \frac{(4 * D + p) \pm \sqrt{(4 * D + p)^2 + 16 * (\sigma_c^2 - D^2)}}{8}$$

Equation 20: Pressure difference to avoid breakouts according to Hoek-Brown [28]

$$A = 3 * \sigma_h - \sigma_H$$

$$p = m * \sigma_c$$

$$\Delta P = \frac{(4 * A - p) \pm \sqrt{(4 * A - p)^2 - 16 * (A^2 - \sigma_c^2 - p * A)}}{8}$$

Equation 21: Pressure difference to avoid the fractures according to Hoek-Brown [28]

It needs to be mentioned that several other failure criteria exist. Nevertheless, the scope of this section is not about stating already known failure criteria. The focus is more on evaluating the influence of CwD on geomechanical properties such as stresses and pressure especially in the near wellbore region. To make this point it is sufficient to use two different failure criteria and describe the impact of CwD based on them.

3.4 The Influence of CwD on Wellbore Geomechanics

One of the main advantages of CwD is that the exposure of the formation to the drilling fluid is much shorter than in regular drilling operations. It is reported that formation strength around the wellbore changes with time [31, p. 1]. Furthermore, also physico-chemical interactions between formation and fluid take place.

Regarding mechanical properties fluid invasion leads to an increase of the near wellbore pressure [31, p. 1]. But we should not forget that as reported earlier [26], also the stress state changes and fluid invasion can also create additional stresses in the near wellbore region.

Another mechanism that should not be underestimated is the frequent contact of the casing joints with the wellbore wall. This contact is of course intended, but it is also necessary to understand the possible influence on the geomechanical properties of the near wellbore region.

3.4.1 Time dependent pore pressure change

Pore pressure in the near wellbore region changes with time. This phenomenon has been addresses in different studies so far [31]. Depending on the permeability of the filter cake and the formation, this fluid invasion can be very low, but it still has an impact. Mokhtari, Tutuncu and Teklu [31] performed numerical simulations based on the following formula.

$$\frac{dp}{dt} = \frac{k}{\mu_f * \beta * \Phi} * [\frac{d^2P}{dr^2} + \frac{1}{r} * \frac{dp}{dr}]$$

Equation 22: Pore pressure changes with time [31]

Where μ_f is the fluid viscosity, k is the permeability, β is the Biot-coefficient, r is the distance from the centre of the wellbore and Φ is the porosity.

The first thing that can be recognized from this differential equation is that the permeability is a very influential parameter. Considering that it would be possible to create a zero-permeability zone around the wellbore immediately while drilling the overall pore pressure could not change with time, but this is far from reality. Nevertheless, if we follow the most common theory that CwD creates an impermeable layer at the wellbore wall the change in pore pressure with time could be greatly reduced. This could have a positive effect on the stability of the borehole regarding breakouts which is shown in the simulations of Mokhtari, Tutuncu and Teklu [31].

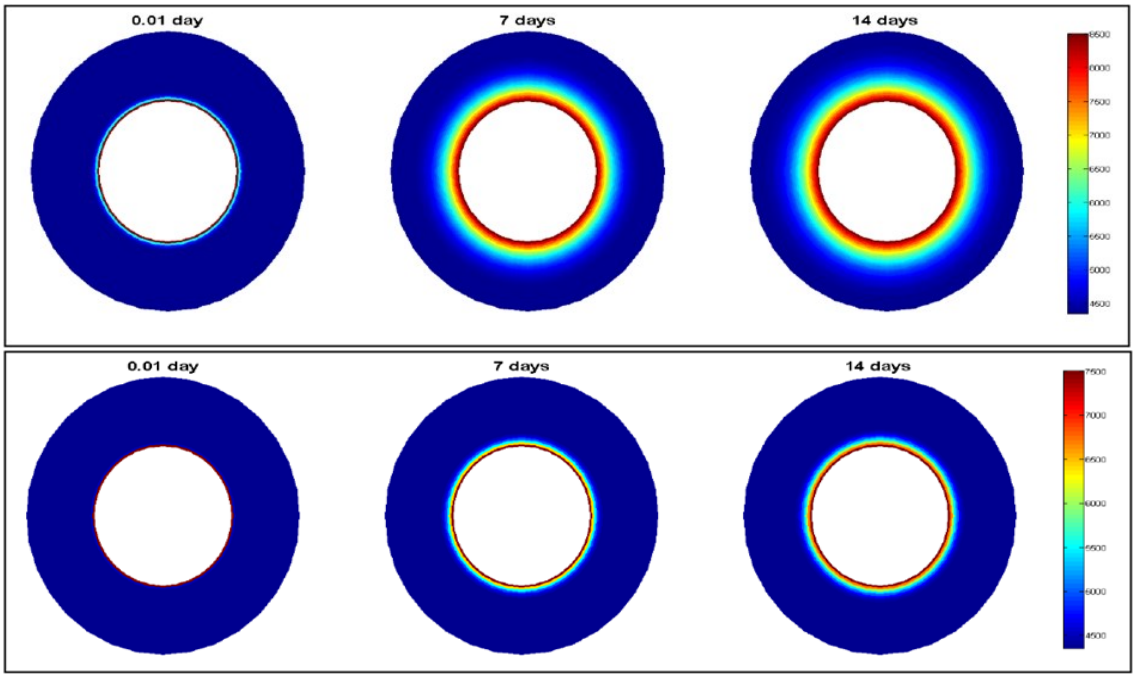

Figure 21: Figure 16: Pressure Distribution in a wellbore with and without a filter cake created by CwD [31]

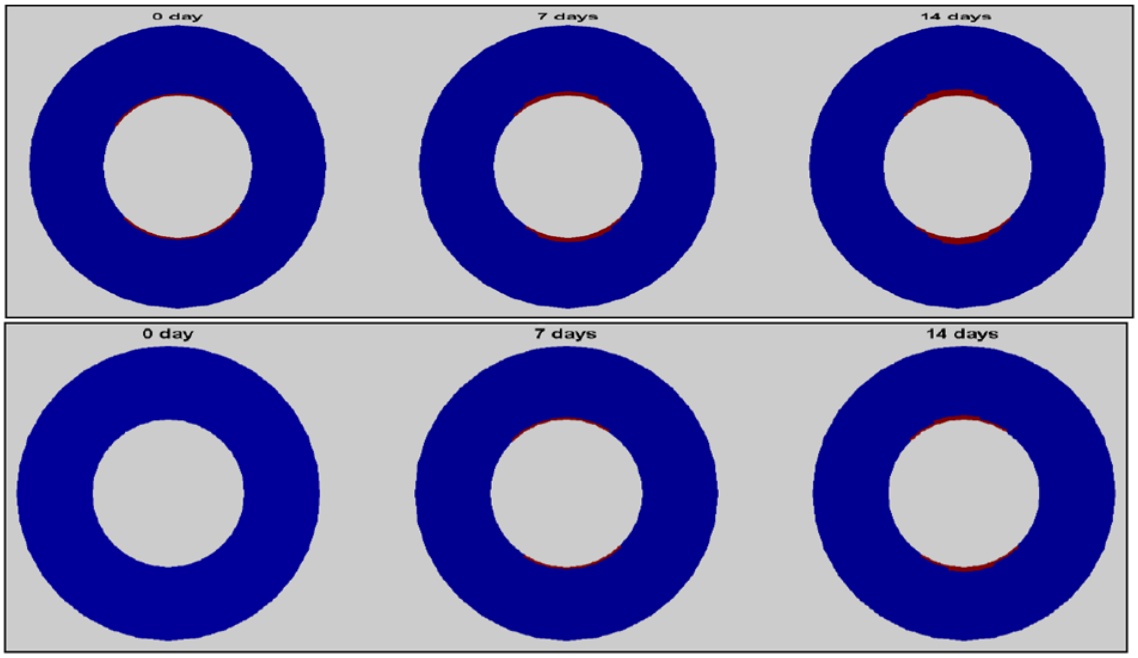

Figure 22: Breakout extent for a wellbore with and without filter cake created by CwD [31]

The breakout extent, which can be seen in red in the figure above is bigger for the situation without a sufficient filter cake created by CwD. This is related to the higher fluid invasion into the formation as can be seen in Figure 21 where the pressure perturbation reaches deeper into the formation.

3.4.2 Stresses during CwD

Pressure is only one aspect when considering the impact of CwD. The most interesting stress is the hoop stress when it comes to wellbore instabilities. This is simply because breakouts and fractures are either related to a maximum or a minimum in hoop stress along the wellbore wall. Both contact forces, as well as the annulus hole size ratio can influence the hoop stress during CwD [32].

Kiran and Salehi [32] have conducted finite element analysis to address this problem and to quantify the effect of the contact forces and the annulus hole size ratio in CwD. The finite element analysis was based on a mathematical model which incorporates the following parameters. Young's modulus E, moment of inertia of the drill system I, radial clearance of casing with borehole r, Cartesian co-ordinate of position of the casing in the vertical direction z, angular displacement of casing ϑ, pitch p, weight of drill system per unit length w, angular velocity of drill system Ω, and outer radius of casing R_o. The contact force λ is calculated based on the equations below and the results are discussed in the following section.

$$\lambda = \frac{-E * I * r * (\theta')^4 + T * r * (\theta')^3 + F * r * (\theta')^2 - \mu * w * \Omega^2 * R_o * sin^2(\theta)}{cos^2(\theta) + \mu * sin^2(\theta)} + w * \Omega^2 * R_o$$

$$F = \frac{8 * \pi^2 * E * I}{p^2} - \frac{3 * \pi * T}{p}$$

$$I = \frac{\pi * (d_o^4 - d_i^4)}{64}$$

$$\theta = \frac{2 * \pi * z}{p}$$

Equation 23: Mathematical model for the FEM analysis [32]

3.4.2.1 Change in Hoop Stress with Varying RPM of Casing

Considering the direct proportionality between the angular velocity of the drill system and the contact force, it is obvious that an increase in rpm leads to an increase in the contact force. The examples below confirm this depending on the horizontal far field stress direction.

Contact force is applied in maximum horizontal far field stress direction

The contact force is applied in the direction of the maximum horizontal stress. This is the direction in which fractures while propagate when they open up. A fracture opens due to tensile failure at a position of minimum hoop stress. From the results of their studies it can be seen that a higher RPM leads to an increase in hoop stress, but only within an angle of 20° from the contact point. Going from 20° up to 90° from the contact point, which would represent the direction of minimum horizontal stress, the influence of increasing RPM is not significant.

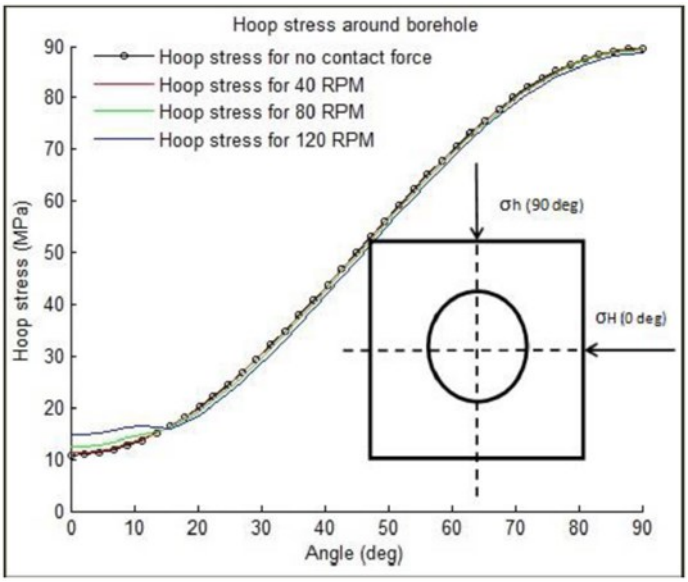

Figure 23: Hoop Stress around borehole when contact force is applied in maximum horizontal far field stress direction

Contact force is applied in minimum horizontal far field stress direction

In this case no improvements in wellbore stability can be achieved due to obvious reasons. The hoop stress is already a maximum at this point. Increasing the hoop stress further at this point would negatively influence the wellbore stability. Wellbore breakouts are much more likely to happen. This already proofs that applying CwD needs to be considered with care because the situation in the wellbore is not as easy controllable than in a simulation.

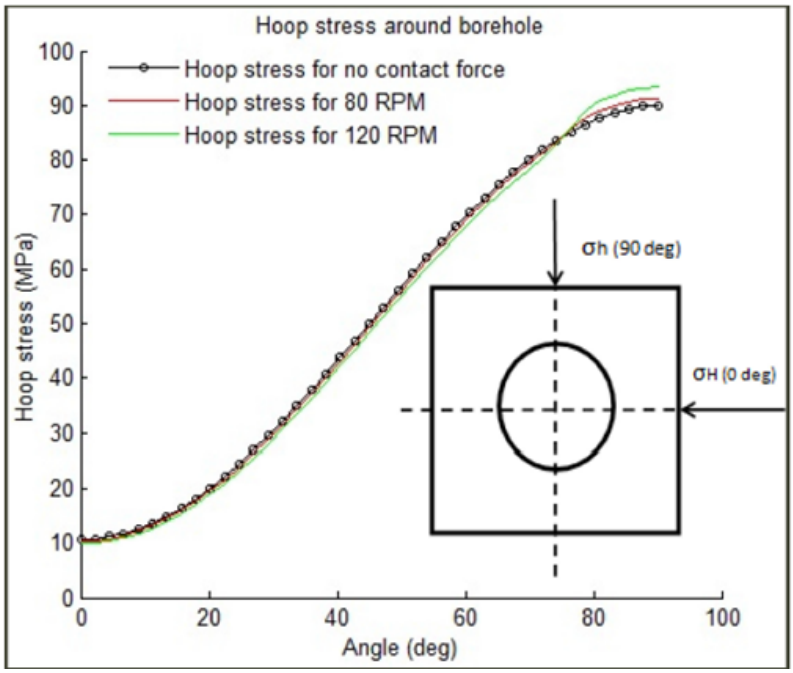

Figure 24: Hoop Stress around borehole when contact force is applied in minimum horizontal far field stress direction

3.4.2.2 Change in Hoop Stress with Variation in Annulus to Hole Ratio

One of the main influence parameters in CwD is the annulus to hole size (A/H) ratio, which is recommended to be in the range of 0.6-0.8 [15].

Contact force is applied in maximum horizontal far field stress direction

The influence of the annulus to hole size ratio on the hoop stress seems negligible. With an increasing A/H ratio from 0.62 to 0.78 the difference in hoop stress is around 1 MPa.

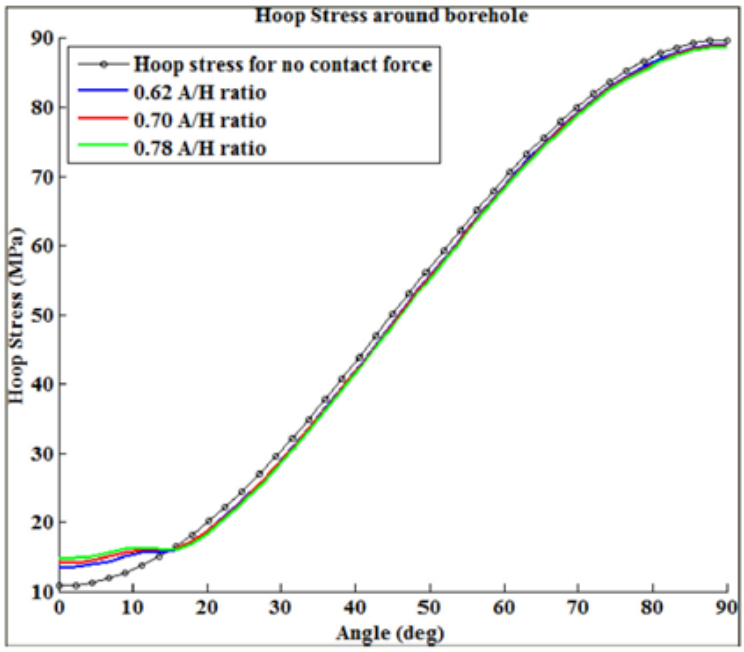

Figure 25: Hoop stress around the borehole with changing annulus to hole size ratio when contact force is applied in maximum far field stress direction

Contact force is applied in minimum horizontal far field stress direction

The same effect can be observed here. In general, there is no significant change of the hoop stress with increasing A/H ratio. Nevertheless, it is still not favourable to have an increase in hoop stress in this stress direction because it contributes to the creation of breakouts.

3.5 Geomechanical Conclusions

Overall, the geomechanical aspects can be concluded as follows. It is obvious when considering wellbore geomechanics that CwD has a positive effect on the wellbore stability. On the one hand this is due to the creation of a filter cake with very low permeability, which hinders fluids to invade the formation. This prevents time dependent pore pressure changes, which in worst case could lead to significant breakouts.

Furthermore, the frequent contact of the casing with the wellbore wall can influence the stability positively because it increases the hoop stress. But this statement needs to be treated with care because this depends also on the direction of the far field stress components. The contact in direction of the maximum far field stress is good because it increases the hoop stress at a point of minimum hoop stress, which could otherwise lead to the creation of a fracture.

On the other hand, if the contact takes place at a point of already maximum hoop stress this could lead to higher instabilities than before. This is due to the reason that breakouts occur in zones of maximum hoop stress. If the hoop stress is further increased by casing contact force the creation of breakouts can be accelerated.

Additionally, it needs to be considered that in situations where fractures are already present there is another theory about the positive influence of CwD. It is recorded that CwD can increase the Fracture Propagation Pressure [1]. This could happen due to tip screen out and is another possible theory about the effectiveness of the smearing effect.

Finally, it can be said that the theories mentioned in this chapter need to be proved by experiments. The wellbore face sealing could be tested by applying pressure on a sample with a predefined filter cake with a certain permeability and observe the seepage of fluid into the sample. The simulations regarding the hoop stress could be tested by using a sample in a load cell and test the influence of contact forces at different stress directions. And finally, to test the theory of the increase in Fracture Propagation Pressure an artificial fracture could be created in a sample. Afterwards CwD experiments are carried out to see if the tip screen-out happens or the fracture is propped due to wellbore face sealing. This can then be tested by fracturing the sample again.

Chapter 4 Existing Laboratory Technologies

The next section describes different technologies that were used to simulate dynamic and static filter cake build-up.

4.1 Static Experiments

4.1.1 Static filter cake filtration cell

The sketch below shows the arrangement of the apparatus for the experiments conducted by Williams and Cannon in 1938 [33, p. 23]. As can be seen this publication is around 80 years old, but features an interesting idea how to conduct filter cake experiments with cores.

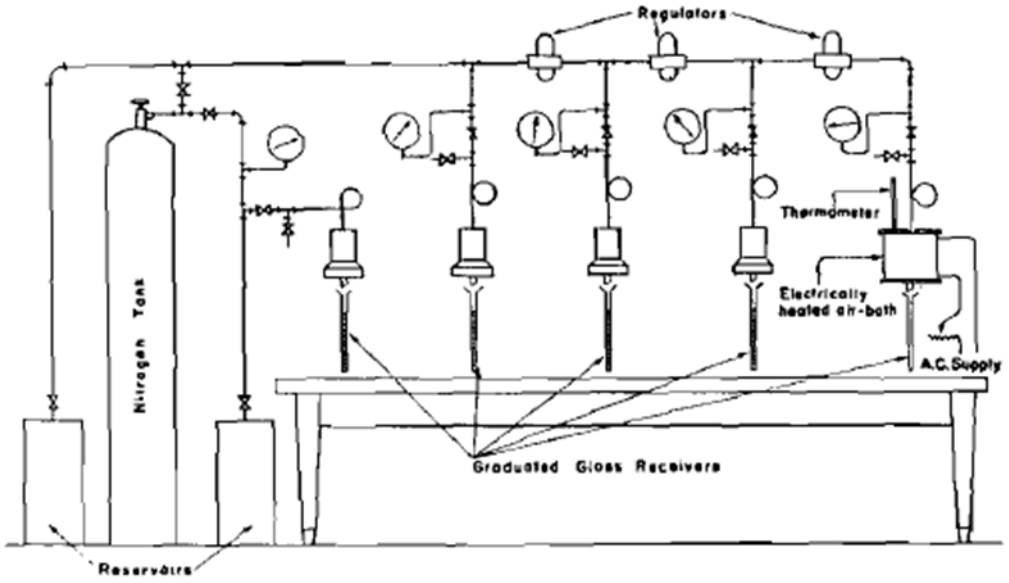

Figure 26: Diagrammatic representation of the filter cells arrangement [33, p. 23]

In one run five filter cells can be used. Each filter cell can be used with a different pressure. Furthermore, there is the opportunity to regulate the temperature via an electrically heated air bath. This allows the user to test up to five different situations during one run. It is also possible to use different cores in one run. Still this system lacks in terms of creating a dynamic environment during the test but using a number of cores in series could be an interesting idea for further experiments.

4.1.2 Hassler Cell

In general, a Hassler Cell is not a tool that is used in filter cake investigations. The main purpose of a Hassler Cell is to evaluate the permeability of cores. Nevertheless, it can also be used to investigate the depth of invasion for a certain drilling fluid into the core. Afterwards the core can be cut in half to investigate the invaded volume of core in detail [9]. Especially, to see how effective bridging particles are working. A combination between a tool that could investigate the filter cake build-up, invasion into the core and simultaneously measures permeability is a possible scenario where the principle of a Hassler Cell could be applied in a new experiment.

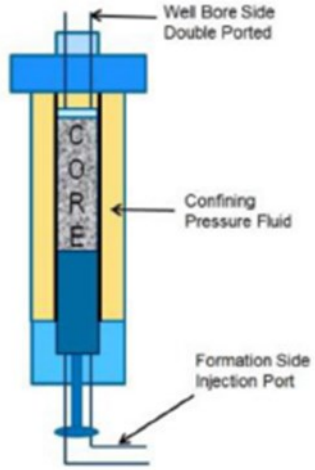

Figure 27: Hassler cell schematic [9, p. 2]

4.2 Dynamic Experiments

4.2.1 High Pressure and Temperature filtration cell by Oilfield Instruments Inc.

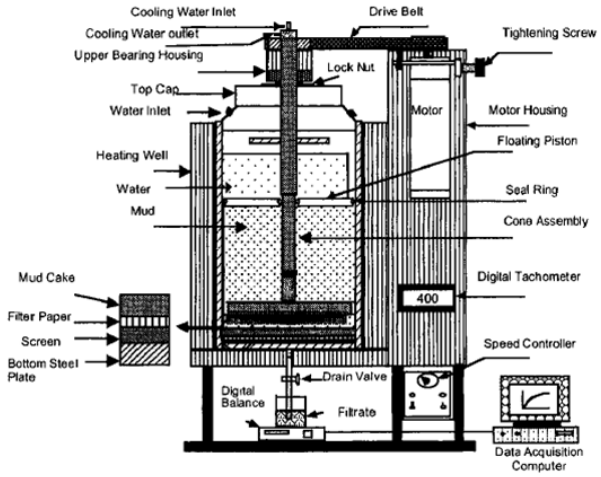

Figure 28: Oilfield Instruments Filtration Cell [2, p. 238]

The filter medium is at the bottom and can be a core or a core in combination with a filter paper. Nevertheless, experiments have shown that filter-paper only is the best choice because otherwise the cores are immediately plugged by the filter cake. Above the filter medium is the mud that is going to be tested. This is separated by a floating piston from a water chamber, which is connected to an external pump that controls the pressure. Above the filter paper is a rotatable cone that creates mud shear rates up to 600 revolutions per second.

4.2.2 Multi-Core Dynamic Fluid Loss Equipment

In this case four cores are tested in parallel in one cell. This means the same pressure is applied to all the cores but different cores can be used. The filtrate is collected individually. A rotating cylinder in the middle of the filtration cell provides constant shear rates onto the core face. After the test the cores can be investigated individually. Another interesting feature of this technology is the possibility to test the return permeability of the different cores after fluid invasion.

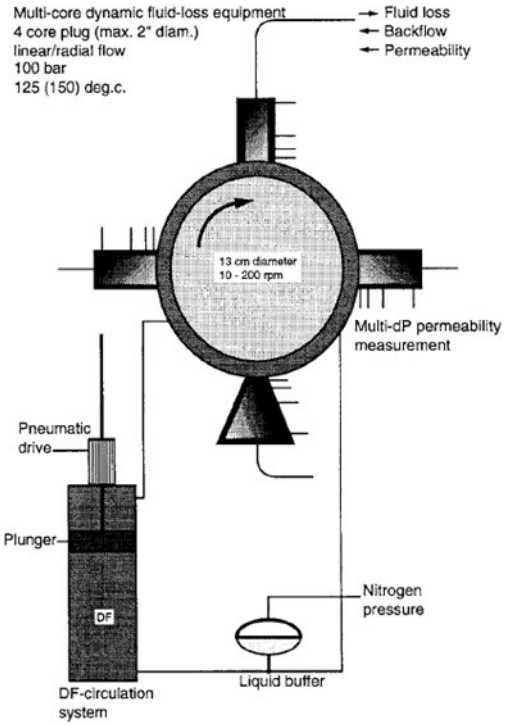

Figure 29: Multi-Core Dynamic Fluid Loss Equipment [34, p. 8]

4.2.3 Dynamic Filtration Apparatus

The arrangement of the experiment by Bezemer and Havenaar [35, p. 293] uses a totally different approach. In this case the outer cylinder of the apparatus is rotating and the inner one is covered in filter paper. The filtrate is collected behind the filter paper. The outer cylinder rotates and a certain shear rate can be applied onto the filter cake. By using small blades mounted on the inner cylinder local high concentrations of clay can be prevented.

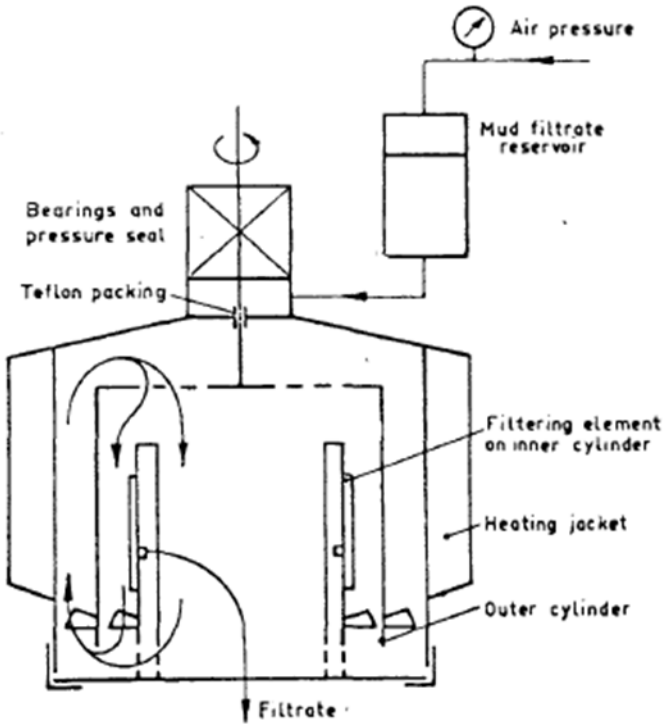

Figure 30: Schematic of the Dynamic Filtration Apparatus [35, p. 293]

4.2.4 Lubricity, Filtration, Drilling Simulator - M2200

This apparatus features a temperature and pressure controlled work environment to simulate downhole conditions. The filter medium is available in different porosities and permeabilities. A shear bob can simulate the rotation of the drill string concentric or off-centre. This produces a certain shear rate on the filter cake. In an optional version, there is even a mud circulation system applied but only for lower pressures and temperatures. The main advantage of this apparatus is that it can rotate a shear bob off-centre, which is exactly what happens during CwD. Nevertheless, it is important to find out if the rotation is simply off-centre or if it performs a similar motion as during CwD. This would mean regular contact with the filter medium during rotation. If so, this would be the only apparatus which could simulate CwD conditions realistically so far.

Figure 31: M2200-Grace Instruments HPHT-Filtration Cell [36]

4.2.5 Dynamic Filtration Unit, US-Patent: 4,790,933

The following figure displays the schematic of a dynamic filtration unit which was invented in 1988.

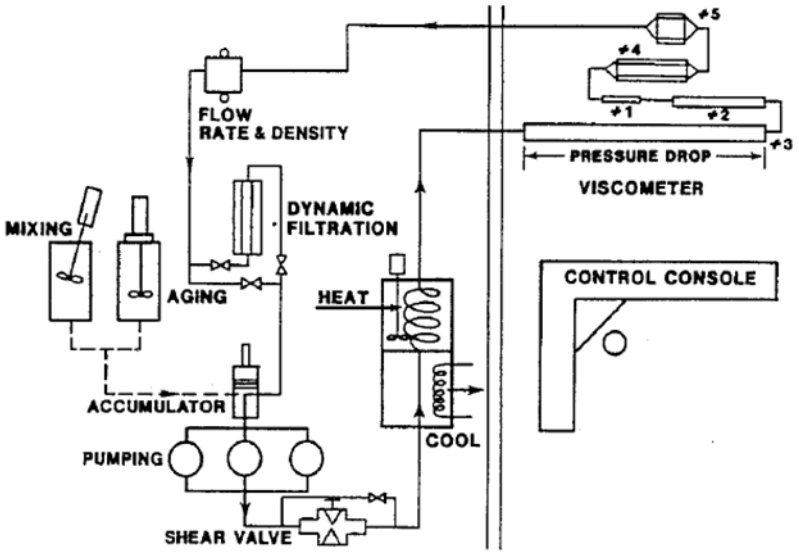

Figure 32: Dynamic Filtration Unit [37, p. 1]

The mud is mixed and transferred to the accumulator where the pressure is kept higher than the vapor pressure. Through a heat exchanger the fluid moves to the viscometer. After the viscometer, the density is measured via a mass flowmeter. Then the fluid enters the dynamic filtration apparatus where the build-up process of the filter cake is investigated. In general, the diagram shows a series of different experiments and seems to be quite simple, but there is an interesting idea behind this patent. Normally filter cake build up is a single parameter which is investigated. In this case the build-up of the filter cake is investigated in parallel with the viscosity and the density of the fluid. Due to that the alteration of the fluid during the build-up process can be observed. This aspect of filter cake build-up is rarely investigated, but it is also not a necessity because during a drilling operation old fluid is continuously replaced by new one.

4.2.6 Dynamic HPHT® Filtration System by Fann

This system uses a shear shaft to create a dynamic environment. An accurate temperature control is possible via a heating jacket. Several different filter cores are available. These specially designed cores come in a variety of porosities and permeabilities. Up to fifty millilitres of filtrate can be collected. This apparatus is more or less a good opportunity if dynamic filtration behaviour should be observed but it is not useful in terms of CwD investigation. This is simply due to the fact that the apparatus cannot be modified in any way as it is delivered as a complete unit.

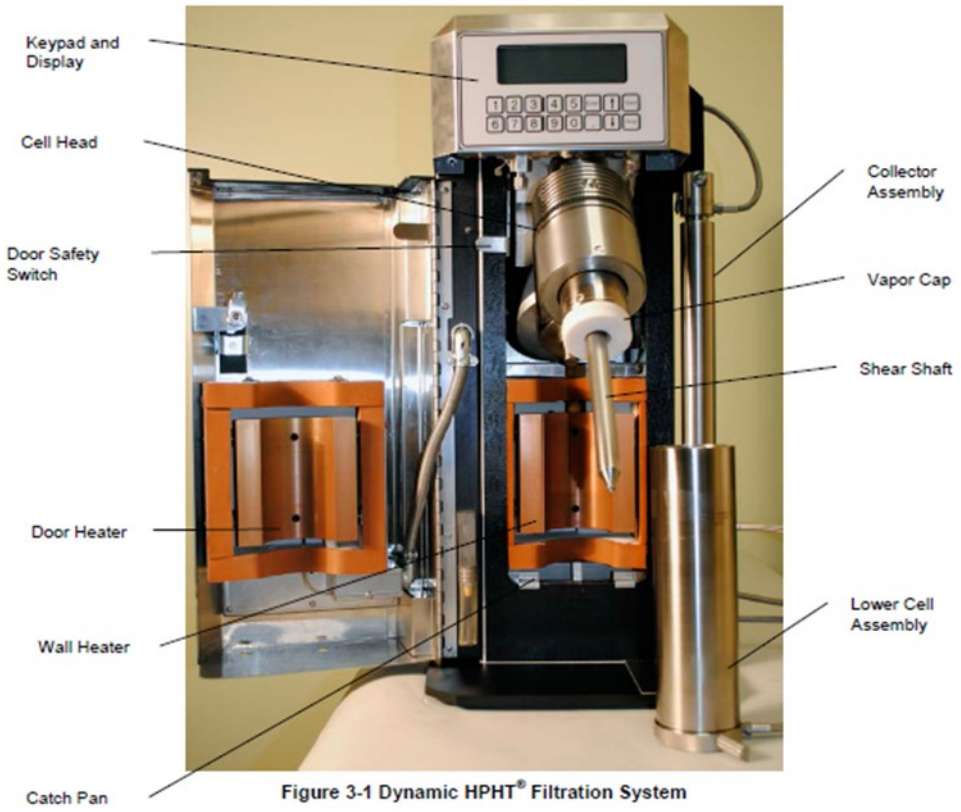

Figure 33: Dynamic HPHT® Filtration System [38]

4.2.7 Lubricity Evaluation Monitor

The device described in the title is mainly used for determining the coefficient of friction between a rotating steel bob, simulating the drill string and a side-loaded wellbore sample, while immersed in a certain drilling fluid [39]. The main idea for this apparatus is a good starting point for a new design proposal. The problem with this apparatus is that it does not focus on the filtration process at all. There are systems out there, which can also simulate the build-up of a filter cake [40]. Nevertheless, the only information about the product is the promise on the website of the vendor that they can do that. There is no further information available about their products unless you want to buy it.

Chapter 5 Experimental Setup

This chapter represents the main part of the thesis and describes the process of developing the final proposed design for an experimental setup. It starts defining the types of experiments which should be carried out with this unit. Furthermore, the most important and critical issues in such an experiment are analysed, based on the idea how a manual for this apparatus would look like. Finally, these issues are tackled with different solutions, which are also described in this chapter. In the end the final design is presented to the reader.

5.1 Type of Experiments

The final design should feature a single unit which can be implemented into a flow loop. The basic version of the design will allow three different experiments to be carried out on a single unit.

- Static filtration test
- Dynamic filtration test
  - With drill pipe in the hole
  - Without drill pipe in the hole
- Pipe Impact Test
  - Regular drill pipe
  - Casing while drilling

5.2 General Considerations

All the experiments can be conducted under a certain confining pressure. This requires a new design of a core holder. One side of the core is exposed to the drilling fluid. The other side of the core can be considered as undamaged by the drilling fluid.

The situation in the wellbore should be reproduced as accurately as possible. That means that the flow of mud should be aligned with the drill pipe. What is meant by that can be seen in the following figure.

Figure 34: Correct position of pipe in the artificial wellbore

The left part of the figure shows the correct position of the pipe in a real drilling situation. The pipe axis is aligned with the flow direction. On the right side of the figure the pipe axis is perpendicular to the flow direction. This does not represent a situation which is encountered in a wellbore.

Furthermore, the setup should feature the possibility to vary pressure and temperature. For the temperature this would require a heat exchanger, which heats the drilling mud for the entire loop. The pressure can be regulated by using regulation valves. Further details are going to be discussed in the different sections of this chapter.

Another important aspect in such an experimental design is the method of measuring the parameters of interest. Besides operational parameters such as pressure, temperature, flow rate it is necessary to measure parameters before and after the test such as permeability of the core sample, filter cake thickness, invasion depth, residual saturation and also the return permeability. How to measure all the different parameters will also be discussed in a separate section of this chapter.

Another important aspect is the applicability for a variety of drilling fluids. As drilling fluids in combination with cuttings can be highly erosive it is critical to choose a material that can deal with a variety of different situations.

5.3 Measurement

This chapter describes the results which should be obtained from the experiment. Furthermore, measurement mechanisms for the parameters are proposed and the value of information from each parameter is discussed. The proposed measurement mechanisms are then incorporated in the design. Not all parameters can be measured during the experiment. Therefore, different tests which are performed on the filter cake and the core, after the experiment, are discussed as well. This should not be mistaken with operational parameters such as temperature and pressure. How those parameters are measured is discussed in the actual design chapter.

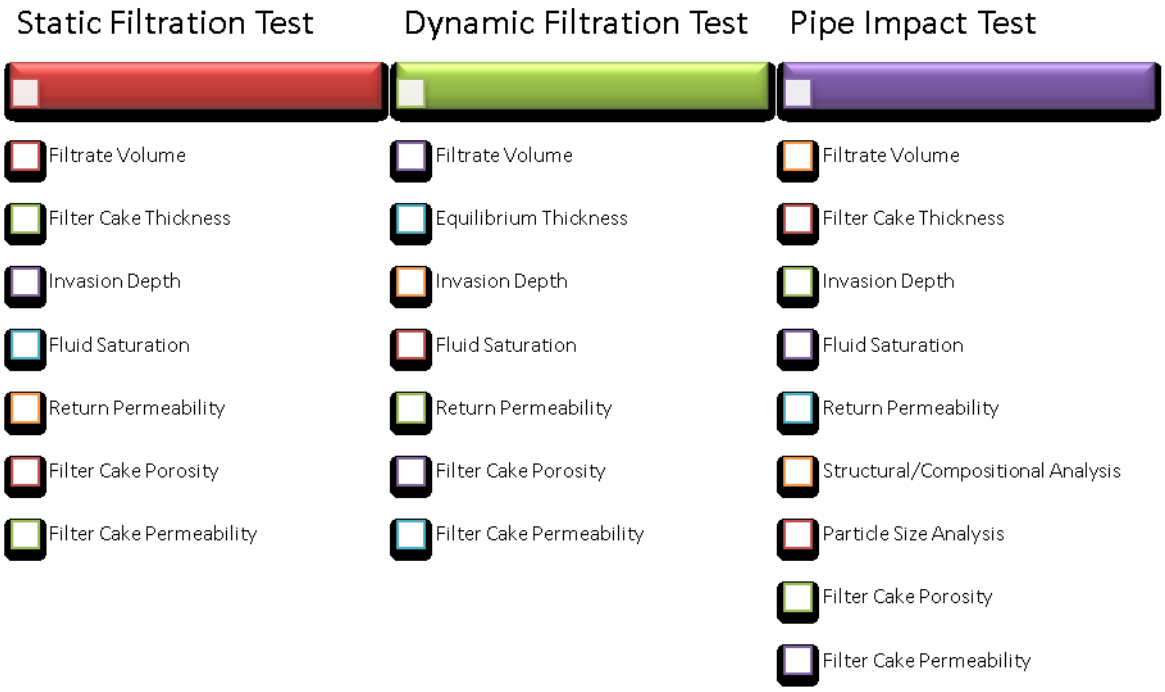

Figure 35: Parameters to be measured, recorded or analysed during the different tests

5.3.1 Filter Cake Porosity and Permeability

Both parameters are already described in the Literature Review Chapter. Porosity can be measured by using the CT-Scan Technique which uses the CT-Number as described in Equation 3. Another useful technique is to calculate the porosity by using the dry and wet weight of the filter cake, the density of the used fluid and an assumption for the grain density.

$$V_g = \frac{Net\ dry\ weight\ of\ the\ cake}{\rho_g}$$

Equation 24: Grain volume of the filter cake

$$V_p = \frac{(Net\ wet\ weight - Net\ dry\ weight)}{\rho_f}$$

Equation 25: Pore volume of the filter cake [6, p. 3]

$$\Phi_C = \frac{V_p}{V_p + V_g}$$

Equation 26: Filter cake porosity from wet and dry filter cake weight measurements [6]

Where ρ_g is the grain density and ρ_f is the fluid density.

This technique is not very accurate because an assumption of the grain density based on the used material is necessary. There is no absolute proof that the grain density is exactly the value of the used solids in the drilling fluid because several different materials could be deposited depending on the composition of the drilling fluid. Nevertheless, it is an easy method and can be used without the need of a CT-scanner.

Regarding permeability most of the techniques used rely on empirical correlations as described in Equation 4. Nevertheless, it is possible to use an equation which uses the continuously measured filtrate volume, the time and the filter cake volume to come up with a value of permeability. The advantage of this method is that the permeability of the filter cake is continuously measured during the test. The disadvantage is that this method was developed for static filtration methods and needs to be verified for dynamic experiments.

$$K = Q_w * Q_C * \frac{\mu}{2 * t * p * A^2}$$

Equation 27: Filter cake permeability calculated continuously [6, p. 5]

Where Q_W is the filtrate volume in cm^3, Q_C is the volume of the filter cake in cm^3, μ is the viscosity of the filtrate in cp, t is the time in seconds, p is the differential pressure in atm and A is the filter cake area in cm^2.

5.3.2 Filtrate Volume

One of the main parameters in filtration tests is the question how much fluid is lost into the formation. This is measured by collecting the amount of filtrate which, passes the filtration surface in a static or dynamic filtration test. For dynamic filtration tests no standardized testing procedures exist. As basis for the collection of filtrate the API-Standard API Recommended Practice 13B-1 is used.

The collected filtrate volume is a very important parameter because it gives information about how fast a certain formation can be sealed by the build-up of a filter cake. This is necessary to know because the invasion of drilling mud into the formation is one of the main damage mechanisms and it is especially important in the reservoir region.

According to API RP 13B-1 the filter press should have a filtration area of 45.2 cm^2 up to 46.4 cm^2. The test is carried out at 100 ± 5 psi and the filtrate is collected over a period of 30 minutes. The filtrate is collected in a graded cylinder.

The filtrate volume is proportional to the square root of the time period used [41, p. 46]

$$V_f = \sqrt{2 * k * \Delta p * (\frac{f_{sc}}{f_{sm}} - 1)} * A * \frac{\sqrt{t}}{\sqrt{\mu}}$$

Equation 28: Filtrate Volume in a static filter press [41, p. 46]

Where k is the permeability of the filter cake, Δp is the pressure differential, f_{sc} is the volume fraction of solids in the filter cake, f_{sm} is the volume fraction of solids in the mud, A is the filter area, t is the time and μ is the filtrate viscosity.

In case that the filtrate volume exceeds the volume of the filtrate receiver during a period of 30 minutes, the API water loss is reported as twice the volume of filtrate after 7.5 minutes. In case that a spurt loss is observed the filtrate volume after 30 minutes is calculated as follows.

$$V_{30} = 2 * \left(V_{7.5} - V_{sp}\right) + V_{sp}$$

Equation 29: API fluid loss after 30 minutes if spurt loss is observed [41, p. 46]

Where V_{sp} is the spurt loss and $V_{7.5}$ is the filtrate volume after 7.5 minutes.

The same theory is applied when the tests are carried out at elevated pressure and temperature. The only difference is a filter cake area which is half the size of the original test [42]. Furthermore, a backpressure receiver is used to collect the filtrate.

Anyway, this is not comparable to a dynamic situation where the shear force acting on the formation stops the build-up of the filter cake. Therefore, the filter cake does not grow anymore and the equilibrium thickness is reached. From that point on the filtrate loss into the formation increases constantly. The difference in both methods can be seen in the following figure.

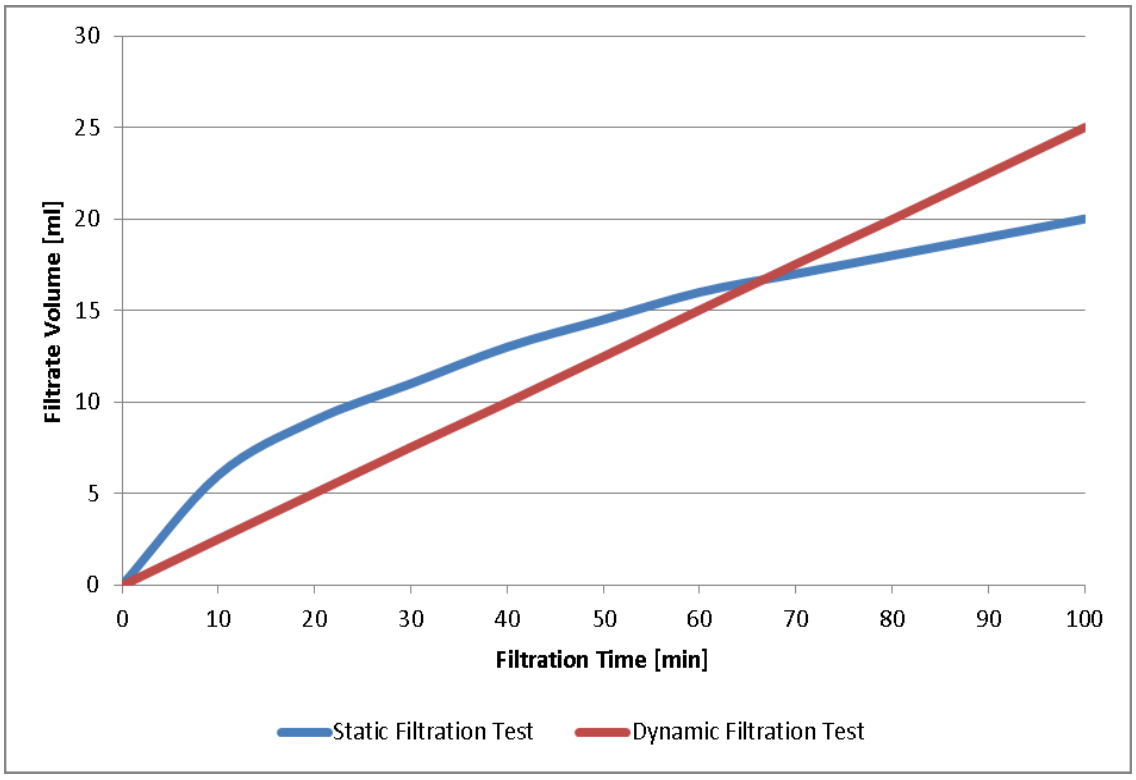

Figure 36: Comparison of filtration behaviour between static and dynamic filtration test

In case of the new experimental design the filtrate volume should be measured according to the proposed method in the recommended practice by the American Petroleum Institute. This means that after starting the experiment the filtrate volume is constantly recorded over a certain period of time by using a graded cylinder for example. If the test is carried out at elevated pressure or temperature a backpressure receiver needs to be used.

5.3.3 Filter Cake Thickness-Equilibrium Thickness

The filter cake thickness is reported after the test is finished. In case of a dynamic test it is necessary to take the shear forces into account. This leads to a certain erosion of the filter cake and an equilibrium thickness is reached. So far there is no standard method in place to record and report the filter cake thickness in case of a dynamic test. Another important issue is that in case of a pipe-impact test local varieties in the filter cake thickness are very likely to be observed. Therefore, reporting an overall value for the thickness would not be valid.

The filter cake thickness is not measured continuously during the test but from the volume of filtrate the height of the filter cake at different time steps can be concluded via the following equation. This relationship has to be treated with care because it is only valid for static filtration tests in a special environment.

$$h_{mc} = \frac{V_f}{A * (\frac{f_{sc}}{f_{sm}} - 1)}$$

Equation 30: Filter cake thickness as a function of collected filtrate volume [41, p. 46]

Having information about the filter cake thickness from a certain test is vital if a drilling mud is applied in real drilling situations. Not only because thick mud cakes could lead to drilling related problems such as differential sticking but also production issues are associated with the thickness of the filter cake [43]. With increasing thickness of the filter cake, the cake-pipe contact area increases and this leads to an increase of magnitude of the sticking force [43].

This and many more drilling related issues lead to the necessity of having an accurate measurement of the filter cake thickness. Four different methods for the measurement of filter cake thickness are discussed in this chapter.

5.3.3.1 Measuring Filter Cake Thickness

Single Value Measurement

The filter cake thickness, independent, of the test (static, dynamic, and pipe-impact) is measured and a single value is reported. This is simply done by using a ruler. The tip of the ruler is immersed in the filter cake and the final value can be concluded from the covered part of the tip or read directly. Another way to measure the filter cake thickness is by putting the ruler beside the filter cake without immersing the tip of the ruler in the filter cake.

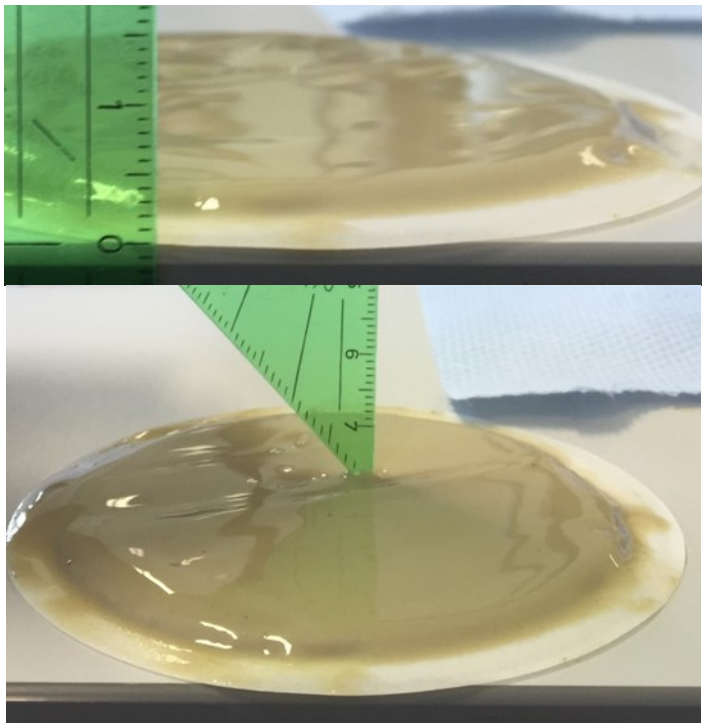

Figure 37: Methods to measure filter cake thickness with a ruler

The proposed methods are not recommended for an accurate measurement of the filter cake thickness. One of the biggest problems is that the measurement is only a single value and gives no accurate information about local varieties in the filter cake thickness. Furthermore, if the tip of the ruler is immersed in the filter cake, the structure of the cake is damaged.

Multiple Value Measurement

The idea of using a multiple value measurement is especially important in case that a pipe-impact test is carried out. The contact of the pipe with the filter cake will lead to local varieties in the filter cake thickness. A proposed scheme for measuring the filter cake thickness can be seen below. The measurement is still carried out by using a ruler or any other device that allows an accurate measurement on a millimetre scale.

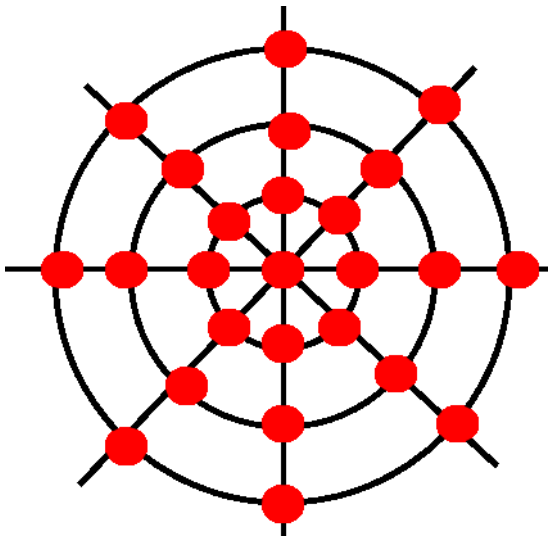

Figure 38: Proposed scheme for multiple point filter cake thickness measurement

The overall information value is much higher compared to a single value measurement. The damage done to the filter cake is much higher because the filter cake is penetrated at several points with the ruler. This could be an issue if further analysis steps regarding the filter cake surface are carried out.

Dial Gauge Method

For this method a precision dial gauge thickness meter is used. Several different options exist. In case of a filter cake a very precise measurement device is required to keep the error as small as possible. The device in the figure below uses a disc which is firmly placed onto the filter cake surface. The thickness of the filter cake can be read directly from the display. The measuring range is ±10 mm with a resolution of 0.001 mm [43, p. 3]. The measurement is done according to a spot pattern and the average value is reported.

The biggest problem with such a device is that it requires direct contact with the filter cake with the potential to damage the surface. This is especially critical if further analysis of the filter cake surface should be carried out.

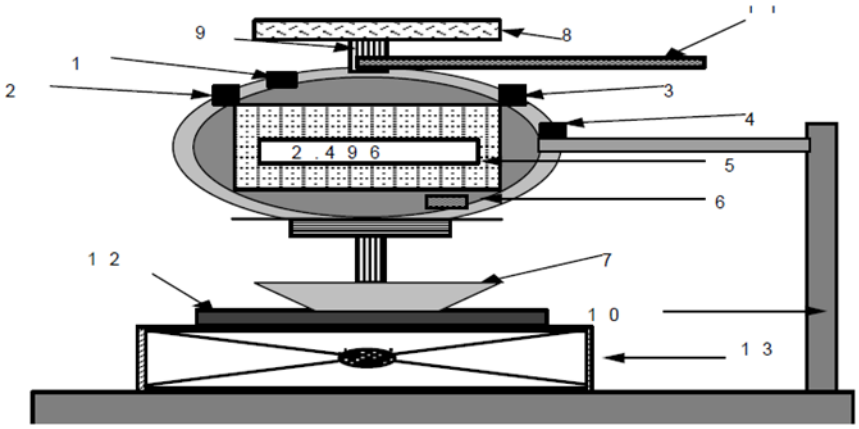

1 - Power Supply 2 - On/Off Switch 3 - Inch/mm Changeover Switch 4 – Direction Changeover Switch
5 - Digital Display 6- Reset Button 7- Disc 8 - Load Platform 9 - Transducer Stem 10 – Stand
11- Lifting Lever 12 - Mud Cake 13 - Lab Jack

Figure 39: Schematic of a precision dial gauge [43, p. 9]

Non-Destructive Method of Cake Thickness Measurement

This method was developed by Amanullah and Tan and published in the year 2000 [43]. They apply a laser methodology to the sample to come up with reliable and accurate results about the filter cake thickness. The used light source is a semi-conductor laser with a wavelength of 670 nm and an output of 1.2 mW maximum [43, p. 2]. It is important to create a spot diameter of maximum 1mm. This guarantees a higher resolution and several measurements at different locations can be taken. For this method a seventeen spot measurement layout is proposed to get a reliable average of the cake thickness.

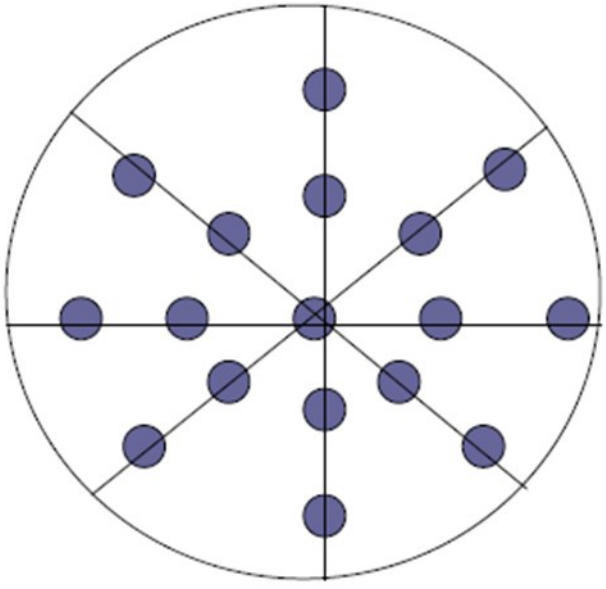

Figure 40: Measurement spot layout [43]

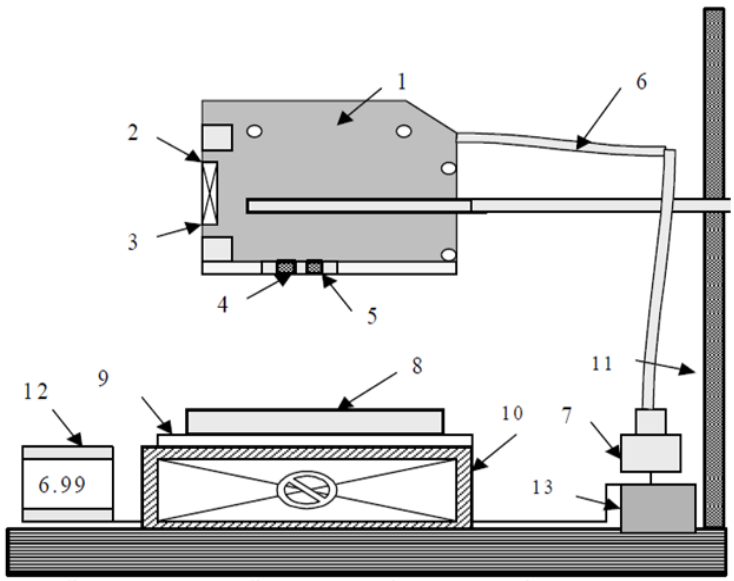

1- Laser Head 2- Far Indicator 3- Near Indicator 4- Emitter 5 - Receiver 6 - Connector 7 - Signal Conditioner
8 - Mudcake 9 - Filter Paper 10 - Lab Jack 11- Stand 1 2 - Multi-meter 13 - Power Supply

Figure 41: Schematic figure of the laser thickness apparatus [43]

Regarding the applicability of such a measurement method it would be interesting if a device could be developed that allows continuous measurement during the filter cake build-up. But for now it is definitely the best method as the author reports the standard deviation with less than 0.025 mm and the coefficient of variation with less than 1 percent.

5.3.4 Invasion Depth

The invasion depth describes how far the drilling fluid has spread into the formation over a certain period of time. This is especially important in those regions where reservoir formations are encountered. If the invasion of drilling fluid into the formation is severe, production related problems can be encountered afterwards.

Quantifying the invasion depth can be done continuously during the experiment or directly after the experiment. The difference between the two methods is going to be discussed in this chapter.

5.3.4.1 Continuous Invasion Depth Measurement

The main advantage of measuring the invasion depth during the experiment is that the build-up of the filter cake can be directly related to the invasion of the core sample. If the build-up of the filter cake is effective the invasion depth should be minimal.

The main idea behind this measurement is the application of Darcy's Law. A reduced permeability due to solids invasion into the core sample leads to a higher pressure drop over a certain length of the core. The normal pressure profile without solids invasion can be compared with the pressure profile measured during the test. From the difference in pressure profiles a conclusion about the invasion depth can be made.

To have an accurate pressure profile a certain number of pressure sensors needs to be installed into the core holder. The number of pressure sensors is dependent on the

length of the core itself. The upper part of the core is more sensitive to these pressure changes due to the fact that it is directly exposed to the drilling fluid. Therefore, in the upper part of the core the number of pressure sensors can be higher. The exact number of pressure sensors is going to be incorporated into the final design depending on the core size.

$$k = \frac{Q * \mu * \Delta L}{\Delta P}$$

Equation 31: Darcy's Law

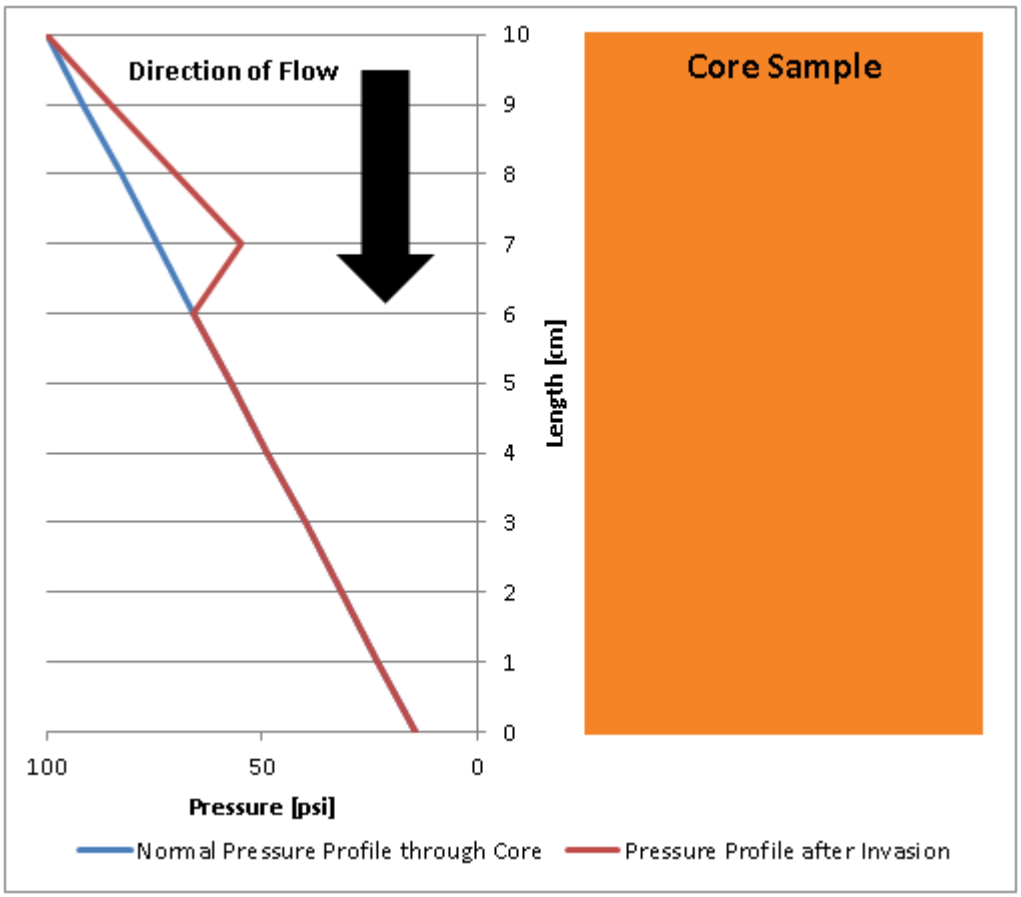

Figure 42: Core pressure profile before and after invasion

5.3.4.2 Post-Test Invasion Depth Measurement

Another opportunity is to measure the invasion depth after the test. This means that only the final invasion depth can be evaluated. This technique is actually applied on cores which are used in a Hassler Cell [9, p. 2]. After testing, the cores are dried in a convection oven. The production fluid is removed from the core and thin sections are prepared by impregnating the sample with blue epoxy resin in a low-pressure vacuum chamber. This preserves the whole sample and minimizes damage on sample and filter cake during sawing. Afterwards the core is cut vertically to expose the cross section.In the next step the cross section is observed via microscope and high resolution images are made. In the images invasion depth can be analysed on the microscopic scale. Furthermore, the invasion mechanism related to the structure of the pores can be

analysed in detail. The technique described above is mentioned in detail in the paper of Li and He [9, p. 2].

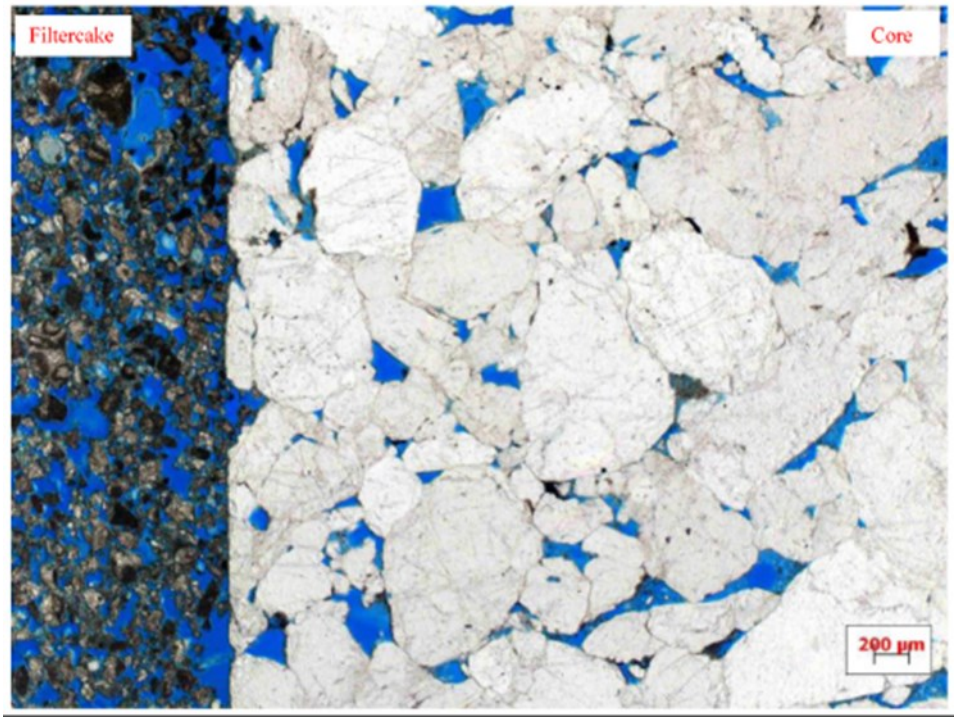

Figure 43: Example picture for investigating invasion depth on a pore size scale in sandstone [9, p. 4]

In comparison, it can be concluded that both techniques, which are described in this chapter are a valid solution to measure the invasion depth. In the case of this experiment the author suggests to use both methods because each method has a value of information that the other one can't deliver. Furthermore, the Post-Test method can be used to validate the results from the continuous measurement method and to calibrate it. If this combination is successful information about the invasion depth can be gathered during filter cake build up and over the whole course of the experiment and afterwards on a pore size scale.

5.3.5 Fluid Saturation

The near wellbore is normally altered by the drilling process [44]. This leads to the problem that in a lot of cases the saturation of the formation is influenced. Especially invasion into the hydrocarbon leg of the reservoir can dramatically decrease the hydrocarbon saturation [44]. Nevertheless, filtrate from a water based mud into the water leg of the reservoir formation won't change the water saturation. Therefore, it is necessary to have accurate "before" and "after" measurements of the water and reservoir fluid saturation in the core sample.

$$S_w = \frac{V_w}{V_p}$$

Equation 32: Water saturation

Where V_W is the volume of water and V_P is the pore volume.

$$S_o = \frac{V_o}{V_p}$$

Equation 33: Oil Saturation

Where V_O is the oil volume and V_P is the pore volume.

The water saturation in a wellbore is usually measured by using resistivity logs in combination with the Archie-Equation. It is obvious that this technique can't be applied in such an experiment. Therefore, for the experiment a different technique needs to be applied.

Two methods can be applied to measure the saturation of fluids in a core sample. Before conducting the experiment the core sample needs to be saturated with reservoir fluid upfront.

5.3.5.1 Distillation Retort Method

The idea behind this method is simply that the fluids inside the core sample are vaporized one after each other. The vapor is lead through a cooling unit which liquefies the vapor. The liquid is collected in a graded cylinder. This method works because oil and water have different boiling points and are vaporized one after each other [45].

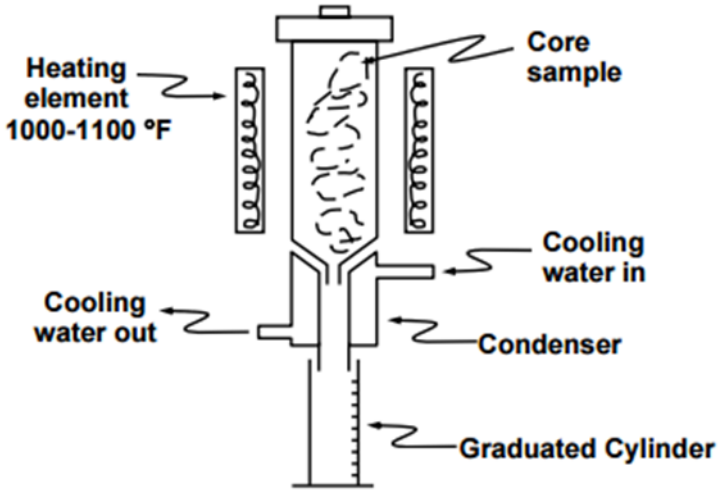

Figure 44: Sketch of the retort distillation apparatus [45]

The main advantages of this method are that it is fast and the values for oil and water saturation are determined with and adequate accuracy [45]. On the other hand the high temperatures normally lead to a destruction of the core sample and disables any further usage. Furthermore, due to the high temperatures, clay bound water can be mobilized and requires correction when the final result is reported. Finally, the effect of

coking and cracking of hydrocarbons needs to be taken into account as well because otherwise and an incorrect amount of oil is reported [45].

5.3.5.2 Solvent Extraction Method

The solvent extraction method is a non-destructive technique to measure the water and oil saturation of a sample. The sample is mounted above a bath of solvent. The core and the solvent are heated. At the beginning the water is vaporized and is lead through a cooling unit. The liquefied water is then measured in a graduated cylinder. Later the solvent starts to boil and is vaporized. As it moves through the core it dissolves the hydrocarbon. The vaporized solvent which includes the hydrocarbon is then liquefied again via a cooling unit and the solvent is collected [45].

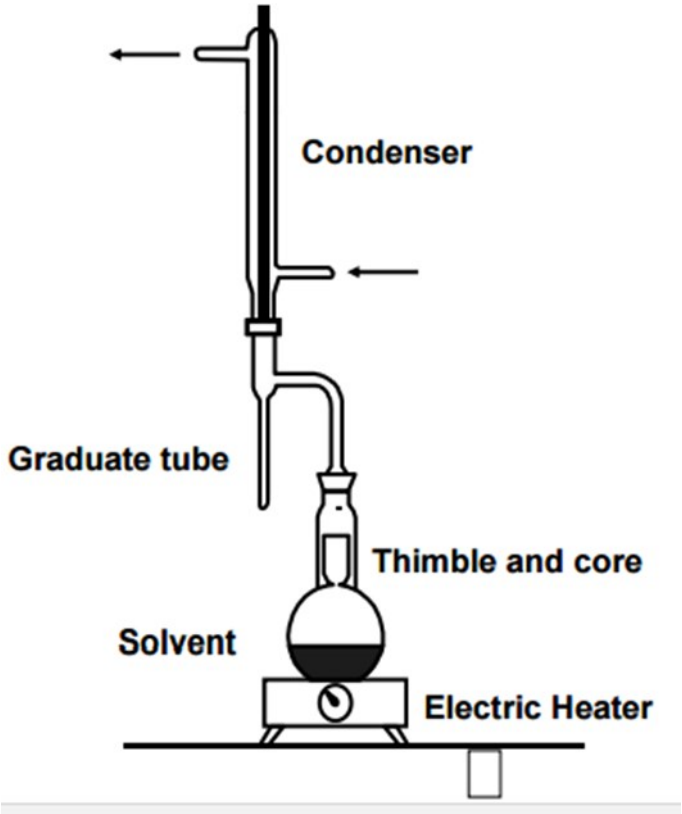

Figure 45: Solvent extraction apparatus for core samples [45]

The method features one major advantage compared to the distillation retort method which is that the core is not destroyed with this method and it can be used for further testing. Still the method has some major disadvantages. First of all, it can take days to extract all the fluid from the core sample and the hydrocarbon volume can't be measured directly because the hydrocarbons are dissolved in the solvent [45]. The only way to get the volume of oil is to weigh the core before and after the extraction and subtract the weight of water.

$$V_o = \frac{\left(W_i - W_{dry}\right) - V_w * \rho_w}{\rho_o}$$

Equation 34: Volume of oil from the solvent extraction method [45]

Where W_i is the initial weight of the core, W_{dry} is the dry weight of the core, V_w is the volume of water, ρ_w is the density of the water and ρ_O is the density of the oil.

Regarding the applicability of both methods for the evaluation of saturation, the solvent extraction method should be used, because the integrity of the core is not altered. The distillation retort method destroys the core and allows no further experiments. Furthermore, it should be possible to construct a solvent extraction apparatus without spending extensive amounts of money. Anyway, analysing the core saturation after the experiment should always be the last part of the analysis because then the filter cake has already been analysed and also the return permeability is already obtained.

5.3.6 Return Permeability

When drilling into a reservoir the build-up of a filter cake can influence the return permeability of the formation. This could lead to production related problems. The easiest way to measure the return permeability is to use the same core holder as used in the experiment and perform a Hassler-Cell experiment opposite to the flow direction of filtrate in the experiment. The measured return permeability can then be compared with the original permeability measurement to assess the damage of the core.

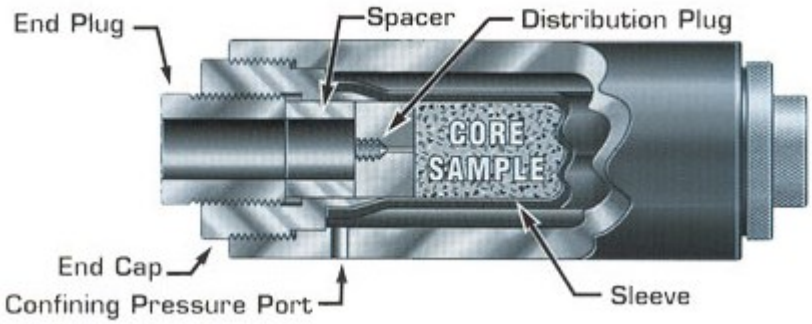

Figure 46: Hassler type core holder example from CoreLab [46]

Two different reservoir fluids are normally considered for the permeability measurement, oil and gas. The permeability can be measured with either a liquid or gas. The absolute permeability is not dependent on the type of fluid that is used for the measurement.

Independently from the type of fluid which is used to determine permeability the main underlying equation is Darcy's Law as shown in Equation 30. The main idea is to have a dried core sample which is covered in a rubber sleeve. Afterwards the core is flushed with fluid at a constant flow rate and the pressure drop through the core sample is recorded [47]. It is important to have laminar flow through the core sample because otherwise Darcy's law is not applicable. This can be tested by plotting the flowrate Q divided by the area A (Q/A) against the pressure difference divided by the core length $(\Delta P/L)$. A straight line indicates the laminar flow through the core sample [48].

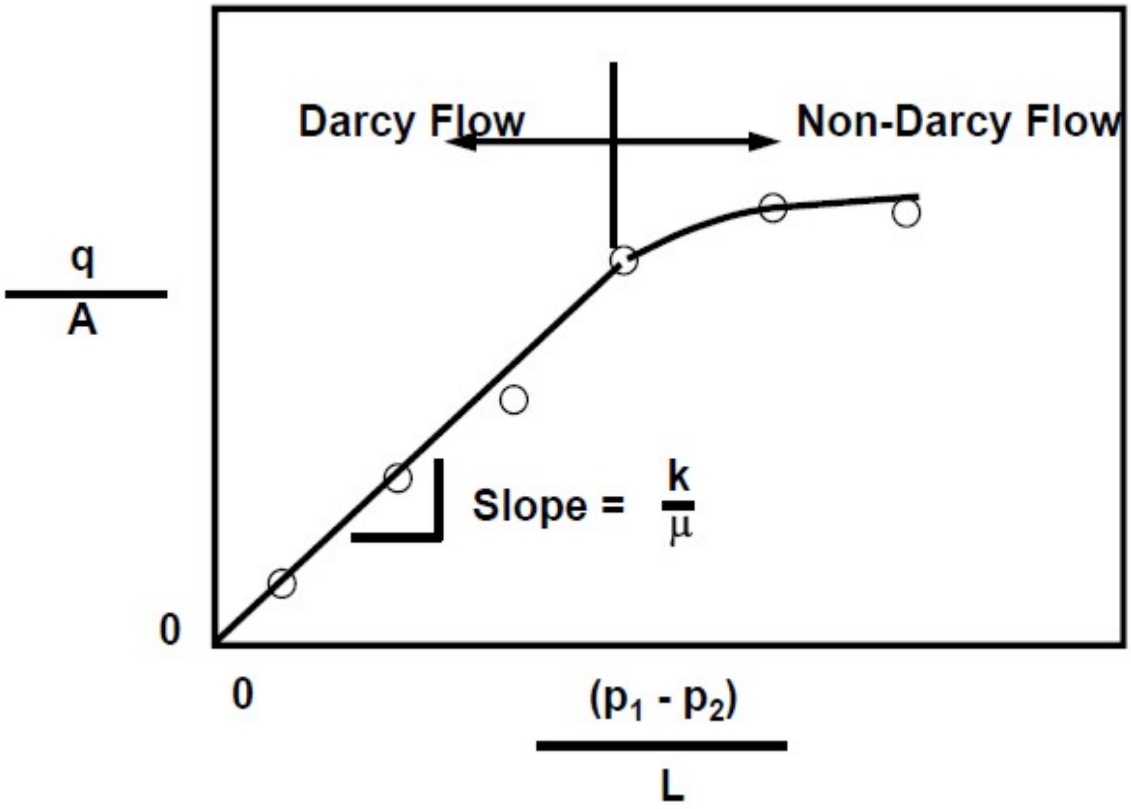

Figure 47: Darcy and Non-Darcy Flow [48]

The main difference between the measurement of liquid and gas permeability is that for the gas permeability a correction needs to be considered. This is due to the reason that gases exhibit a so-called slippage on the grain surface. A liquid has zero velocity on the grain surface but a gas has a finite velocity on the grain surface. Due to that the flowrate for a certain pressure difference is higher resulting in a higher permeability if this is not corrected [48].

$$k_g = k_\infty * (1 + \frac{b}{P_m})$$

Equation 35: Klinkenberg's Permeability Equation

Where k_g is the gas permeability, k_∞ is the absolute permeability and P_m is the mean pressure.

To calculate the correct permeability of the core sample the gas permeability is measured at different mean pressures. Then $1/P_m$ is plotted against the measured gas permeability. The absolute permeability can be read from the diagram when the $1/P_m$ is zero which corresponds to a mean pressure of infinite. At such a pressure the gas behaves like a liquid and the absolute permeability for the core is correct. Furthermore the factor b can be estimated from the slope of the line [49].

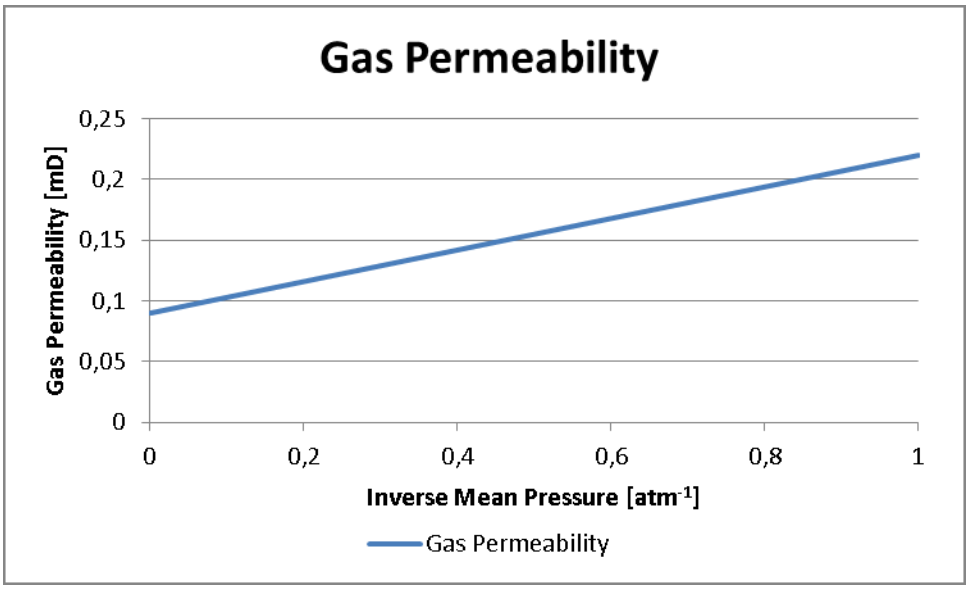

Figure 48: Gas Permeability at different mean pressures

For the measurement of permeability, it does not make a difference which fluid is used. Furthermore, the permeability is one of the most important parameters in this experiment. It needs to be measured before and after the experiment. Therefore, it is important to have a core holder which can be easily deployed from the apparatus and use it directly for the measurement of permeability. This needs to be considered when the core holder is designed.

5.3.7 Structural/Compositional Analysis

The structural analysis should give detailed insights into the filter cake structure. This is especially interesting for a filter cake which is created during a CwD operation. Nevertheless, also the structure of a regular filter cake should be investigated to analyse the differences in detail. Three highly sophisticated techniques are described in this chapter and their usability for such an experiment.

5.3.7.1 Scanning Electron Microscope Technique

Before the scanning electron microscope (SEM) can be used the filter cake needs to be prepared. This needs to be done by the so-called freeze drying technique, which removes water from the frozen filter cake by sublimation [6, p. 8]. Tiny pieces of filter cake are cut from the sample and a shock freezing procedure at -140°C is performed. This needs to be done as fast as possible to avoid the growth of large ice crystals. Then the water is removed by sublimation without passing the water through the liquid stage. The sample is then ready for the SEM [6, p. 8].

In the context of this thesis the SEM technique will not be further described in detail. Nevertheless, the following explanation from the website of nanoscience Instruments [50] should be sufficient. Images are produced by scanning the filter cake with a focused beam of electrons. The electrons interact with atoms in the sample. This produces various signals which contain information about the samples topography and composition [50].

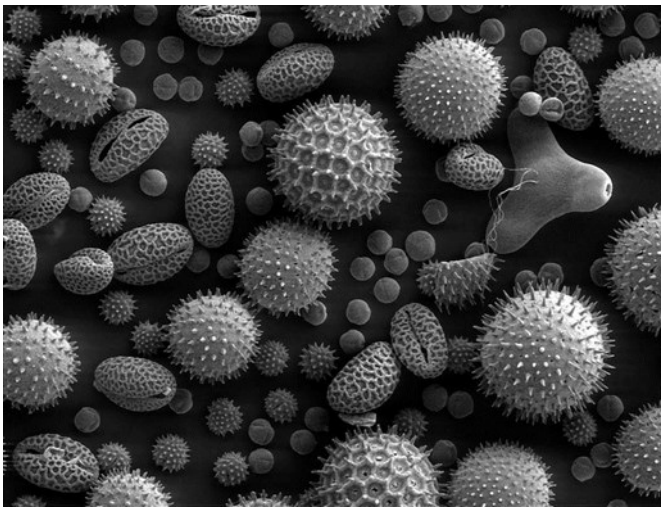

Figure 49: Example picture for the details from a SEM [51]

5.3.7.2 X-Ray Diffraction and X-Ray Fluorescence Analysis

X-Ray diffraction is a special application of X-Ray crystallography, which is used for determining the atomic a molecular structure of a crystal. The crystalline atoms cause a beam of incident X-rays to diffract into many specific directions. By measuring the angles and intensities of these diffracted beams a three-dimensional picture of the density of electrons within the crystal can be produced. From the electron density, the mean positions of the atoms in the crystal can be determined [52].

This technique is then applied onto a dried piece of filter cake. Furthermore, the piece of filter cake needs to be in powder form. The X-Ray diffraction is then used to identify the crystalline solids in the filter cake powder. This is only a qualitative analysis to determine the different phases of the structure [6, p. 9].

The X-Ray fluorescence analysis is then used to quantitatively determine the elemental composition in the filter cake [6].

A CT-scan uses several X-ray images taken from different angles to construct cross-sectional slices of the object of interest [53] With processing software a three dimensional picture can be constructed and also the inner structure of an object can be observed without cutting it. Furthermore, in filter cake investigations the so called CT number can be used to identify the mineralogy in the filter cake and also the core sample [6, p. 9].

All these techniques described above are connected with expensive experimental equipment which is not standard equipment in most laboratories. Anyway, the best method with the highest value of information would be to use the CT scan or the SEM. The only problem with the SEM is that it is a single spot method. This means that

several parts of the filter cake need to be freeze dried to have a representative result of the whole sample. It only makes sense to apply the X-Ray diffraction method if the structure of the filter cake is not of interest. Only the quantity of different lithologies can be observed with this method.

5.3.8 Particle Size Distribution

The importance of the particle size distribution is already described in the literature review part of this thesis. Before any measurements of the particle size can be made it needs to be tested if the experimental unit itself can provide the necessary force on the core face to crush the artificial cuttings which are fed into the system. If this is not possible already fine grained cuttings need to be fed into the system to simulate the effect of CwD.

Several different methods exist to assess the particle size distribution in a fluid. At the beginning stage of such an experiment only the basic analysis by using sieves is described because it can easily be used and does not require extensive additional laboratory equipment.

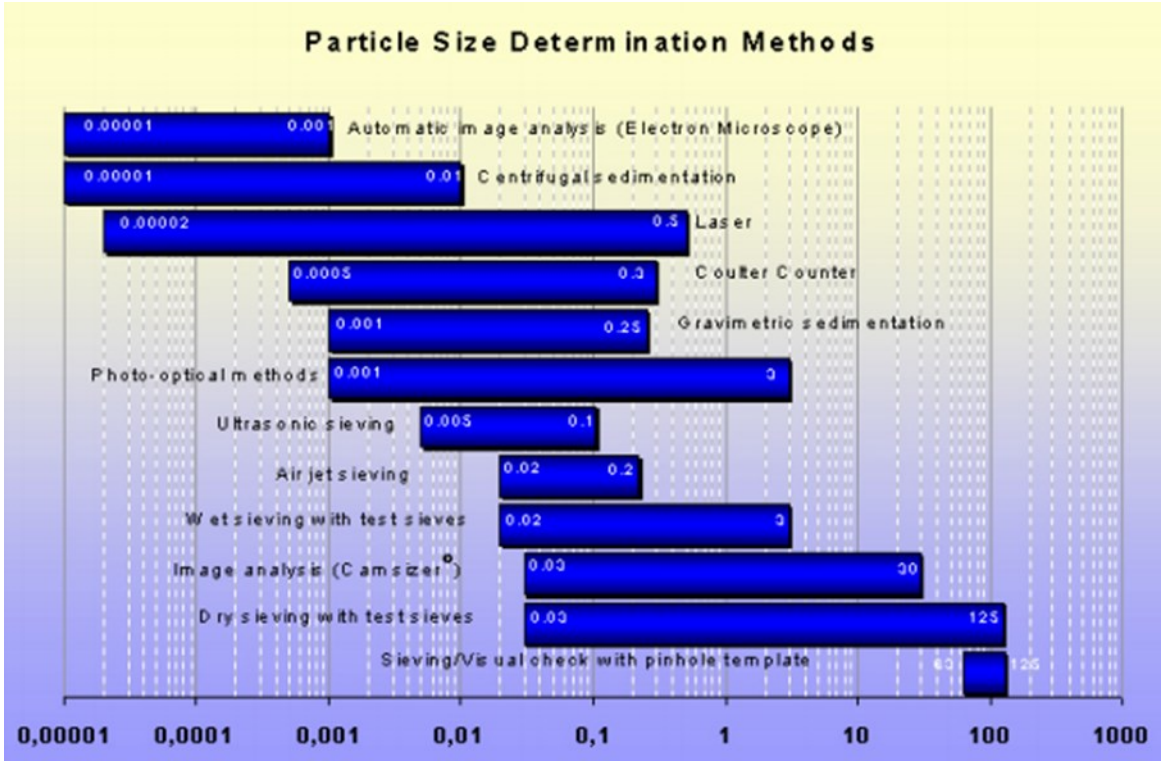

Figure 50: Particle size determination methods [54]

The main idea of sieve analysis is to use a series of sieves and a representative sample from the drilling fluid for analysis. As the sieves are moved either horizontally or vertically the grains are separated from each other and either retain on the sieve surface or they fall through onto the next sieve [54]. From the weights of grains on the different sieves and the knowledge about the mass of the whole sample a particle size distribution can be created. The choice of sieves depends mainly on the sample and the size of the grains that are going to be analysed [54]. In case of a CwD experiment the

size of the artificial cuttings determines which sizes of sieves should be used for the analysis.

Figure 51: Example for different sieve sizes [55]

Regarding the applicability for the experiment, it is not necessary to determine the particle size distribution before because it is already known when only artificial materials with a known distribution are used. After the experiment a sieve analysis can be performed to see whether the cuttings have been crushed or deposited on the core face. Anyway different particle size distributions can be used to test the change in fluid loss properties of a drilling fluid. Furthermore it is important to know how different distributions influence the filter cake structure, the invasion depth and all the other parameters related to the characterization of the filter cake.

5.4 Proposed Experimental Design

The actual design of the unit can be subdivided in three different parts. Each part is discussed in a separate chapter.

- Core holder
- Main body
- Drill pipe design

It needs to be mentioned that the drill pipe design has its focus not on the actual design of the pipe but on the mechanism, that enables the pipe to be movable in the vertical direction in the artificial borehole.

5.4.1 Core Holder

The design of the core holder is based on different considerations as described in the list below.

- **Mechanical Stability**
  - The core holder needs to withstand the force of constant pipe contact onto the core itself and the confining pressure inside.
- **Corrosion resistance**
  - The upper part of the core holder is exposed to the drilling fluid all the time and needs to be resistant against the corrosive nature of certain drilling fluids.
- **Variable Diameter**
  - Depending on the size of the plug or the core the inside diameter of the rubber seal inside the core holder needs to be variable in diameter.
- **Assembling and Disassembling**
  - The process needs to be easy and cleaning of the separate parts should be simple as well.

5.4.1.1 Core Diameter and Core Length

The core diameter depends on the system that is used to recover the core. As a benchmark the systems of three major service companies are provided in the table below.

Company	Technique	Core Diameter	Core Length
Schlumberger	XL-Rock Sidewall Cores [56]	1,5 inch	2,5 inch
Schlumberger	Conventional Coring [57]	1,75-5,25 inch	Depends on Barrel Size
Schlumberger	Mechanical Sidewall Coring Tool [58]	0,92 inch	1,5-1,75 inch
Baker Hughes	PowerCOR Service [59]	1 inch	1,8 inch
Baker Hughes	HT30™ Max coring system [60]	4 inch	270 ft
Weatherford	Conventional, Rotary Sidewall coring [61]	0,9-5 inch	Depends on Barrel Size

Table 3: Core sizes with different retrieving techniques

By taking a look at the table above it is clear that the core holder needs to hold core diameters from 0.92 inch up to 5.25 inch. The only way to achieve that inside the core holder is to use different sizes of rubber seal and different diameters for the top cap to keep the rubber seal in place.

5.4.1.2 Confining Pressure

The maximum confining pressure which can be applied on cores depending on the provider of the core holder is 15,000 psi [62]. Depending on the gap between body of the core holder and the rubber seal a certain force is acting on the top cap of the core holder. The screws, which hold the top-cap, need to be strong enough to keep the top-cap in place. For a 5 millimetre gap, considering the overall size of the core holder as it is shown in the design, this results in a force of 12.9 kilo-Newton. This force can be subdivided on four screws. Each screw should then support 3,225 kilo-Newton. The correct size of the screws needs to be determined when the core holder is finally created.

5.4.1.3 Material

All the material, which is in contact with drilling fluid, requires a certain resistance against a corrosive environment. For the construction of the core holder it would make sense to use a material which lasts long without the need to replace it. Therefore, as already used by other core holder producers [62], Hastelloy is the preferred material. Hastelloy is a trade name for a nickel-alloy produced by the company Haynes International [63]. The material is highly resistant over a big temperature range.

5.4.1.4 Design

The Core Holder was designed using AutoCAD 2014. A conceptual sketch of the core holder can be seen below.

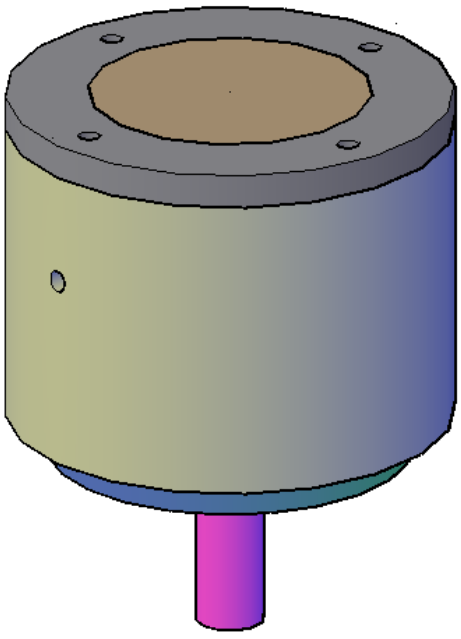

Figure 52: Conceptual sketch of the core holder for the test apparatus.

Cutting the core holder along the y-axis provides more detail about the inside structure.

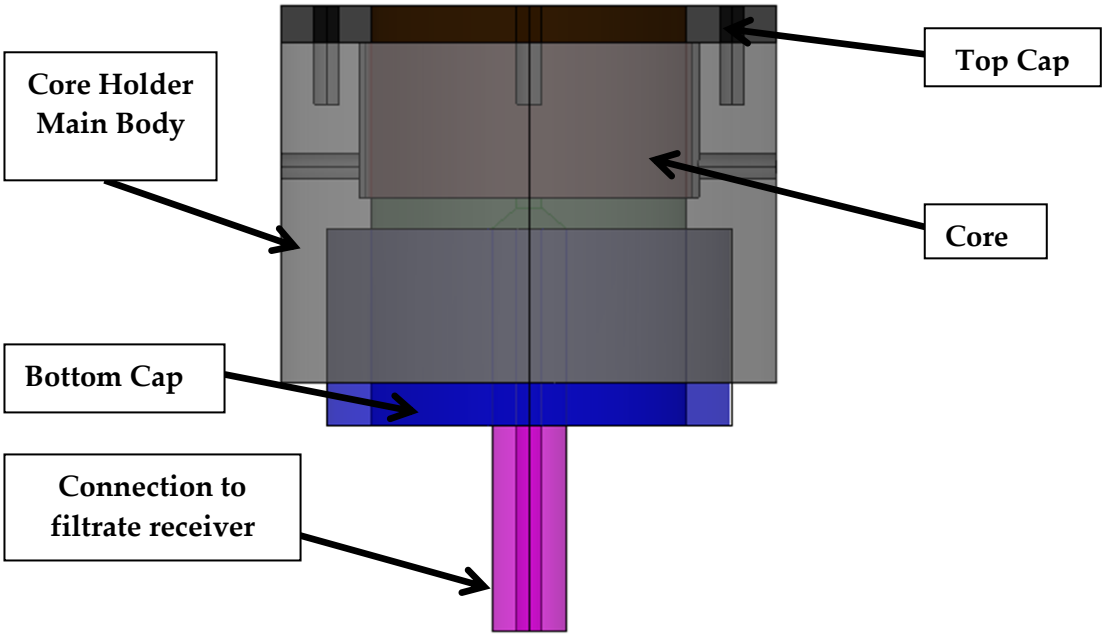

Figure 53: Cut through the y-axis of the core holder

The size of the core holder is 20 centimetres in diameter. The core holder design should make it possible to use 5 inch cores with a maximum length of 12 inches. If such a long core is used it is possible to use pressure taps to have a continuous invasion depth measurement. For smaller cores, especially sidewall cores, which are much smaller in size, spacers need to be used to mount them into the core holder.

Overall a good design for the core holder, which is based on already available designs was obtained. It is obvious that the design is not ready to be manufactured but it gives a good idea what is expected from this core holder. In cooperation with an experienced mechanical engineer it should be easy to create a final design ready for manufacturing very fast.

5.4.2 Main body

In this chapter mainly the pipe body of the apparatus is described. The dimensions of the pipe body can be adapted depending on the usage. The design makes it possible to apply it directly in an existing flow loop by exchanging a piece of pipe or to use the apparatus separately with its own circulation system.

Operating parameters, such as temperature of the fluid and pressure inside the pipe segment, are measured by sensors, which are placed at specific points in the system. Furthermore, pressure inside the system is regulated by using pressure regulation valves (pressure regulator, backpressure regulator). The measurement section needs to be long enough to avoid fluid turbulences during measurement. All the points mentioned above are discussed in more detail in separate sections of this chapter.

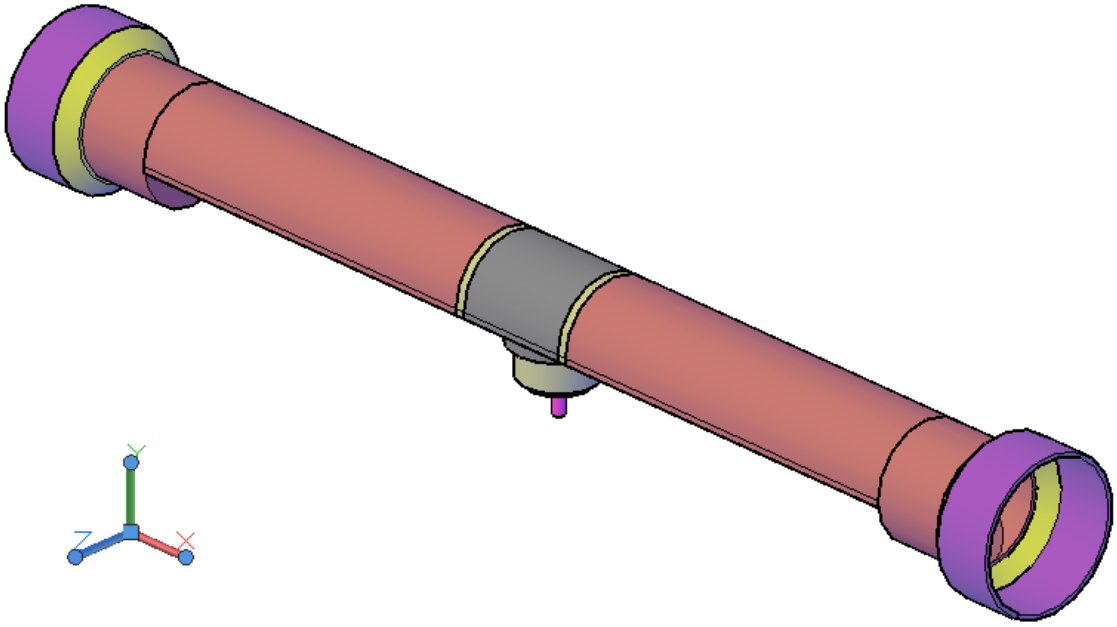

Figure 54 Schematic of the pipe body with the core holder in the middle

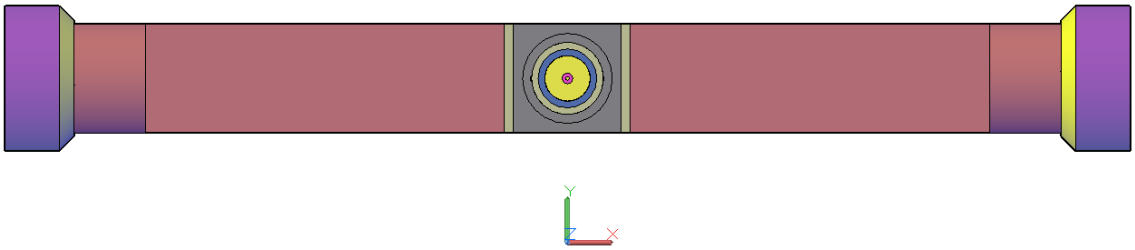

Figure 55: Pipe body seen from below

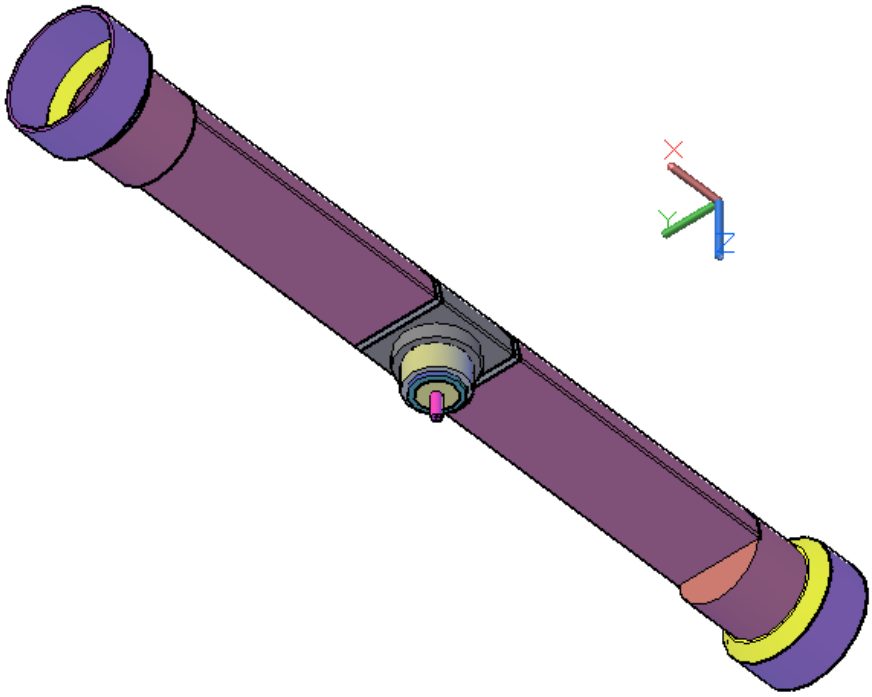

Figure 56: Pipe body seen from below in combination with the core holder

5.4.2.1 Pressure

Pressure and temperature need to be measured inside the system to relate these operating parameters to the final result of the filter cake build up. Pressure is sensed by mechanical elements such as plates, shells, and tubes, which are designed to deflect when pressure is applied [64]. There are several methods available to measure pressure inside a pipe but only the ones proposed for the final design of the apparatus are described in detail.The main idea is that when pressure is applied via a transducing element an electrical output is created which can then be read as a pressure signal. Nevertheless, mechanical devices are still frequently used in the industry. Both types of devices are described in the section below.

Widely used in the industry is the measurement based on the principle of Bourdon. The device uses a closed C-shape tube that tends to go back into its original shape when pressure is applied inside. Via a mechanical link the free tip moves the needle along the scale which displays the pressure.

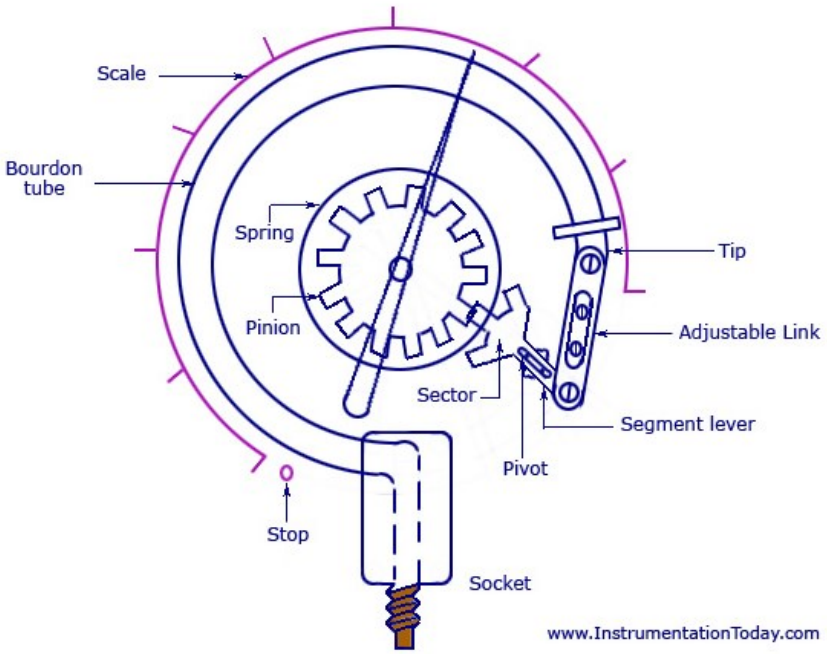

Figure 57: Bourdon pressure gauge [65]

A more sophisticated type of pressure gauge would be a so called strain gauge based pressure transducer. The working principle can be explained as follows. The sensing element is a diaphragm which is deflected in a certain manner when pressure is applied. This causes surface strains which can be sensed by a strain gauge attached to the diaphragm. This causes a change in the resistance of the strain gauge which can be related to a certain pressure [66]. This method of measuring pressure is more accurate as already small changes in resistance can be measured by using a Wheatstone bridge circuit [66].

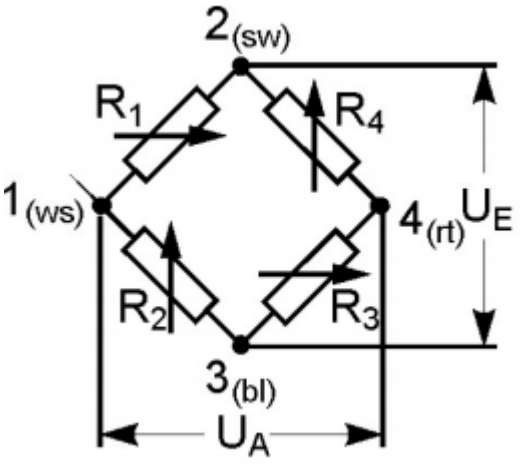

Figure 58: Wheatstone bridge circuit [67]

The measurement principle of a Wheatstone bridge is described by Hoffman [67] as follows. The nodes 2 and 3 are connected to the input voltage U_E. In a balanced state the ratio between the output voltage U_A and the input voltage U_E is zero but in case that the resistors R1 to R4 vary an output voltage is going to be created. The output voltage can then be related to the change in strain which can be related to the applied pressure.

The pressure gauges are placed along the pipe body. One pressure gauge should be placed directly at the core holder to have an accurate measurement of pressure at the zone of interest. One gauge should be place at the beginning of the measuring section and one at the end before the pressure regulation valve to have an idea about frictional pressure losses. Behind the pressure regulation valve a pressure gauge is placed as well to monitor if the fluid pressure is at the desired value after passing the valve.

While running an experiment, the pressure inside the system needs to be kept at a certain value. According to API RP-13B-1 [42] a high-pressure filtration cell should have a working pressure of 600-1300 psi. This would be the ultimate goal for pressure and high temperature pipe impact tests in this unit. Nevertheless, in this work only a low pressure unit is designed to set the stage for further development into a high pressure and temperature unit.

Therefore, the pressure requirements inside the pipe body should not exceed the lower limit of the HPHT unit of 600 psi. This results in an operating range up to 600 psi for this unit.

The pressure is contained by using a pressure regulator at the beginning of the measuring section and a backpressure regulator at the end. The idea is that the fluid arrives from the pump and is then regulated to the operating pressure of the system. The backpressure regulator at the end of the measuring section keeps the pressure in the measuring section constant.

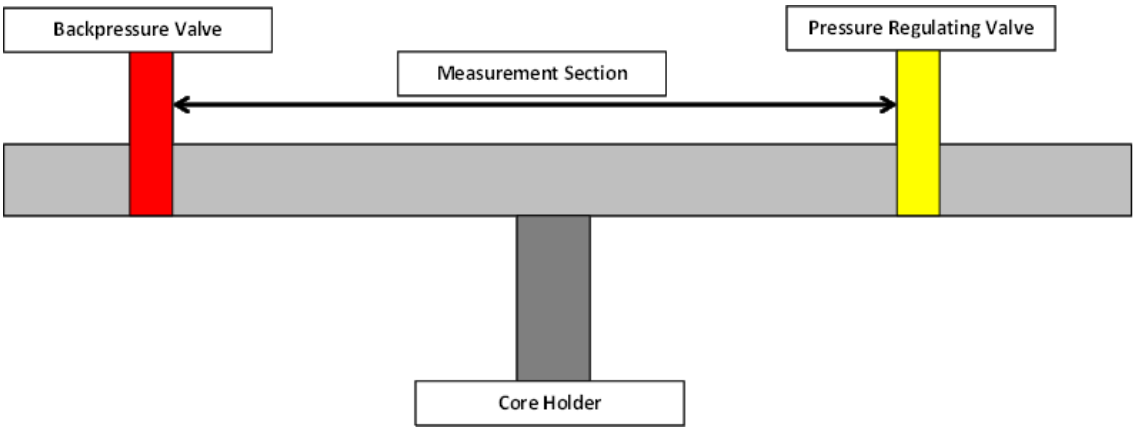

Figure 59: Schematic of the pressure valve arrangement

5.4.2.2 Temperature

By measuring temperature during the experiment relations between different temperatures of the fluid and the filter cake build-up can be observed separately. Temperature inside the pipe is measured by using temperature sensors. The easiest way to do that would be to use bimetal thermometers where the sensing element sticks directly into the fluid. But for a more advanced type of measurement, which allows recording of temperatures electronically, a so called Resistance Temperature Detector (RTD) is required. In both cases the temperature sensor needs to be connected to the pipe body pressure tight.

The measurement principle for the thermometer works as follows. It uses a bimetal helix, which is contained in the sensing element that sticks into the fluid. The two metals have different thermal expansion coefficients. Therefore, one material unwinds faster than the other as the temperature rises. The helix is directly connected to the pointer on the scale. If the temperature rises the unwinding action causes the pointer to move. If the temperature drops the helix winds tighter and the pointer moves into the opposite direction [68].

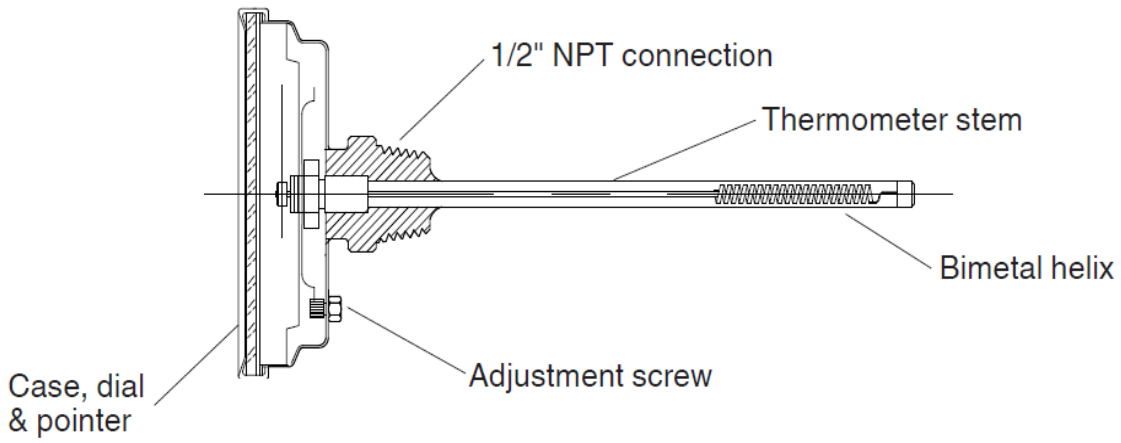

Figure 60: Example sketch of a bimetal-thermometer [68]

The working principle of the RTD relies on the fact that certain materials show a change in resistance when the temperature changes. The sensing element in a RTD is provided with a constant current. If the temperature changes, the resistance of the element changes, which in fact leads to a different output voltage. This change in voltage can then be related to the temperature [69]. Obviously this device works only if the sensor is calibrated upfront. This technology can be combined with a data logging device [70] which delivers a temperature record over the whole duration of an experimental run.

The measurement of temperature is only necessary directly at the core holder where the filtration action takes place. As the fluid temperature only changes due to the exchange of heat with the pipe wall there is no need to measure temperature of the fluid at any other points in the system. Nevertheless, it is necessary to take a certain time before starting the filtration action to condition the whole system at the desired temperature. In an advanced version of the system a clamp thermometer could be used which measures the temperature of the pipe wall, which can then be converted to the fluid temperature. The advantage of such a system, even if it does not measure fluid temperature directly, is that no obstruction is in the path of the fluid in the measurement section.

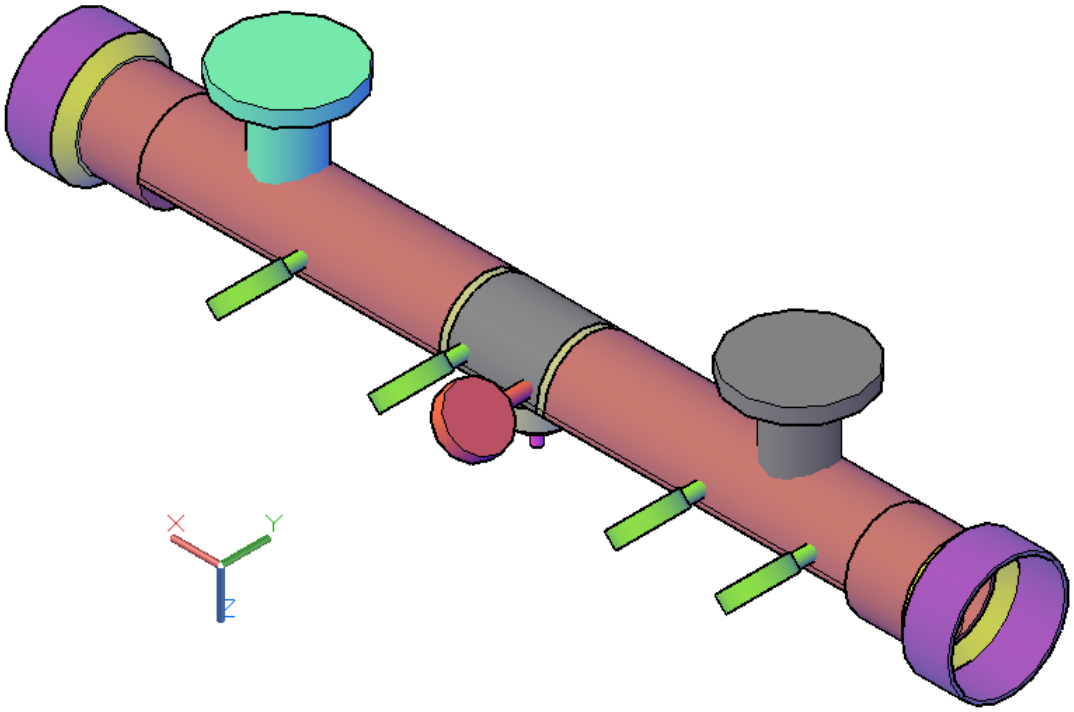

Figure 61: Pipe body with proposed positions for pressure (green) and temperature sensors (red) and pressure regulator (black) and backpressure regulator (blue)

5.4.2.3 Shear Stress

Especially in a dynamic environment measuring the shear stress is important because it influences the force balance, as described in the literature review chapter, directly. The shear stress can't be measured directly but it can be calculated from the flow velocity and the fluid properties. The calculated shear stress depends on the fluid model. The calculation of the shear rate in this case is based on the Herschel-Bulkley

fluid model. This model was chosen because it incorporates the Newtonian, the Bingham and the Power-Law fluid as well.

$$\tau = \tau_y + K * \gamma^n$$

Equation 36: Herschel-Bulkley fluid [71, p. 242]

τ is the shear stress, τ_y is the yield stress of the fluid to be tested, K describes the consistency index and n the flow index [71, p. 242]. The assumption for the experiment is that above the core face the fluid flow can be represented as a slot because the cross-section is not circular.

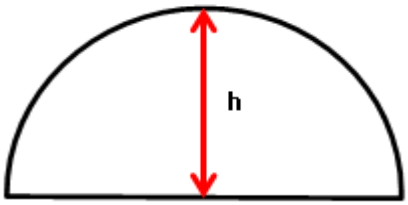

Figure 62: Cross-section of the measuring section

For the calculation of the wall shear stress, which represents the shear stress across the core face, it is necessary to calculate the pressure drop there. For a Herschel-Bulkley fluid the pressure drop can only calculated by trial and error methods due to the complexity of the formula which is shown in the Appendix. The second input parameter for the calculation of the pressure drop is the flow rate, which is simply determined by the flowrate that the pump delivers. With that information, the pressure drop can be determined and finally the wall shear stress is calculated by the following formula where h represents the height of the slot.

$$\tau_W = \frac{h}{2} * \frac{dp_f}{ds}$$

Equation 37: Wall shear stress [71]

The wall shear stress can then be directly converted to the shear force if the area of the core face is known.

$$F_S = \tau_W * A$$

Equation 38: Shear force calculated from the wall shear stress

Finally, the shear force onto the core face can be calculated and it is directly controlled by the flow rate. This determines the equilibrium height during the dynamic filter cake build-up. The deposition force is controlled by the pressure that is set in the measurement section. Therefore, both forces can be controlled directly via different mechanisms. This allows separate control of both mechanisms without influencing each other.

5.4.2.4 Material and Dimensions

From a material point of view the whole pipe body should be made out of a corrosion and temperature resistant material. The final decision for the material needs to be made before the unit is build depending on the final dimensions because Hastelloy is only available up to 4.5 inches in diameter [63]. Regarding the dimensions of the pipe body the measurement section needs to be long enough to ensure undisturbed laminar flow in the area of interest. This needs to be considered when building the pipe body. The diameter of the pipe is directly dependent on the size of the core holder. Considering that in the final section of the chapter the introduction of a drill-pipe into the system is going to be discussed the final dimensions of the system are going to be discussed at the end of this chapter. Simply due to the reason that all of the parts are then designed and can be adapted accordingly to the rest of the system.

5.4.3 Drill-Pipe Design

The drill-pipe design is the most important part for the pipe-impact and CwD tests. For the static and dynamic filtration test it is recommended to remove the pipe from the assembly to reduce the obstructions in the flow-path of the drilling fluid.

The pipe needs to be exchangeable due to different sizes of cores. The length of the pipe is determined by the diameter of the core which is used. The pipe assembly needs to be movable in the vertical direction to simulate the frequent contact of pipe with the core face. Furthermore, the assembly is equipped with a load cell to measure tensile and compressive forces during the up and down movement of the assembly. The assembly is powered by an electric motor with a drive shaft which is connected with the drill-pipe by a drive belt.

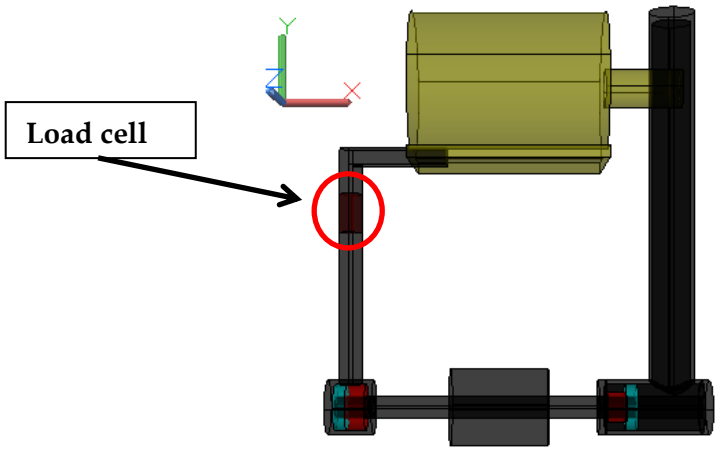

Figure 63: Drill-pipe assembly with electric motor (yellow) and bearings (blue) and seal (red)

The whole assembly is mounted on a lifting platform. The platform can move up and down at a certain speed. This represents the drill-pipe movement in the bore hole. The design represents the actual situation in the borehole where the drill-pipe is parallel to the flow direction. The revolutions per minute of the drill-pipe are controlled by the electrical motor. The contact frequency is controlled by the speed of the lifting platform.

Another important feature of the pipe assembly is that it has to withstand the high pressure in the pipe. Furthermore, fluid leakage to the outside is not desired. To prevent that, the two rods which move up and down will go through a stuffing box. Stuffing boxes are regularly used two allow movement of a pipe into a high-pressure region.

Regarding the material of the drill-pipe it would not make sense to use another material than Hastelloy [63], especially because the drill-pipe has to withstand the corrosive nature of certain drilling fluids and the frequent contact with the core face. The dimensions of the pipe are discussed in combination with the other parts of the apparatus in the final section of this chapter.

5.5 Dimensions

The following dimensions are based on a 5 inch core. This is not the size of core which is mostly expected for such experiments. Nevertheless it would make sense to design the apparatus for the biggest core size available. Smaller cores can be used in the apparatus by using spacers and thicker rubber seals. All dimensions are given in centimetres.

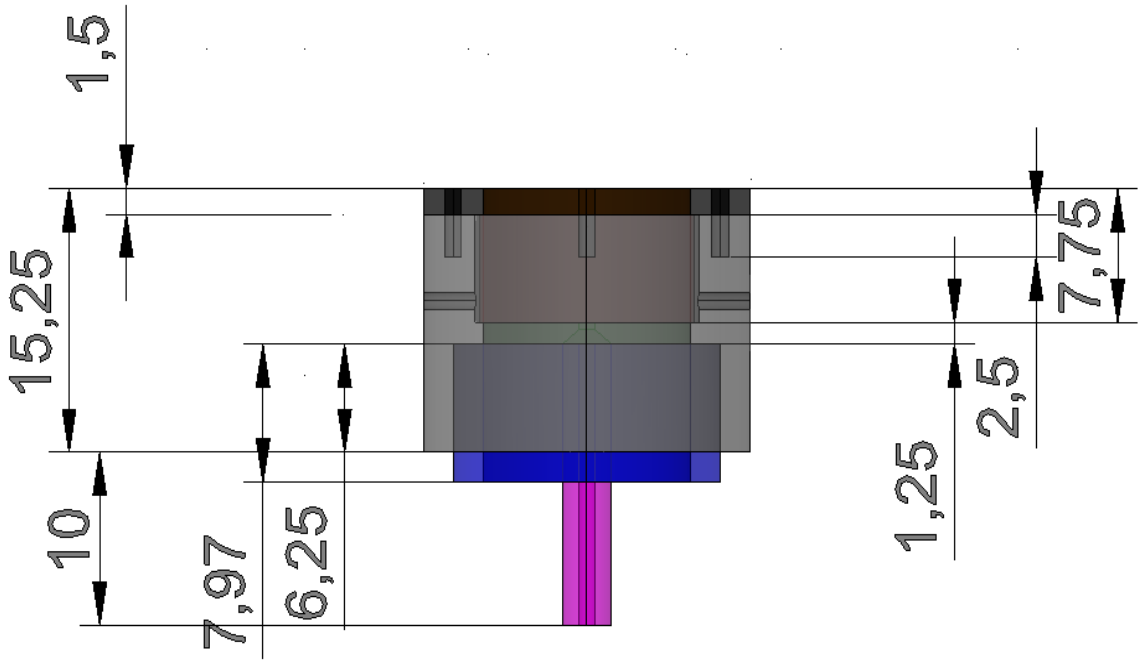

Figure 64: Core holder seen from the front with dimensions

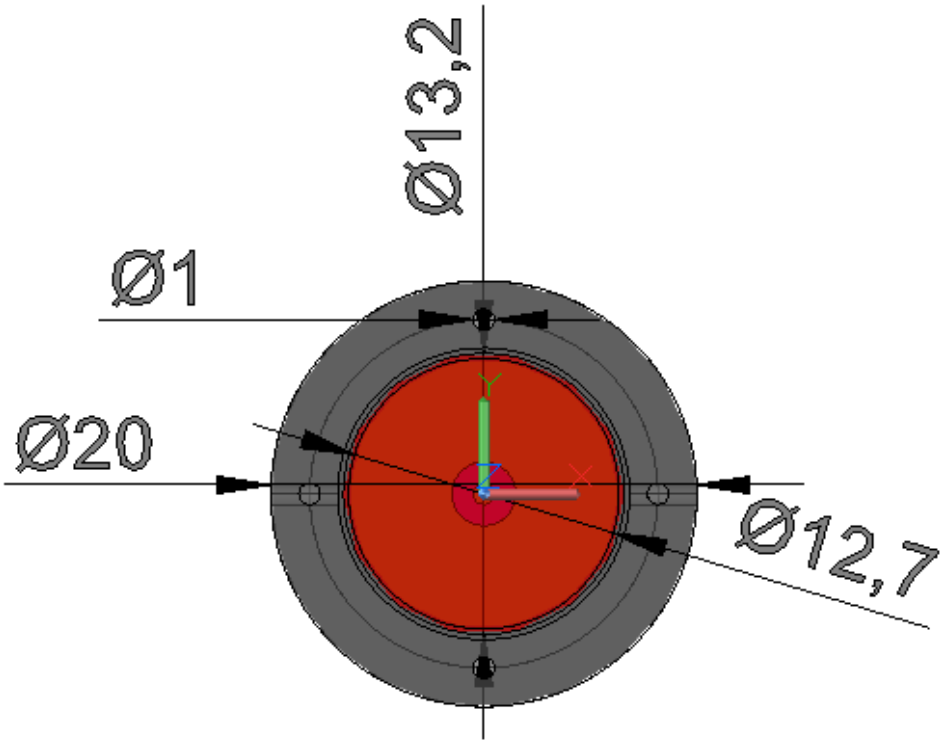

Figure 65: Core holder seen from the top

The size of the core holder determines the size of the pipe body. Nevertheless, this is just a proposal for the final size. It is obvious that if the unit is built in this size an available flow loop needs to be adapted if it should be used together with this device.

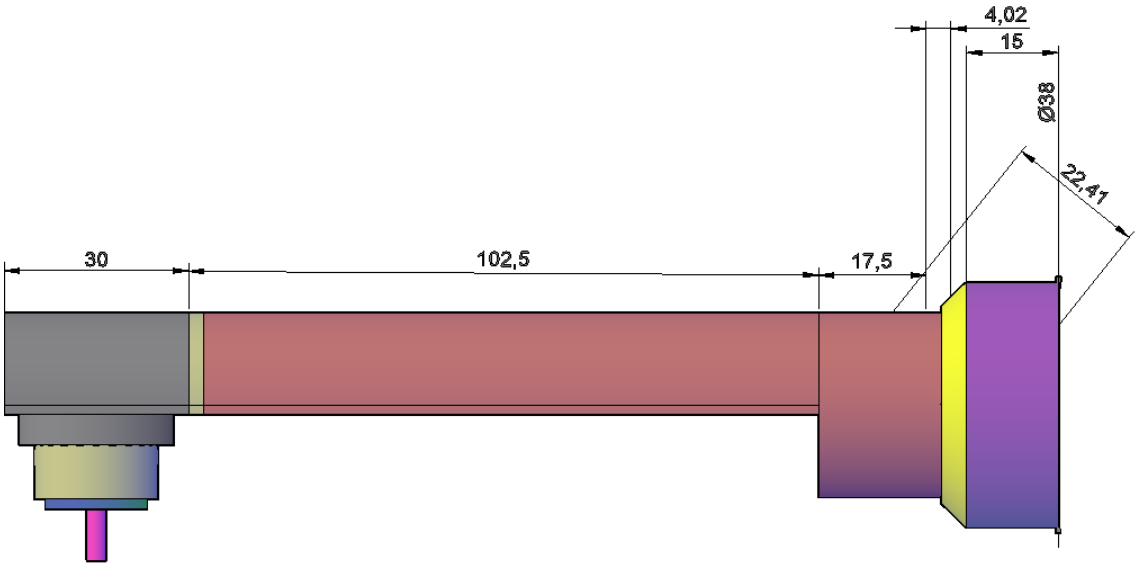

Figure 66: Right side of the pipe body

Only the right side of the pipe body is displayed here. For the dimensions it makes no difference because both sides are equal in size. The measurement section itself is 235 centimetres long. The length is based on the concept of the hydrodynamic entrance length. The entrance length is defined as the necessary distance a fluid needs to travel inside a pipe to have a fully developed parabolic flow profile [72]. For laminar flow the following formula defines the required entrance length.

$$L_E = 0{,}06 * R_e * D_H$$

Equation 39: Definition of the entrance length for laminar flow [72]

Where *Re* is the Reynolds number and D_H is the hydraulic diameter.

$$D_H = \frac{4 * A}{P}$$

Equation 40: Hydraulic Diameter [73]

Where *A* is the area of the pipe crosssection and *P* is the wetted perimeter.

Depending on the flowrate, the fluid viscosity, the fluid density, the pipe diameter and the pipe shape the entrance length varies. For a Reynolds number of 2300 as transition from laminar to turbulent flow [74] with a pipe radius of 14 centimetres the entrance length would be 34 metres which is not reasonable at all. Therefore, for the design a different definition for the entrance length was used.

$$L_E = 10 * D$$

Equation 41: Definition of entrance length for turbulent flow [75]

Considering the half pipe shape and the radius of the pipe the dimensions shown in Figure 66 were chosen. This entrance length does not mean that the flow inside the pipe is turbulent. Anyway before building the apparatus a compromise, including the space specifications need to be considered. Furthermore additional research considering flow dynamics and streamline simulations is required to avoid problems.

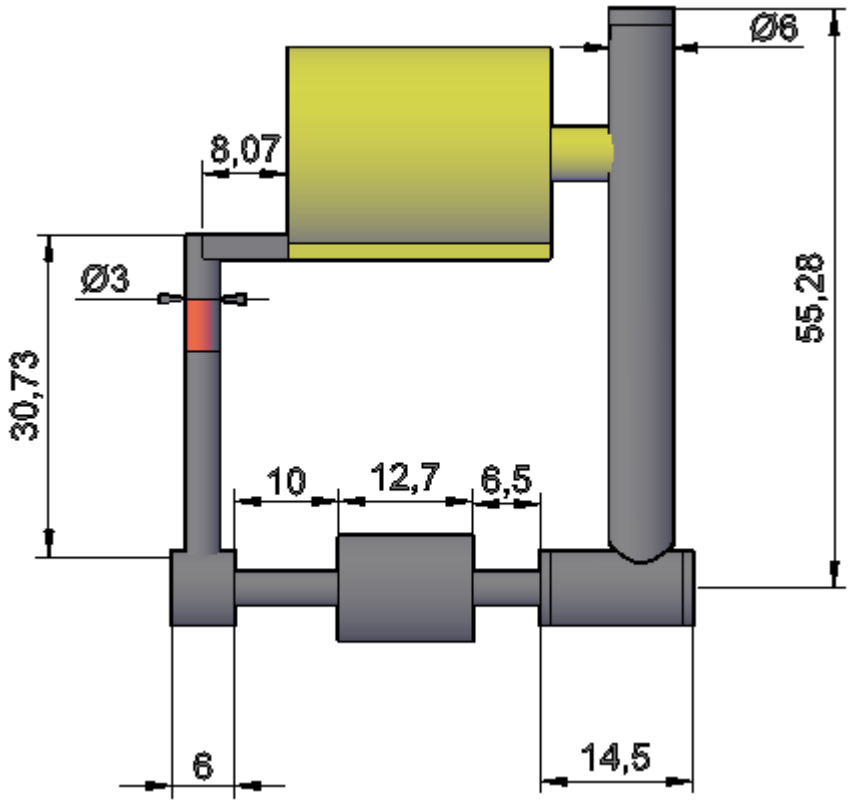

Figure 67: Drill-pipe assembly seen from the front

Considering the dimensions of the drill-pipe assembly it is obvious that the lifting ramp where the motor is placed must support a high weight.

The dimensions for the whole apparatus are based on the biggest core size possible. This leads obviously to dimensions that seem to be oversized. Nevertheless, for a test version of this apparatus the size can be reduced and the system could be tested on a small-scale model. If it turns out to be successful, upscaling the whole construction to the diameters proposed in the thesis would ultimately lead to a powerful tool in observing filter cakes in different drilling situations.

A smaller version with a much smaller pipe assembly could be incorporated into an existing flow loop because the main design does not change. If the testing unit is realized in the proposed size a new large volume flow loop is required. The design of such a flow loop would be a research topic by itself but it would be a unique tool for the testing of fluid flow on a larger scale.

Chapter 6 Experimental Procedures

In this chapter the exact experimental procedures are described. Each experiment (static, dynamic, pipe impact) is discussed in a separate section. It is important to have the procedures ready before the apparatus is build. This has also an influence on the final design. Especially to determine the positions for valves, bypass lines and equipment which is not directly related to the detailed design of the apparatus.

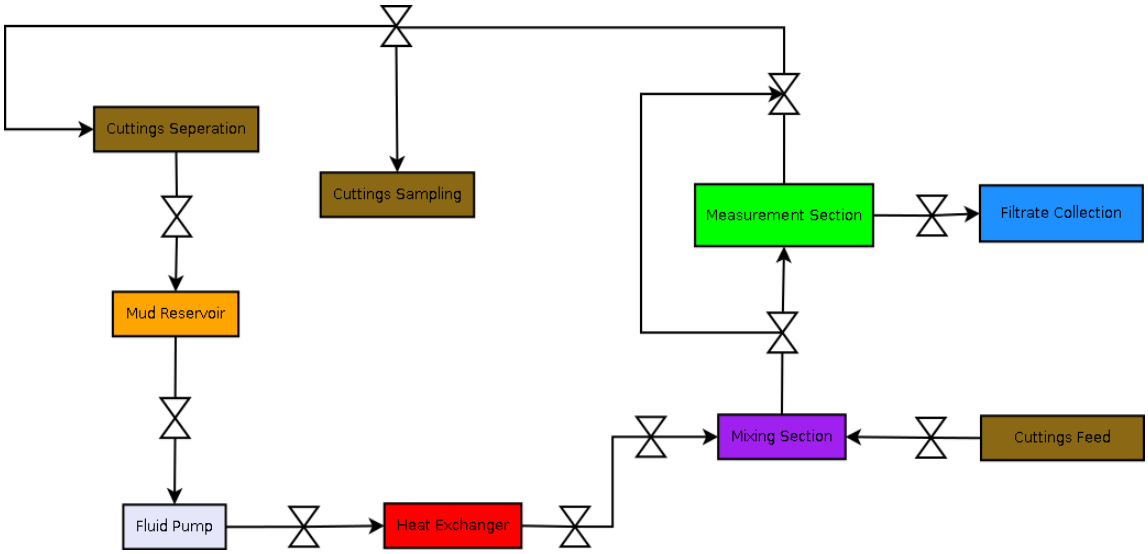

Figure 68: Flow schematic of the circulation system

6.1 General

Before every test can begin the core holder with the core needs to be assembled and afterwards mounted into the apparatus.

1. After saturating the core with the desired fluid the core is placed inside the rubber seal.
2. Afterwards the rubber seal is mounted into the core holder body.
3. The core is fixed from the bottom with a distribution plug.
4. The distribution plug is fixed with the bottom cap of the core holder.
5. On the top the core is fixed with the top cap.
6. The top cap is screwed onto the core holder body with four screws.
7. The connection pipe to the filtrate receiver is screwed into the bottom cap.
8. After that the whole assembly is mounted into the apparatus.
9. If necessary, a backpressure receiver is connected to the connection pipe.
10. A graded cylinder is placed below the core holder.

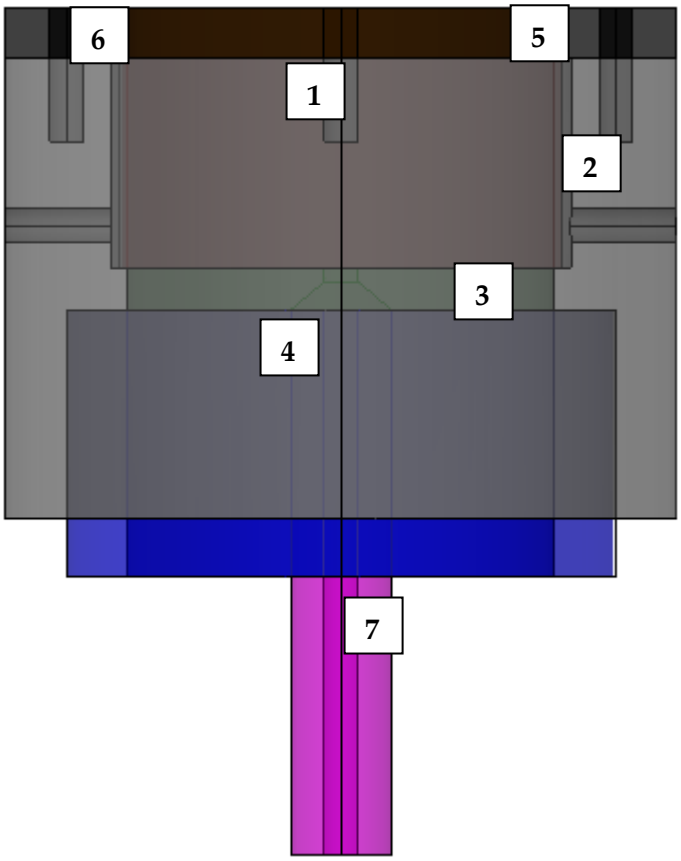

6.2 Static Filtration Test

During the static filtration test no circulation is required. Furthermore, no cuttings are fed into the system. This would only lead to blockage of lines and settling in the measurement section. The drill-pipe assembly is removed from the system. Both valves before and after the measurement section are closed to create a closed compartment, with the only possible flow path for the drilling fluid through the core.

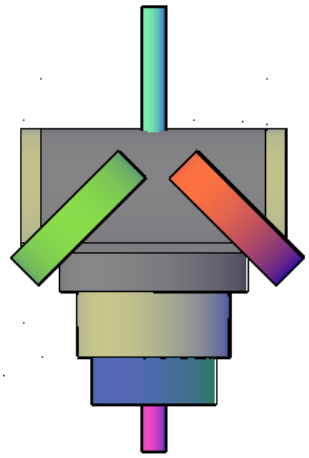

Figure 69: Core holder with shut-off valve indicated in grey on both sides

1. The core holder is screwed into the testing apparatus
2. The pressure lines to build up the confining pressure are attached to the core holder
3. Then the drilling fluid is poured into the sample chamber until it is completely filled with mud
4. Confining pressure is applied on the core sample up to 5000 psi
5. When the confining pressure has reached a steady value the pressure line to the sample chamber is attached.
6. A pressure of 100 psi is applied onto the drilling fluid
7. The pressure is kept for 30 minutes and filtrate is collected and every 5 minutes the volume is recorded
8. After 30 minutes the confining pressure is released from the core holder
9. Then the pressure is released and the drilling fluid is discarded from the sample chamber
10. The core holder is unscrewed from the apparatus
11. The top cap is removed from the core holder and the core together with the rubber seal is removed from the core holder
12. The rubber seal is removed from the core and the core and the filter cake are ready for further analysis

6.3 Dynamic Filtration Test

In the dynamic filtration test the fluid is circulated at a certain rate to create the required shear rate onto the core face. This is controlled by the flowrate that is set at the pump. Cuttings are not fed into the system as they are not required in these types of experiment. There is no standard procedure for carrying out a dynamic filtration test with regards to pressure or time. Nevertheless, the time interval for the experiment needs to be long enough to reach the equilibrium thickness of the filter cake. The drill pipe assembly is also removed from the system to avoid obstructions in the flow path.

1. The core holder is assembled as described before
2. The core holder is mounted into the experimental apparatus
3. The pressure lines to build up the confining pressure are attached to the core holder
4. Meanwhile the drilling fluid is already circulated through the heat exchanger and the bypass line to heat up the whole system
5. The temperature is measured at several points in the circulation system, when the temperature is constant the system is ready to be used

6. Then the drilling fluid is circulated through the measurement section without already setting the working pressure
7. Confining pressure is applied on the core sample up to 5000 psi
8. When the measurement section has reached the required temperature, the pressure regulator and the backpressure regulator are set to the working pressure
9. When the pressure is constant, the test duration begins
10. During the test filtrate is collected in a graded cylinder and the volume is recorded every 5 minutes
11. The test duration depends on the shear rate and the working pressure of the system
12. When the fluid loss is linear, dynamic fluid loss has stopped and the static filtration process has started. At this point the experiment can be stopped.
13. The pump is stopped and the heat exchanger is turned off
14. The drilling fluid is discarded from the system and should be stored for further usage and analysis
15. The core holder is unscrewed from the apparatus
16. The top cap is removed from the core holder and the core together with the rubber seal is removed from the core holder
17. The rubber seal is removed from the core and the core and the filter cake are ready for further analysis

6.4 Pipe Impact Test

This type of test uses the circulation system and the drill pipe assembly. Depending on the core size a different size of drill pipe can be used, which matches the core size. Cuttings are also feed into the system. The cuttings feed starts after the pump and the cuttings are removed from the circulation system before they enter the mud reservoir. This should avoid that cuttings of a certain size may damage the pump. The cuttings are sampled directly after the measurement section.

1. The core holder is assembled as described before
2. The core holder is mounted into the experimental apparatus
3. The pressure lines to build up the confining pressure are attached to the core holder
4. Meanwhile the drilling fluid is already circulated through the heat exchanger and the bypass line to heat up the whole system

5. The temperature is measured at several points in the circulation system, when the temperature is constant the system is ready to be used
6. Then the drilling fluid is circulated through the measurement section without already setting the working pressure
7. Confining pressure is applied on the core sample up to 5000 psi
8. Rotation of the drill pipe is started and the load sensor is activated
9. When the measurement section has reached the required temperature, the pressure regulator and the backpressure regulator are set to the working pressure
10. The up and down movement of the pipe is activated at the desired contact frequency
11. When the pressure is constant, the test duration begins
12. During the test filtrate is collected in a graded cylinder and the volume is recorded every 5 minutes
13. Every 5 minutes a cuttings sample is taken from the circulation system to see if it is possible to crush the cuttings with the drill pipe
14. The test duration depends on the shear rate and the working pressure of the system
15. When the fluid loss is linear, dynamic fluid loss has stopped and the static filtration process has started. At this point the experiment can be stopped.
16. The pump is stopped and the heat exchanger is turned off
17. The drilling fluid is discarded from the system and should be stored for further usage and analysis
18. The core holder is unscrewed from the apparatus
19. The top cap is removed from the core holder and the core together with the rubber seal is removed from the core holder
20. The rubber seal is removed from the core and the core and the filter cake are ready for further analysis

The proposed experimental procedures are far from complete. When the apparatus is built, there are several details which are going to be added to the procedures. Furthermore, the test durations for the static filtration test, the dynamic filtration test and the pipe impact test need to be determined depending on the applied pressure and the shear rate. The pipe contact frequency can be set specifically for each experiment.

Chapter 7 Results and Conclusion

7.1 Results

The main result of this thesis is a design for a multipurpose unit for testing a variety of situations for filter cake build-up. Depending on its final size the unit could be implemented into an already existing flow loop. If testing of large diameter cores is required, a new design for a flow loop, which produces high circulation rates, is necessary. The design features three different applications, which are static filter cake build-up, dynamic filter cake build-up and a pipe impact test. CwD can be simulated by using large diameter pipe, which has regular contact with the core face and by feeding artificial cuttings into the circulation system.

The final design consists of three parts which are the core holder, the main body and the drill-pipe assembly. The core holder allows confining pressures up to 5000 psi and exposes one side of the core to the drilling fluid. The core holder is going to be made out of Hastelloy.

The main body has a half pipe shape and is equipped with a temperature sensor and four pressure sensors. Furthermore, two shut-off valves are indicated in the design two allow static filtration tests. The pressure is regulated by a pressure regulation valve at the beginning of the measurement section and a backpressure valve at the end for pressure maintenance.

The drill-pipe assembly is aligned with the flow direction. The design features an electric motor which drives the pipe rotation. Via two stuffing boxes pressure is maintained in the pipe body. A load sensor is used to measure the forces during up and down movement of the assembly. The vertical movement is controlled because the whole assembly rests on a lifting ramp.

Furthermore, three experimental procedures were developed based on the final design. These procedures are so far only proposals because they need to be adapted after the unit is build.

7.2 Conclusion

Based on the literature review the comparison between regular filter cake and one created by smearing it can be concluded that the particle size distribution (PSD) is of vital importance. The PSD has a high influence on the filtrate volume and the filter cake structure. Furthermore, the porosity and the permeability of the filter cake are influenced by the PSD.

Considering the geomechanical aspects of CwD it seems that it has a positive effect on the wellbore stability. This is due to the creation of a filter cake with very low permeability which hinders fluid to invade the formation. Therefore, time dependent pore pressure changes are prevented, which in worst case would lead to significant breakouts.

The frequent contact of the casing with the wellbore wall is also considered as positive, but it is not verified yet. The contact leads to an increase of the hoop stress and can prevent the creation of fractures if the contact happens at the point of maximum horizontal far field stress. If the contact happens at the point of minimum horizontal far field stress it is more likely to create breakouts due to the increase in hoop stress. Therefore, it can be concluded that the positive effect of CwD depends highly on the contact direction in the wellbore.

Regarding the experimental research of filter cake created by smearing, so far, no experiment exists which simulates the build-up. Also, no experiment exists which allows a direct comparison between a filter cake created by smearing and a regular filter cake.

When the experimental design is realized, it will enable the user to test the build-up of filter cake in different situations in the wellbore. Pressure, temperature, shear rate and particle size distribution are parameters which can be directly controlled during an experiment. This should allow the user to test different dependencies of parameters on the filter cake quality simultaneously.

Finally, it can be concluded that CwD requires additional research regarding the different influence parameters and the differences of filter cake quality and structure compared to normal operations. This research can be realized by building the proposed unit.

Appendix A Equations

A.1 Stresses around the wellbore

$$\sigma_\theta = \frac{1}{2} * (\sigma_H - \sigma_h) * \left(1 + \frac{R^2}{r^2}\right) - \frac{1}{2} * (\sigma_H - \sigma_h) * \left(1 + \frac{3 * R^4}{r^4}\right) * \cos 2 * \theta - P_W * \frac{R^2}{r^2}$$

$$\sigma_r = \frac{1}{2} * (\sigma_H - \sigma_h) * \left(1 - \frac{R^2}{r^2}\right) + \frac{1}{2} * (\sigma_H - \sigma_h) * \left(1 - 4 * \frac{R^2}{r^2} + \frac{3 * R^4}{r^4}\right) * \cos 2 * \theta - P_W * \frac{R^2}{r^2}$$

$$\sigma_z = \sigma_v - 2 * \nu * (\sigma_H - \sigma_h) * \cos 2 * \theta$$

Equation 42: Stresses in the near wellbore region [23]

A.2 Herschel Bulkley pressure drop

$$Q = \frac{2 * w * \left(\frac{h}{2}\right)^{2+\frac{1}{n}} * \left(\frac{1}{K} * \frac{dp_f}{ds}\right)^{\frac{1}{n}} * \left(1 - \frac{\tau_y}{\frac{h}{2} * \frac{dp_f}{ds}}\right)^{1+\frac{1}{n}} * \left(\frac{\tau_y}{\frac{h}{2} * \frac{dp_f}{ds}} + \frac{1}{n} + 1\right)}{\frac{1}{n+1} * \frac{1}{n+2}}$$

Equation 43: Herschel-Bulkley pressure drop equation [71]

Bibliography

[1] E. van Oort and S. O. Razavi, "Wellbore Strengthening and Casing Smear: The Common Underlying Mechanism," in *IADC/SPE Drilling Conference and Exhibition*, Fort Worth, Texas, 2014.

[2] Dewan and Chenevert, "A Model for Filtration of Water-base Mud During Drilling: Determination of Mudcake Parameters," in *Petrophysics. Vol. 42*, Austin, Texas, Society of Professional Well Log Analysts, 2001, pp. 237-250.

[3] Elkatatny, Mahmoud and Nasr-El-Din, "A New technique to Characterize Drilling Fluid Filter Cake," in *SPE European Formation Damage Conference*, Noordwijk, The Netherlands, 2011.

[4] Elkatatny and Nasr-El-Din, "Properties of Filter Cake of Water-Based Drilling Fluid under Dynamic Conditions using Computer Tomography," in *IADC/SPE Drilling Conference and Exhibition*, San Diego, California, 2012.

[5] Elkatatny, Mahmoud and Nasr-El-Din, "A New Approach to Determine Filter Cake Properties of Water-Based Drilling Fluids," in *SPE/DGS Saudi Arabia Section Technical Symposium and Exhibition*, Al-Khobar, Saudi Arabia, 2011.

[6] Geri, Al-Mutairi and Mahmoud, "Different Techniques for Characterizing the Filter Cake," in *SPE Middle East Unconventional Gas Conference and Exhibition*, Muscat, Oman, 2013.

[7] Chandler und Dangou, „Potential Increase of Formation Damage at Horizontal Wells as a Result of Changing Dynamic Filter Cake Properties with the Shear Rate," in *SPE European Formation Damage Conference*, Scheveningen, The Netherlands, 2009.

[8] Jiao und Sharma, „Investigation of Dynamic Mud Cake Formation: The Concept of Minimum Overbalance Pressure," in *Annual Technical Conference and Exhibition*, Houston, Texas, 1993.

[9] Li und He, „Journey Into Filter Cakes: A Microstructural Study," in *International Petroleum Technology Conference*, Doha, Qatar, 2015.

[10] M. Stephens und W. He, „Bridging Particle Size Distribution in Drilling Fluid and Formation Damage," in *SPE European Formation Damage Conference*, Noordwijk, The Netherlands, 2011.

[11] M. Karimi, A. Ghalambor, M. Montgomery and E. Moellendick, "Formation Damage and Fluid Loss Reduction due to Plastering Effect of Casing Drilling," in *SPE European Formation Damage Conference*, Noordwijk, The Netherlands, 2011.

[12] M. Karimi, E. Moellendick and C. Holt, "A Review of Casing Drilling Advantages to Reduce Lost Circulation, Improve Wellbore Stability, Augment Wellbore Strengthening, and Mitigate Drilling-induced Formation Damage," in *SPE/IADC Middle East Drilling Technology Conference and Exhibition*, Muscat, Oman, 2011.

[13] Beardmore, Scott, McKeever, Greener and Watts, "Particle Size Distribution Improves Casing-While-Drilling Wellbore-Strengthening Results," in *IADC/SPE Drilling Conference and Exhibition*, New Orleans, Louisiana, 2010.

[14] Salehi, Karimi, Shahri, Aladsani and Ezeakacha, "All in One for Casing while Drilling Technology: Numerical, Analytical, and Experimental Results and Field Observations," in *SPE Annual Technical Conference and Exhibition*, New Orleans, Louisiana, 2013.

[15] Salehi, Mgboji, Aladsani und Wang, „Numerical and Analytical Investigation of Smear Effect in Casing Drilling Technology: Implications for Enhancing Wellbore Integrity and Hole Cleaning," in *SPE/IADC Drilling Conference and Exhibition*, Amsterdam, The Netherlands, 2013.

[16] M. Karimi, E. Moellendick and C. Holt, "Plastering Effect of Casing Drilling; a Qualitative Analysis of Pipe Size Contribution," in *SPE Annual Technical Conference and Exhibition*, Denver, Colorado, USA, 2011.

[17] Gidley, Holditch und Nierode, „Recent Advances in Hydraulic Fracturing," in *Rock Mechanics and Fracture Geometry*, Richardson, Texas, Monograph Series, SPE, 1989, pp. 57-63.

[18] SPE-International, "PetroWiki, Fracture Mechanics," SPE-International, [Online]. Available: http://petrowiki.org/Fracture_mechanics#cite_note-r2-2. [Accessed 29 11 2016].

[19] B. Pasic, N. Gaurina-Medimurec und D. Matanovic, „Wellbore Instability: Causes and Consequences," *Rudarsko-geološko-naftni zbornik,* Bd. 19, Nr. 1, pp. 87-98, 2007.

[20] SPE-International, "PetroWiki, Elastic wellbore stress concentration," SPE-International, [Online]. Available: http://petrowiki.org/Elastic_wellbore_stress_concentration. [Accessed 29 11 2016].

[21] Geomechanic Technologies, "Advanced Wellbore Stability Analysis," Geomechanic Technologies, 2012. [Online]. Available: http://www.geomechanics-technologies.com/wellbore_stability.html. [Accessed 21 February 2017].

[22] Kirsch, „Die Theorie der Elastizität und die Beduerfnisse der Festigkeitslehre," *Zeitung Verein Deutscher Ingenieure,* Bd. 29, Nr. 42, pp. 797-807, 1898.

[23] Hiramatsu und Oka, „Determination of the stress in rock unaffected by boreholes or drifts, from measured strains or deformations," *International Journal of Rock Mechanics and Mining Sciences & Geomechanics Abstracts,* pp. 337-353, 1968.

[24] Fjaer, Holt, Horsrud, Raaen und Risnes, Petroleum Related Rock Mechanics 2nd Edition, Amsterdam, The Netherlands: Elsevier, 2008.

[25] B. Aadnoy, E. Kaarstad und M. Belayneh, „Elastoplastic Fracture Model Improves Predictions in Deviated Wells," in *SPE Annual Technical Conference and Exhibition*, Anaheim, California, USA, 2007.

[26] Y. Baohua, Y. Chuanliang, T. Qiang, D. Jingen und G. Shen, „Wellbore Stability in High Temperature and Highly-depleted Reservoir," *Eectronic Journal of Geotechnical Engineering,* pp. 909-922, 2013.

[27] M. Zoback, D. Moos, L. Mastin und R. Anderson, „Wellbore breakouts and in situ stress," *Journal of geophysical research,* Bd. B7, Nr. 90, pp. 5523-5530, 1985.

[28] Gholami, Moradzadeh, Rasouli und Hanachi, „Practical application of failure criteria in determining safe mud weight windows in drilling operations," *Journal of Rock Mechanics and Geotechnical Engineering,* Bd. 1, Nr. 6, pp. 13-25, 2014.

[29] M. Zoback, Reservoir Geomechanics, Cambridge, United Kingdom: Cambridge University Press, 2010.

[30] Hoek und Brown, Underground excavations in rock, London: E&FN Spon, 1980.

[31] M. Mokhtari, A. Tutuncu und T. Weldu Teklu, „A Numerical Modeling Study for the Impact of Casing Drilling on Wellbore Stability," in *SPE Unconventional Resources Conference*, Calgary, Alberta, Canada, 2013.

[32] Kiran und Salehi, „Finite Element Analysis of Casing Drilling Smearing Effect," in *SPE Deepwater Drilling and Completions Conference*, Galveston, Texas, USA, 2014.

[33] M. Williams und Cannon, „Evaluation of Filtration Properties of Drilling Mud," in *American Petroleum Institute*, 1938.

[34] Leerloijer, Kuijenhoven und Francis, „Filtration Control, Mud Design and Well Productivity," in *Formation Damage Control Symposium*, Lafayette, USA, 1996.

[35] Havenaar und Bezemer, „Filtration Behavior of Circulating Drilling Fluids," in *SPE 40th Annual Fall Meeting*, Denver, Colorado, 1966.

[36] Grace Instrument, "M2200," 20 August 2016. [Online]. Available: http://www.graceinstrument.com/M2200.php. [Accessed 9 September 2016].

[37] Scott Quigley und H. Seal, „Dynamic Filtration Unit and Process of Use". USA Patent 4,790,933, 13 December 1988.

[38] fann, "Dynamic HPHT Filtration Cell," fann, 20 August 2016. [Online]. Available: http://www.fann.com/fann/products/drilling-fluids-testing/filtration-dynamic-hpht/dynamic-hpht-filter.page. [Accessed 9 September 2016].

[39] Slater und Amer, „New Automated Lubricity Tester Evaluates Fluid Additives, Systems and their Applications," in *11th Offshore Mediterranean Conference and Exhibition*, Ravenna, Italy, 2013.

[40] Core Lab, "Lubricity Evaluation Monitor," Core Lab Reservoir Optimization, 1 11 2016. [Online]. Available: http://www.corelab.com/cli/drilling-and-stimulation/lubricity-evaluation-monitor-lem-4100. [Accessed 1 11 2016].

[41] A. Bourgoyne, M. Chenevert, K. Millheim und Young, Applied Drilling Engineering, Richardson, Texas, USA: Society of Petroleum Engineers, 1986.

[42] American Petroleum Institute, Recommended Practice for Field Testing of Water based Drilling Fluids, Washington D.C.: API Publishing Services, 2003.

[43] Tan und Amanullah, „A Non-Destructive Method of Cake Thickness Measurement," in *SPE Asia Pacific Oil and Gas Conference and Exhibition*, Brisbane, Australia, 2000.

[44] SPE International, "PetroWiki, Saturation Evaluation," SPE International, [Online]. Available: http://petrowiki.org/Saturation_evaluation. [Accessed 26 December 2016].

[45] King Saud University, „King Saud University, Fluid Saturation," [Online]. Available: http://faculty.ksu.edu.sa/arefi/_layouts/mobile/view.aspx?List=18957bb9-3c20-499e-a29a-3f8572e257a6&View=d75ccc5c-674f-414d-b9bc-aebcd8453e61. [Zugriff am 26 12 2016].

[46] CoreLab, "CoreLab, Hassler Type Core Holder," CoreLab, [Online]. Available: http://www.corelab.com/cli/core-holders/hassler-type-core-holders-rch-series. [Accessed 27 January 2016].

[47] AAPG, "AAPG Wiki, Permeability," AAPG, [Online]. Available: http://wiki.aapg.org/Permeability. [Accessed 27 December 2016].

[48] E.R. Crain, "Crains Petrophysical Handbook," [Online]. Available: https://www.spec2000.net/09-coreperm.htm. [Accessed 27 December 2016].

[49] University of Stavanger, „Klinkenberg Permeability Measurements: Problems and Practical Solutions," [Online]. Available: http://www.ux.uis.no/~s-skj/ipt/Proceedings/SCA.1987-2004/1-SCA1991-20EURO.pdf. [Zugriff am 27 December 2016].

[50] nanoScience Instruments, "nanoScience Instruments, Scanning Electron Microscopy," nanoScience, [Online]. Available: http://www.nanoscience.com/technology/sem-technology/. [Accessed 17 1 2017].

[51] Dartmouth College Electron Microscope Facility, "Botanical Pollen SEM," Dartmouth College, [Online]. Available: http://remf.dartmouth.edu/images/botanicalPollenSEM/. [Accessed 17 1 2017].

[52] Montana State University, "Integrating Research and Education," [Online]. Available: http://serc.carleton.edu/18400. [Accessed 17 1 2017].

[53] Radiopaedia, "Radiopeadia, Computed Tomography," TrikeApps, [Online]. Available: https://radiopaedia.org/articles/computed-tomography. [Accessed 17 1 2017].

[54] Retsch, "The Basic Principles of Sieve Analysis," Retsch Gmbh & Co KG, Haan, 2004.

[55] ShineSaga, „Sieve Analysis of Soil," [Online]. Available: http://www.shinesaga.com/2014/07/sieve-analysis-of-soil.html. [Zugriff am 31 12 2016].

[56] Schlumberger, „XL-Rock, Large-volume rotary sidewall coring service," Schlumberger, 2012.

[57] M. V. Tony Smithson, „Downhole Coring," *Oilfield Review*, Nr. 27, pp. 63-64, 2015.

[58] Schlumberger, „Mechanical Sidewall Coring Tool," Schlumberger, Houston, 2004.

[59] Baker Hughes, „PowerCOR Service," Baker Hughes, 2010.

[60] Baker Hughes, „First HT30 Max Coring System Run Saved 1.5 Days Rig Time and Delivered Excellent Core Quality," Baker Hughes, Qatar, 2016.

[61] Weatherford, „Wellsite Services," Weatherford, 2015.

[62] DCI Test Systems, „DCI-Core-Holder Configurations," DCI Test Systems, West North Salt Lake.

[63] Haynes International, "Product Forms, Pipe and Tubing," Haynes International, [Online]. Available: http://www.haynesintl.com/alloys/product-forms/pipe-and-tubing. [Accessed 17 1 2017].

[64] R. E. Bicking, "Sensors Online," Questex, [Online]. Available: http://www.sensorsmag.com/sensors/pressure/fundamentals-pressure-sensor-technology-846. [Accessed 6 1 2017].

[65] Instrumentation Today, "Bourdon Tube," Instrumentation Today, [Online]. Available: http://www.instrumentationtoday.com/bourdon-tube/2011/09/. [Accessed 6 1 2017].

[66] Dynisco, "www.dynisco.com," 2017. [Online]. Available: http://www.dynisco.com/stuff/contentmgr/files/1/2604e6ab8ea5dedf1e46af7a3d771c37/pdf/straingage.pdf. [Accessed 22 February 2017].

[67] K. Hoffman, "Hottinger Baldwin Messtechnik GmbH," 2017. [Online]. Available: https://www.hbm.com/fileadmin/mediapool/hbmdoc/technical/s1569.pdf. [Accessed 22 February 2017].

[68] WIKA, "Wika Instrument," [Online]. Available: http://www.wika.us/upload/BR_CAT_Mechanical_Temperature_en_us_17803.pdf. [Accessed 6 1 2017].

[69] AZO Materials, "www.azom.com," AzoNetwork, 2017. [Online]. Available: http://www.azom.com/article.aspx?ArticleID=5573. [Accessed 22 February 2017].

[70] Omega, "www.omega.de," Omega Engineering, 2017. [Online]. Available: http://www.omega.de/pptst/OM-CP-OCTRTD.html. [Accessed 22 February 2017].

[71] R. Mitchell und S. Miska, Fundamentals of Drilling Engineering, Richardson: SPE, 2011.

[72] University of Sydney, "Aerodynamics for students," University of Sydney, 2005. [Online]. Available: http://www-mdp.eng.cam.ac.uk/web/library/enginfo/aerothermal_dvd_only/aero/fprops/pipeflow/node9.html. [Accessed 22 February 2017].

[73] Native Dynamics, "Neutrium," Native Dynamics, 2017. [Online]. Available: https://neutrium.net/fluid_flow/hydraulic-diameter/. [Accessed 22 February 2017].

[74] The Engineering ToolBox, "Reynolds Number," The Engineering ToolBox, 2017. [Online]. Available: http://www.engineeringtoolbox.com/reynolds-number-d_237.html. [Accessed 22 February 2017].

[75] I. B. Misalam, "University Malaysia Pahang," [Online]. Available: http://umpir.ump.edu.my/8331/1/cd8228_62.pdf. [Accessed 22 February 2017].

Acronyms

CwD	Casing while Drilling
WBS	Wellbore Strengthening
FIP	Fracture Initiation Pressure
FRP	Fracture Reopening Pressure
FPP	Fracture Propagation Pressure
FPR	Fracture Propagation Resistance
PSD	Particle Size Distribution
LCM	Lost Circulation Material
CT	Computer Tomography
PSD	Particle Size Distribution
UBD	Underbalanced Drilling
SEM	Scanning Electron Microscopy
RTD	Resistance Temperature Detector

Symbols

σ_1	Maximum Principal Stress	[Pa]
σ_2	Intermediate Principal Stress	[Pa]
σ_3	Minimum Principal Stress	[Pa]
σ_H	Maximum Horizontal Stress	[Pa]
σ_h	Minimum Horizontal Stress	[Pa]
σ_θ	Hoop Stress	[Pa]
σ_r	Axial Stress	[Pa]
σ_z	Radial Stress	[Pa]
τ	Shear Stress	[Pa]
ΔP	Pressure Difference	[Pa]
Q	Flowrate	[m^3/s]
k_{mc}	Mudcake Permeability	[mD]
k_{mc0}	Reference Permeability at 1 psi	[mD]
k_g	Gas Permeability	[mD]
k_∞	Absolute Permeability	[mD]
Φ_{mc}	Porosity of the mudcake	[ ]
Φ_{mc0}	Reference Porosity at 1 psi	[ ]
Φ_f	Formation Porosity	[ ]
P_w	Pore Pressure on the wellbore wall	[Pa]
P_0	Far Field pore pressure	[Pa]
φ	Internal Angle of Friction	[°]
θ	Angle of Interest	[°]
α,β	Biot's Coefficient	[ ]
μ_i	Internal coefficient of friction	[ ]
μ_f	Filtrate viscosity	[cp]
ν	Poisson's Ratio	[ ]
F_x	Hydrodynamic Force	[N]
F_y	Pressure Force	[N]
C	Cohesion	[Pa]
C_0	Unified Compressive Strength	[Pa]

h	Slot height	[m]
w	Slot width	[m]
R	Wellbore radius	[m]
r	Radius of Interest	[m]
K	Consistency Index	[Pas]
n	Flow Index	[ ]
τ_y	Yield Stress	[Pa]
τ_W	Wall Shear Stress	[Pa]
f	Coefficient of Friction	[ ]
f_{sc}	Volume fraction of solids in the cake	[ ]
f_{sm}	Volume fraction of solids in the mud	[ ]

List of Figures

List of Tables

List of Equations